

Early Hydration of Cementitious Systems

THÈSE N° 4554 (2009)

PRÉSENTÉE LE 10 DÉCEMBRE 2009

À LA FACULTÉ SCIENCES ET TECHNIQUES DE L'INGÉNIEUR
LABORATOIRE DES MATÉRIAUX DE CONSTRUCTION
PROGRAMME DOCTORAL EN SCIENCE ET GÉNIE DES MATÉRIAUX

ÉCOLE POLYTECHNIQUE FÉDÉRALE DE LAUSANNE

POUR L'OBTENTION DU GRADE DE DOCTEUR ÈS SCIENCES

PAR

Patrick JUILLAND

acceptée sur proposition du jury:

Prof. P. Stadelmann, président du jury
Prof. K. Scrivener, Dr E. Gallucci, directeurs de thèse
Dr P. Bowen, rapporteur
Dr R. Flatt, rapporteur
Prof. A. P. Nonat, rapporteur



ÉCOLE POLYTECHNIQUE
FÉDÉRALE DE LAUSANNE

Suisse
2009

Abstract

Underground job sites such as tunnels and mines rely on the quality of recently sprayed concrete to secure freshly excavated zones. Rapid setting and early high strength development are required for safety as well as for the rapid progression of the construction site. This is ensured by the addition of accelerating admixtures. These admixtures are of various chemical formulations and have different impacts on the early hydration kinetics. It is therefore important to understand their impact on the mechanism of hydration.

However, knowledge on the early hydration mechanisms, though extensively studied, is still incomplete. The present investigation studied the mechanisms taking place at the solid-liquid interface during the early hydration of cementitious compounds. Crystal dissolution theory developed in the field of geochemistry was applied to alite in order to explain the rapid slow-down of the reactions taking place after the first rapid dissolution. To assess the validity of this theory, alite was synthesised in laboratory. Annealing of alite powders of narrow particle size distributions were carried out to assess the influence of the density of crystallographic defect on the duration of the induction period. Morphological observations of alite surfaces dipped in solutions of different saturation states were also performed in order to observe the rate controlling mechanism of dissolution. On the basis of these experimental results as well as an extensive literature review, a new model is proposed for the early hydration of alite in which dissolution is the rate controlling factor up to the onset of the acceleration period.

Parameters affecting the kinetics of hydration such as the influence of mixing speed or the accelerating effect of calcium chloride is discussed bearing in mind the concept of crystal dissolution.

Finally, the impact of alkali-free accelerators on the kinetics of hydration was also studied. The reactions of hydration were monitored by isothermal calorimetry and in-situ XRD. It is found that these admixtures lead to a massive precipitation of ettringite which might impair the ability of gypsum to control the C_3A hydration leading to a competition between the silicate and the aluminate reactions to fill up the available pore space.

Key words: Hydration; Alite; Induction period; Dissolution; Mixing; Alkali-free accelerators; Shotcrete.

Résumé

La sécurité de zones excavées lors de l'exécution de travaux souterrains tels que tunnels ou mines dépend essentiellement de la qualité du béton fraîchement projeté. Une prise instantanée ainsi qu'une rapide augmentation des propriétés mécaniques à jeune âge sont nécessaires pour des raisons de sécurité mais aussi afin d'accélérer la progression des travaux. Ces diverses mesures sont atteintes grâce à l'utilisation d'accélérateurs de prise. Ces adjuvants influencent les cinétiques d'hydratation à jeune âge de manière différente selon leur nature chimique. Il est donc important de connaître leur impact sur les mécanismes d'hydratation.

Malgré les connaissances déjà acquises dans le domaine de l'hydratation, notre compréhension reste toutefois incomplète. La présente étude s'intéresse donc à mieux comprendre les phénomènes prenant place à l'interface solide-liquide des matériaux cimentaires durant les premières heures de l'hydratation. En nous basant sur la théorie de la dissolution des cristaux développée dans le domaine de la géochimie, nous avons été en mesure de trouver une nouvelle théorie permettant d'expliquer le soudain ralentissement des réactions quelques minutes après que la phase cimentaire ait été mise en contact avec l'eau. Afin de vérifier ces hypothèses, des tests de recuit sur des poudres d'alite caractérisées par une étroite distribution de taille ont été menés afin de montrer l'influence de la densité de défauts cristallins. Des études morphologiques de surfaces d'alite plongées dans des solutions possédant différents états de saturation ont également été entreprises afin d'observer les mécanismes de dissolution opérant dans ces conditions. Sur la base de ces résultats expérimentaux ainsi que d'une revue littéraire relativement étendue, un nouveau modèle d'hydratation est présenté dans lequel la dissolution est le facteur limitant jusqu'à la fin de la période d'induction.

D'autres paramètres pouvant également affecter les cinétiques d'hydratation tels que la vitesse de mélange ou encore la présence de chlorure de calcium sont discutés en nous basant sur ces nouveaux concepts liés aux mécanismes de dissolution.

Finalement, les cinétiques d'hydratation de systèmes plus complexes comprenant la présence des accélérateur de prise sans alcalins sont étudiées principalement par calorimétrie et diffraction des rayons X in situ. Il est montré que ces accélérateurs de prises provoquent une précipitation rapide et massive d'ettringite pouvant amener à une déstabilisation de l'hydratation de la phase C_3A , cette dernière pouvant dès lors entrer en compétition avec l'hydratation des phases silicates pour remplir l'espace de la solution poreuse.

Mots clés: Hydratation; Alite; Période d'induction; Dissolution; Mélange; Accélérateur sans alcalins; Béton projeté.

Contents

Abstract	i
Résumé	ii
1 Introduction	1
2 Theory: Hydration and Crystal Dissolution	3
2.1 Early Hydration of Ordinary Portland Cement	3
2.2 Early hydration of Tricalcium Aluminate	5
2.2.1 Hydration of C_3A without sulfate addition	5
2.2.2 Hydration of C_3A in presence of sulfate addition	6
2.2.3 Role of sulfate content	7
2.3 Early Hydration of Alite	9
2.3.1 Protective membrane	12
2.3.2 Double layer theory	13
2.3.3 Nucleation and growth	16
2.4 Crystal dissolution	20
2.4.1 Surface and crystallographic defects	20
2.4.2 Role of crystallographic defects and solution saturation on crystal dissolution	28
2.4.3 Relation between dislocation density and rate of dissolution .	33
2.4.4 Effect of impurities on dissolution	38
3 Assesement of Dissolution Theory to Alite Early Hydration	43
3.1 Influence of Alite Crystal Structure on its Early Hydration Kinetics .	43
3.1.1 Surface observation of coarse anhydrous alite	43
3.1.2 Induction period and crystallographic defects	44
3.2 Morphological Studies of Early Hydrated Alite	48

3.2.1	Surface study of coarse alite in normal alite paste	48
3.2.2	Effect of solution saturation state	51
3.3	Previous evidence of the role of crystallographic defects on the reaction of cementitious materials	53
3.3.1	Effect of calcium hydroxide addition	56
3.3.2	Effect of free lime addition	59
3.4	Effect of inorganic addition	59
3.5	Discussion	62
3.5.1	Large difference from solubility limit of C_3S	62
3.5.2	NMR studies of early hydration of C_3S	64
3.5.3	Calculations of dissolution rate	65
3.6	Proposed mechanisms of early hydration of alite	68
3.7	Summary	71
4	Effect of Mixing on the Early Hydration of Cementitious Systems	73
4.1	Effect of speed of mixing on the hydration kinetics of alite pastes . .	74
4.2	Influence effect on real cementitious systems	83
4.2.1	Portland Cement systems	83
4.2.2	Retarded/Superplasticised PC systems	87
4.2.3	Accelerated systems	91
4.3	Discussion: Effect of mixing conditions on the early hydration of cementitious systems	94
5	Influence of Alkali-Free Accelerators on the Kinetics of Hydration of Portland Cement	101
5.1	Kinetics of hydration on accelerated paste systems	102
5.1.1	Influence of accelerator type	102
5.1.2	Influence of accelerator dosage	112
5.1.3	Influence of cement type	114
5.1.4	Influence of acid formic content using accelerator A	116
5.2	Shotcrete	119
5.3	Discussion and Summary	123
5.3.1	Role of sulfate on hydration of accelerated systems	123
5.3.2	Competition between aluminate and silicate reactions	124

6 Conclusion and Perspectives	125
Acknowledgments	138
Annexe I	139
Annexe II	140
Curriculum Vitae	142

List of Figures

2.1	Typical calorimetry curve for a Portland cement paste.	4
2.2	Development of microstructure during the hydration of Portland cement. From [1]	5
2.3	Schematic evolution of the C_3A heat flow hydrating in presence of gypsum.	6
2.4	Ionic concentrations (aluminium:▲, sulphates: ●, calcium: ■ and calculated hydroxide: ◆) and conductivity evolutions during hydration of 7.4 mmol of C_3A and gypsum (1.5 mmol) in 50 mL of a solution saturated with respect to the Portlandite (L/S=25). Adapted from [2]	7
2.5	Heat evolution rate curves during the hydration of C_3A in solutions saturated with respect to Portlandite (w/b = 25) carried out with increasing quantities of gypsum. From [2]	8
2.6	Influence of the gypsum content (0%, 2%, 3%, 4%, 5% and 6%) on the heat flow generated by a mass mixture of 80% of C_3S and 20% of C_3A . the water to binder ratio is 1 and the temperature is 25 °C. From [3]	8
2.7	Scheme showing the influence of the gypsum content on the heat flow generated by PC having various amount of gypsum addition. Adapted from [4]	9
2.8	Solution phase analysis with the associated heat development monitored by isothermal calorimetry. From [5].	10
2.9	Simulation vs experimental data of alite particles having a narrow particle size distribution centred around 38 μm . (a) Simulation using the nucleation and growth mechanism and (b) using the “densification” process. Black data are the heat flow of alite hydration and grey data, the associated degree of hydration. Plain curves are experimental data. From [6]	11
2.10	Water-rich region of the $CaO-SiO_2-H_2O$ phase diagram showing the solubility curves of two types of C-S-H. Curves A represent three possible solubilities for C-S-H formed by precipitation either from solutions of a calcium salt and sodium silicate or from solutions of $Ca(OH)_2$ and silicic acid. Curve B represents the solubility of a C-S-H formed from a hydrating C_3S . From [7].	13

2.11	Change in C/S ratio of a hydrated C_3S surface as a function of hydration time. From [8]	14
2.12	Schematic representation of the charge distribution close to a negatively charged surface and the associated potential evolution. Adapted from [davis:1990]	15
2.13	Calcium ion and silica concentrations in solution during the first 4 hours of hydration at a w/ C_3S ratio of 0.7. From [9]	17
2.14	Variation with lime concentration of the percentage of hydration against time during the hydration of Ca_3SiO_5 grains, l/s=50. The characteristic periods are indicated for the curve obtained at 16 mmol/L. From [10]	17
2.15	Interactions of water with quartz surfaces and associated surface energy changes (schematic). From [11]	22
2.16	Scheme illustrating some of the defects which may occur at a free surface. The examples shown are (1) a vacancy on a terrace, (2) a vacancy at a step, (3) an adatom on a terrace, (4) an adatom at a ledge or step, (5) an edge dislocation-surface intersection, (6) a screw dislocation-surface intersection and (7) a kink site. Note that in the removal of an atom at a kink site, the kink is regenerated. Adapted from [12]	24
2.17	Schematic representation of a crystallographic lattice with (a) a screw dislocation, (b) an edge dislocation. The vector \vec{b} is the Burgers vector and $\vec{\xi}$ is the line vector of the dislocation.	25
2.18	Schematic representation of a perfect edge dislocation lying in the prism plane of sapphire, with a Burgers vector of the type $\langle \bar{1}010 \rangle$. The crystal is represented by the stacking of three different layers. From [13]	26
2.19	X-ray diffraction patterns of C_3S after 0h (unmilled), 10h, 20h and 30h of milling. From [14].	27
2.20	Time dependence of intensities for the 101 reflection of $Ca(OD)_2$ for the hydrated unmilled and hydrated milled Ca_3SiO_5 . Experimental data are represented by unfilled symbols. From [14].	27
2.21	Dissolution mechanisms: (a) two-dimensional vacancy islands: nucleation of small pits at perfect surfaces with or without the help of impurities; (b) etch pit: formation at the outcrops of a dislocation with the surface; and (c) step retreat taking place at pre-existing roughness. Mechanisms (a) and (b) are fast dissolution processes occurring at far from equilibrium conditions. (c) is a slow dissolution mechanism occurring at close to equilibrium conditions.	28

2.22	In situ AFM images of a dissolving $10\bar{1}4$ surface showing the abrupt leap in pit density when the saturation index decreases from (A) $S = 0.012$ to (B) $S = 0.007$ and the resemblance of the surface morphologies at (B) $S = 0.007$ and in (C) distilled, deionised water. From [15].	29
2.23	Dependence of the two activation energy barriers ΔG_{crit}^n (2D vacancy islands) and ΔG_{crit} (etch pit) in function of the undersaturation for an albite crystal having $\gamma = 0.05 \text{ mJ.m}^{-2}$, $\Omega = 100 \text{ cm}^3.\text{mol}^{-1}$, $\ \vec{b}\ = 7 \text{ \AA}$ and $G = 30 \text{ GPa}$. Values from [Burch et al., 2003]. In part I, II and III, it is respectively the step retreat, the etch pit formation at dislocations and the formation of 2D vacancy islands that become the rate determining mechanisms.	31
2.24	AFM images of quartz (100) surfaces produced from different solution chemistries illustrate dissolution process that occur across driving force and solution chemistry after equivalent extents of reaction. (a) When $S = 0.10$ and the solution contains 0.0167 M CaCl_2 , the surface is covered with a high density of small pits with flat bottoms and with steep flanks. (a') At an intermediate driving force of $S = 0.65$ in a salt solution of 0.0167 M CaCl_2 , a mixture of larger and smaller flat bottom pits form across the surface. (b) When $S = 0.10$ in H_2O , surface are dominated by large etch pits with sloping sides that converge at dislocation sources. Pits are separated by relatively flat regions on the surface. (c) At a low driving force of $S = 0.90$ in 0.0167 M CaCl_2 , surfaces shows only straight edges steps with no evidence of pitting. The associated equations between the different processes are equation 2.13 for the transition 2D vacancy islands-impurity defects and dislocations-etch pit opening and equation 2.14 for the dislocations-etch pit opening and the step retreat process. Adapted from [16].	32
2.25	Comparison of the full dissolution theory (see Equation (5)) with experimental data. (A) Albite at pH 8.8 and 80°C . (B) Gibbsite at pH 3 and 80°C . (C) Labradorite at pH 3 and 25°C . (D) Smectite at pH 3 and 80°C . (From [17]).	33
2.26	Highly schematic illustration of the parallel processes involved in crystal dissolution. The horizontal length of each arrow indicates the relative rate of each process (actual rates can differ by many orders of magnitude). The vertical thickness of each arrow represents the relative quantity of material dissolved and delivered to aqueous solution by that process. Thus, while point and linear defects react most rapidly, they deliver less dissolved material to solution than slower dissolution of faces and pits occurring at edges, ledges and corners. From [18].	34
2.27	Si concentration history for the dissolution of oligoclase in four conditions: unshocked and recovered from three shock-loading experiments. Values of Si dissolution rates corresponding to steady-state slope of curves are provided in units of $10^{-12} \text{ mol.m}^{-2}.\text{s}^{-1}$. Data were obtained from experimental runs performed at 25°C and pH 4.0. From [19].	35

2.28	Dissolution rate data versus annealing temperature. Units of rate are titanium moles $\text{cm}^{-2}.\text{s}^{-1}.$ 10^{-15} . The error bars identify the 99 percent confidence interval of the regression slope. The horizontal line corresponds to the dissolution rate of the unshocked starting material. The open circle is the shocked and unannealed sample. From [20] . . .	37
2.29	Experimental results for the release of silica during dissolution of diopside powders as a function of age. Data for the unwashed powder aged 2.2, 2.7, and 7.0 months. Filled and open symbols are used to calculate rates of dissolution for various stages. From [21]	38
2.30	Schematic representation of the hydrous oxide surface, showing planes associated with surface hydroxyl groups (S), inner-sphere complexes (a), outer-sphere complexes (β) and the diffuse ion swarm (d). In case of an inner-sphere complex with a ligand (e.g., F^- , HPO_4^{2-}) the surface hydroxyl groups are replaced by the ligand (ligand exchange). From [22]	39
2.31	Schematic representation on the influence of adsorbed impurities on the shape of retreating step.	40
2.32	AFM image of phosphate poisoning on calcite growth in solution. In the presence of phosphate, step advance is dramatically reduced, steps become jagged and eventually growth stops all together. From [23] . .	40
2.33	Optimized bond lengths and angles for the static molecular models of H_4SiO_4 , NaH_3SiO_4 and LiH_3SiO_4 . From [24].	41
2.34	Free energy change of dissolving a calcium ion into (a) water, (b)0.59 M, (c) 2.38 M and (d) 3.58 M salt water. Adapted from [25]	42
3.1	SEM micrographs of anhydrous surface of coarse alite samples.	44
3.2	(a) Particle size distributions of reference and thermally treated (200° and 750°C for 6 hours) alite used for this experiment and (b) associated XRD pattern showing the change from polymorph MIII to TI for the sample treated at 750°C	45
3.3	Isothermal calorimetry curves of alite quenched in air, quenched in air and subsequently annealed at 200°C or 750°C for 6 hours. (a) Induction period and (b) hydration over 24 hours.	46
3.4	Particle size distribution of alite used in this study [26].	46
3.5	Diffraction pattern of the reference alite in grey showing the MIII polymorph and the thermally treated sample in black showing TI polymorph.	47

3.6	Heat evolution of alite untreated (reference) and treated at 650° for 6 hours of narrow particle size distribution. (a) 61 μm during the first dissolution period (in-situ measurement), the grey curve is the reference sample and the black one is the thermally treated sample and, (b) 38 μm and 82 μm for the main peak of hydration. Dashed curves are the reference samples and the plain curves are the thermally treated samples. All measurements were performed at 20°C and the water to cement ratio was kept at 0.4.	48
3.7	Calorimetry curve of an alite paste mixed 2 minutes by hand mixing. Number 1, 2, 3 and 4 (10 minutes, 3, 5 and 7 hours respectively) represent times where surface investigation was performed.	49
3.8	SEM micrographs of surface of coarse alite samples hydrated after, (a) and (b) 10 minutes, (c) and (d) 3 hours, (e) and (f) 5 hours and (g) and (h) 7 hours of hydration.	50
3.9	FIB reconstruction of (a) an alite surface hydrated in paste for 7 hours and (b) the bottom view image. The dimension of the box are 1.75 μm x 1 μm x 400 nm.	51
3.10	SEM micrographs of alite immersed during 2 minutes in (a) deionised water, (b) saturated lime solution, and 30 minutes in (c) deionised water and (d) saturated lime solution.	52
3.11	(a) Calorimetry curves of tricalcium silicate thermally treated showing the effect of crystallographic defects on the length of the induction period resulting from different thermal treatment. (b) Associated thermal treatments. From [27].	54
3.12	SEM micrographs of C_3S samples with 1.1% wt. Cr_2O_3 after 1 minute in etchant (0.4% HF with 0.6% HNO_3 in ethyl alcohol) [28].	54
3.13	High-resolution SEM micrographs of hydrated C_3S surface at $w/c = 1.0$ [8].	55
3.14	Morphology of ordinary Portland cement at different times of hydration ($w/c = 0.5$). (a) After 180 minutes of hydration and (b) after 240 minutes. From [29].	55
3.15	Topographic observation by AFM of alite surface hydrating in a saturated lime solution (deflection mode). From image E-F-G-H it is possible to observe the dissolution of specific crystallographic planes. It can also be observed that the presumed C-S-H appearing in the 1 st preferential area (image B) as well as the one in the 2 nd area are dissolving with time (AFM images from [30])	56
3.16	Dissolution of 1.5 mg of C_3S in 200 mL of calcium hydroxide solution of 0, 5.5 and 11 mM. Speed of mixing is kept constant for all experiments. From [31].	57
3.17	Heat evolution and electrical conductivity curves plotted against hydration time for C_3S hydration (a) in water at a $w/c=18$ and (b) in a 22 mM lime solution at $w/c=16$, from [32].	57

3.18	Delayed addition experiment of CH during the hydration of C_3S at $w/c=70$. From [33].	58
3.19	Heat flow of alite at early age with different amount of $MgCl_2$. From [34].	60
3.20	Rates of heat evolution from hydrating C_3S with organics salts at a $w/c = 0.4$ for (a) 4 hours of hydration and (b) 24 hours of hydration. From [35].	60
3.21	SEM micrographs of surfaces of coarse alite samples dipped into a 2 $CaCl_2$ solution for 30 minutes.	62
3.22	(a) Chemical potential phase diagram showing the chemical potential solubility isotherms for various compounds of interest in the $CaO-SiO_2-H_2O$ system, relative to the oxides in their standard states at 298.15 K. Points above and to the right of a phase boundary represent supersaturation with respect to the solid. The slope of a line at any point represents the $CaO:SiO_2$ ratio according to $R_S^C = -d\mu_s / -d\mu_c$. The precision is roughly $\pm 2n$ kJ/mol for compounds containing n oxides (e.g., ± 8 kJ/mol for C_3S). From [7].	63
3.23	Dependence of the activation energy barriers for the nucleation of 2D-vacancy islands (ΔG_{crit}^n) and etch pit formation (ΔG_{crit}) with different assumed solid-liquid interfacial energies; $\gamma = 500$ mJ.m $^{-2}$ for albite and $\gamma = 1060$ mJ.m $^{-2}$ for alite. The other parameters are kept the same as in Figure 3 except for the molar volume, which is equal to 70 cm 3 .mol $^{-1}$ for alite. The intersection between the abscissa and the plain curves give the values of $ \Delta G_{crit}^* /RT$ above which etch pits can form at dislocations.	64
3.24	Graph showing the formation of hydrated monomeric silicate species as determined by CP NMR during the hydration of C_3S in the absence and presence of admixtures. Adapted from [36].	65
3.25	Comparison of the full dissolution theory (Equation 3.4) with experimental data and transition state theory (Equation 3.3). Albite at pH 8.8 and 80C. (From [37]). The dotted dashed, black lines correspond, respectively, to values of $n=0.1, 0.5$ and 1.0 in Equation (6).	66
3.26	Schematic representation of the rate of dissolution of alite as a function of the undersaturation. The black squares represent the experimental data obtained by Damidot and co-workers (see Table 3.1) [38] and the plain curve is the assumed evolution of the rate of dissolution of alite as a function of the undersaturation. The light grey zone correspond to Portlandite saturation which is assumed to be close to $\Delta G_{crit}^*/RT$ (the width correspond to the uncertainty in silicate ions concentration). This value delimits the fast dissolution regime controlled by etch pit formation (zone II) and the slow regime of dissolution where only step retreat takes place (zone I). Arrows 1, 2 and 3 show the evolution of the undersaturation during respectively the fast dissolution stage, the induction or “dormant” period and finally the acceleration period. . .	69

3.27	Cryo-FIB cross sections where the arrows indicate the discontinuous hydration layer (cement suspension containing 0.2% of polycarboxylate-ether-based superplasticizers, after 24 min of hydration) From [39].	70
3.28	Hydration scheme at early age of reaction. (a) An alite grain is represented in cross section. Dislocations and grain boundaries are represented by dashed lines. A simple differentiation is made between areas of high surface energy (in black) and surfaces of lower surface energy (in grey). (b) When the alite grain is put in contact with water, we assume that some primary hydrates will precipitate (metastable C-S-H in dark grey) but not as a continuous membrane. Areas of lower surface energy might remain only partially hydroxylated and will therefore present some etch pitting at the point of emergence of dislocations. (c) Finally, when supersaturation with respect to stables hydrates is reached, stable nuclei of C-S-H and CH start to grow, which marks the end of the induction period and the beginning of the acceleration period. Metastable C-S-H might remain present at least during the first 20 hours as detected by Rodger and co-workers by NMR cross-polarisation [36].	71
4.1	Evolution of the kinetics of hydration for an alite paste ($w/c=0.4$) mixed two minutes at various mixing speeds.	74
4.2	Evolution of the kinetics of hydration for an alite paste ($w/c=0.4$) mixed two minutes at various mixing speeds starting with a saturated lime solution.	77
4.3	Schematic representation of the velocity profile of the surrounding solution close to the surface of a cement grain for a) low shearing conditions and b) high shearing conditions. The dark grey area represents alite and the medium and light greys represent schematically the Stern and diffuse electrical layers respectively. It can noticed that the double layer becomes thinner for higher shearing conditions according to Sangwal [40].	78
4.4	Micrographs of polished section of alite samples at the maximum heat flow mixed twice by (a) hand mixing (16h00 of hydration), (b) at 915 rpm (13h30 of hydration) and (c) at 1600 rpm (12h30 of hydration).	80
4.5	Micrographs of polished section of alite samples at 7 days of hydration mixed twice by (a) hand mixing, (b) at 915 rpm and (c) at 1600 rpm.	81
4.6	Effect of C-S-H seed made with a molar Ca/Si ratio of 1 on the early hydration kinetics of C_3S hydration. The seed amounts refer to the mass of solid C-S-H per mass of C_3S . From [41].	83
4.7	Evolution of the kinetics of hydration for an PC paste ($w/c=0.4$) mixed two minutes at various mixing speeds.	84
4.8	Heat of hydration for pastes (dashed lines) and mortars (solid lines) with a size of beads of 0.3 - 0.4 mm for (a) the PC and (b) the alite systems at different mixing speeds.	85

4.9	Time to reach the maximum peak of heat flow during the acceleration period in function of the average diameter of aggregates at three different speed of mixing for (a) alite systems and (b) PC systems. Note that hand mixing being negligible compared to mechanical mixing, it is graphically reported as 0.	86
4.10	Effect of speed mixing on (a) a retarded/superplasticized cement paste and (b) a retarded/superplasticized alite paste using the two steps mixing procedure.	88
4.11	Plot of (a) the time at the end of induction period and (b) the rate of heat evolution in function of the speed of mixing.	89
4.12	Heat flow for pastes and mortars in presence of RS admixture with beads of 0.3 - 0.4 mm for (a) the cement and (b) the alite system at different level of speed.	90
4.13	Time to reach the maximum peak of heat flow during the acceleration period in function of the average diameter of aggregates at three different speed of mixing for (a) alite systems and (b) PC systems in presence of a RS admixture.	91
4.14	Effect of speed mixing on an accelerated cement paste using the two steps mixing procedure.	92
4.15	Comparison between a pure PC system and an accelerated PC system at two different speeds of mixing.	92
4.16	Heat flow for pastes and mortars in presence of RS admixture with beads of 0.3 - 0.4 mm for an accelerated PC system at different level of speed.	93
4.17	Time to reach the maximum peak of heat flow during the acceleration period in function of the average diameter of aggregates at three different speed of mixing for accelerated PC systems.	94
4.18	Temperature evolution before and after mixing for paste of (a) alite and (b) PC.	95
4.19	Effect of different initial temperatures for the same mixing procedure.	96
4.20	C ₃ A particles after hydration in the presence of $1.5 \cdot 10^{-3}$ M of CaSO ₄ . No hydration time as well as no w/c are specified. From [42]	98
4.21	Ratio between values obtained for the time to reach the maximum peak at a given speed over the one obtained by hand mixing (a) for paste systems, (b) for mortars systems, in function of mixing speed.	99
5.1	Isothermal calorimetry curves of 3 PC systems mixed 2 minutes at 500 rpm with a w/c=0.4 at 20°C.	102
5.2	Isothermal calorimetry curves for the 3 accelerated systems at 20°C.	104
5.3	Isothermal calorimetry curves of 3 accelerated systems at 26°C.	105

5.4	Evolution of C_3S and CH amount for the accelerated system A. . . .	106
5.5	Evolution of ettringite and gypsum amount for the accelerated system A.	107
5.6	Evolution of C_3S and CH amount for the accelerated system B. . . .	108
5.7	Evolution of ettringite and gypsum amount for the accelerated system B.	109
5.8	Evolution of C_3S and CH amount for the accelerated system C. . . .	110
5.9	Evolution of ettringite and gypsum amount for the accelerated system C.	111
5.10	Comparison of the evolution of ettringite amount for the three accelerated systems.	112
5.11	Isothermal calorimetry curves of systems A at 20°C with 2%, 4% and 6% of accelerator at (a) 500 rpm and (b) 1600 rpm.	113
5.12	Isothermal calorimetry curves of systems B at 20°C with 2%, 4% and 6% of accelerator at (a) 500 rpm and (b) 1600 rpm.	113
5.13	Isothermal calorimetry curves of systems C at 20°C with 2%, 4% and 6% of accelerator at (a) 500 rpm and (b) 1600 rpm.	114
5.14	Zoom on the maximum heat flow of the three different cements without admixture showing the second hump related to the C_3A reaction. Arrows represent the onset of the main aluminate reaction since a smaller hump is present before each of these.	115
5.15	Kinetics of hydration for three different PC (Siegentaler, Wildegger and Vigier) accelerated by 6% of accelerator A monitored by isothermal calorimetry at 25°C	116
5.16	Isothermal calorimetry curves for various amount of acid formic content present in the alkali-free accelerator A (percentage by weight of accelerator).	117
5.17	Comparison of ettringite peak evolution between accelerated systems A and C.	117
5.18	X-ray diffraction patterns showing the evolution of the ettringite peak over 3 hours of hydration for accelerated system A containing (a) 0%, (b) 3%, (c) 6.5%, (d) 9.5%, (e) 12.5% and (f) 15% of formic acid content. Diffractograms are recorded every 22 minutes.	118
5.19	Heat flow evolution for a mortar sample before projection monitored by semi-adiabatic calorimetry (sharp line) and a shotcrete sample (system A) after projection monitored by isothermal calorimetry (bold line).	120
5.20	Comparison between the heat flow monitored by semi-adiabatic and isothermal calorimetry.	120

5.21	SEM micrographs of polished section of shotcrete samples after (a-b) 6h30, (c-d) 12h and (e-f) 24 hours of hydration.	122
5.22	Effect of gypsum addition on the kinetics of hydration of an accelerated mortar sample.	123

List of Tables

2.1	Causes of the induction period and its termination	19
2.2	Surface energy and adsorption energies for water and hydroxyl on low-energy pure wollastonite surfaces [43].	22
2.3	Variation in dislocation densities and associated rate of dissolution for different minerals	36
3.1	Average and calculated dissolution rate for pure C_3S in different lime solution after 0.1 second of dissolution $W/S=0.5$ and $SSA=4625$ $cm^2.g^{-1}$. (Adapted from [38].)	68
4.1	Limiting process for various substances arranged in order of solubilities in pure water [44]	76
4.2	Characteristics of silica beads.	85
5.1	Range of composition for accelerators A, B and C	103
5.2	A/\bar{S} for the three different systems	115
6.1	Phases composition determined by XRD-Rietveld refinement	140
6.2	Elements analysis determined by XRF	140

Chapter 1

Introduction

In cement chemistry, hydration denotes the totality of the reactions occurring when an anhydrous cementitious compound is mixed with water. The ability of a substance to act as hydraulic cement depends on its reactivity to water and that the reactions lead to solids products of low solubility and higher solid volume. These hydrated products give then rise to the various engineering properties such as mechanical strength or volume stability. In this class of materials, Portland Cement (PC) is the most well known compound and the most used worldwide. Its hydration is a complex process due to different chemical reactions taking place in parallel upon contact with water. Many studies of this process have been made over the years. Although alite (impure C_3S) does not completely represent the hydration of PC due to differences in chemical composition, it has often been studied to simplify the investigation of the hydration kinetics as it is the major compound of clinker and dominates the early age kinetics.

Despite the large number of experiments undertaken, controversies still remain on the factors limiting the very early hydration of alite. For instance many theories have been proposed to explain the abrupt slow down of the reaction after only a few minutes and the following period of low reaction rate usually known as the induction or “dormant” period. In this respect, comprehension of the anhydrous cement–water interface is of fundamental importance as it could help to design specific admixtures with particular effects on the hydration kinetics depending on the desired effect.

The use of admixtures such as inorganic salts, retarding molecules, superplasticizers or even supplementary cementitious materials (SCM) is not new and already allows the kinetics of hydration of Portland cement (PC) to be modified. In certain fields of application, such as tunnels, mines or repair, the requirement in terms of settings and early strength gain have led to the development of complex mixes. The achievement of the requirements mentioned above mainly relies on the shotcrete process. Shotcrete refers to a process by which mortar or concrete is pneumatically projected at high velocity onto a surface [45], [46]. The sprayed concrete undergoes placement and compaction at the same time due to the force with which it is projected from the nozzle. It can be impacted onto any type or shape of surface, including vertical or overhead areas due to an instantaneous setting provided by the addition of accelerator admixtures [47]. The last generation of this family of compounds is alkali-free due to safety and ecological requirements. These compounds are generally

alumino-sulfate based materials and provide an instantaneous setting by the rapid and massive precipitation of ettringite but the addition of such compounds lead to more complex kinetics of hydration.

As the utilisation of admixtures is increasing worldwide in all fields of civil engineering applications, the comprehension of the mechanism by which they interact with hydration reactions needs to be understood.

This thesis aims to study the mechanisms of early hydration as well as the different parameters susceptible to modify the early hydration kinetics of cementitious systems, such as the influence of mixing and the addition of alkali-free accelerators.

This document is structured as follows:

1. **Chapter 2** develops the theoretical background related to the kinetics of early hydration of cementitious compounds. Special attention is given to the causes responsible for the induction period. Then a review on the mechanism of crystal dissolution is also presented as it is generally accepted that hydration of cement is a dissolution-precipitation mechanism. The dissolution processes has not received much attention in the cement field compared to the field of geochemistry. It is therefore why the examples are mainly related to the dissolution of natural minerals.
2. In **Chapter 3**, with the help of specific experiments, we will try to assess the applicability of the dissolution mechanisms encountered in natural minerals to alite. A new mechanism for the early hydration of alite is then proposed.
3. **Chapter 4** shows then the influence of mixing speeds on the kinetics of early hydration of different cementitious systems. The results obtained are discussed bearing in mind the concepts presented in chapters 2 and 3. Other parameters such as the addition of aggregates and organic admixture are also studied.
4. **Chapters 5** is dedicated to the influence of alkali-free accelerators on the hydration kinetics and its impact on the two most reactive phases: alite and C_3A .
5. Finally **Chapter 6** gives the general conclusions of this thesis followed by some perspectives for future works.

Chapter 2

Theory: Hydration and Crystal Dissolution

2.1 Early Hydration of Ordinary Portland Cement

Cement is a synthetic compound produced by firing raw materials such as limestone and clay or shale at high temperature, typically 1450°C [48]. The polycrystalline material resulting is called clinker. This latter is composed of four principal phases: alite (impur C_3S), belite (C_2S), tricalcium aluminate (C_3A) and a calcium aluminoferrite solid solution (C_4AF). It is then ground in presence of gypsum to produce the commonly known Portland cement (PC). Grinding agents may be used in order to facilitate the grinding process and lower the energy associated to this process. Typical surface area of the resulting particle are in the range of $300\text{-}350\text{ m}^2/\text{kg}$ [48].

Many features of the early hydration of PC are very similar to the hydration of alite as this phase is the major constituent (50% to 70% by weight of cement). Some important differences, especially regarding the microstructural development and the phase assemblage, arise from the presence of tricalcium aluminate. This phase is the most reactive one among the clinker phases and reacts with gypsum in solution to form ettringite. However, despite the fact that aluminate reacts very rapidly, the hydration kinetics are dominated by the alite hydration. Specific descriptions of the hydration process of these two phases are presented in the following sections. Hydration reactions of PC can be monitored by isothermal calorimetry as its hydration is an exothermic process. A typical curve is given in Figure 2.1.

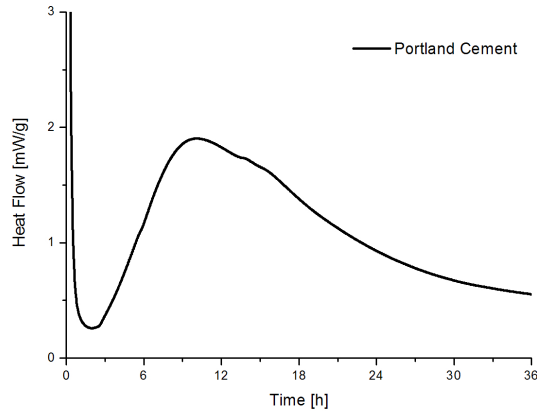


Figure 2.1: Typical calorimetry curve for a Portland cement paste.

During the early period of hydration, fast dissolution of the anhydrous phases takes place resulting in a sharp exothermic peak. Ettringite precipitates almost instantaneously. This burst of heat is followed by a sudden slow down of the reaction and in some cases may be followed by a period of low chemical activity called the induction period.

The main peak corresponds to the massive precipitation of the main hydration products of alite: a calcium silicate gel of variable chemical composition, C-S-H and calcium hydroxide also called Portlandite, CH. This reaction progressively slows down as the volume occupied by the solution is being consumed by the precipitation of the hydrates [6].

A schematic microstructural development of the cement hydration is given in Figure 2.2 [1].

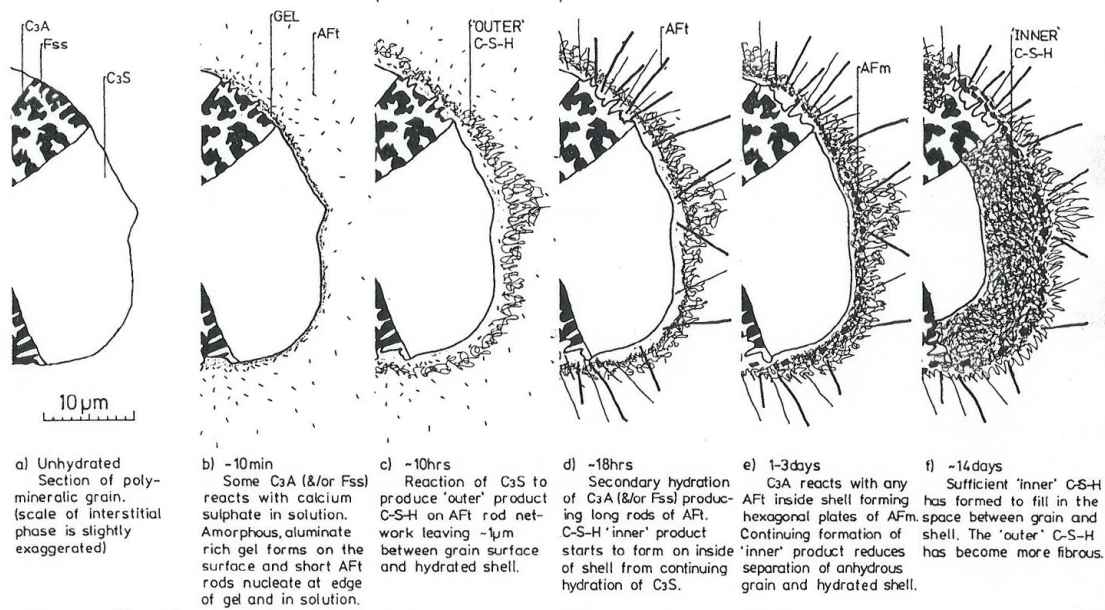


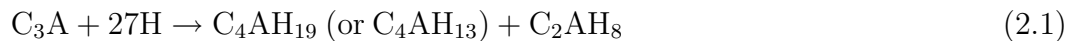
Figure 2.2: Development of microstructure during the hydration of Portland cement. From [1]

2.2 Early hydration of Tricalcium Aluminate

Among the mineral phases in ordinary Portland cement, tricalcium aluminate, C_3A , is the most reactive and can have a significant influence on the early hydration as well as the rheology [5]. In OPC production, gypsum is added during the grinding process as this compound acts as a set regulator for the aluminate hydration.

2.2.1 Hydration of C_3A without sulfate addition

The hydration of C_3A is generally considered to be the fastest among the four main phases, and rapid hydration known as “flash-set” can occur in the absence of gypsum. Within a few seconds of contact with water, irregular flakes of poorly crystalline AFm phases develop on the surface of the clinker grains. These flakes then convert into a permeable network of hexagonal hydrates, C_4AH_{19} and C_2AH_8 . As hydration proceeds further the hexagonal hydrates convert into the cubic hydrogarnet phase, C_3AH_6 [5]:



Depending on the relative humidity (RH), either C_4AH_{19} or C_4AH_{13} that can be observed. Below 88 percent of RH, C_4AH_{19} loses part of its interlayer water to form C_4AH_{13} [5]. Carbonation results in hemicarboaluminate and monocarboaluminate formation at the expense of the calcium aluminium hydrate [49].

2.2.2 Hydration of C_3A in presence of sulfate addition

The hydration of C_3A in presence of gypsum controls the rate of reaction as well as the setting. The first stable hydrate formed in that case is ettringite:



This hydrate forms as long as sulphate ions are available in solution for reaction. Once the sulfate is completely consumed, ettringite is no more stable and becomes then the new sulphate source for the formation of the new stable hydrate, the monosulphoaluminate AFm phase:



The heat evolution of the C_3A hydration in presence of gypsum is schematically represented on Figure 2.3. Three main stages are present:

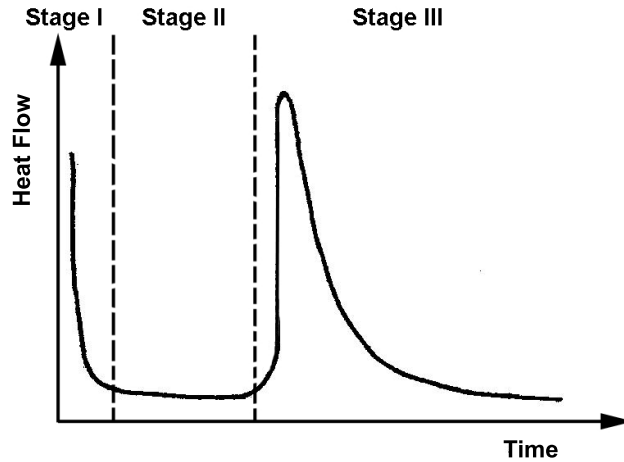


Figure 2.3: Schematic evolution of the C_3A heat flow hydrating in presence of gypsum.

1. Stage I: The initial phases (C_3A and gypsum) dissolve rapidly to form ettringite. After a few minutes, the reaction decelerates rapidly due either to the formation of a protective membrane around the C_3A particles [50] or due to the sulphate adsorption on reactive sites on the surface of the C_3A [2], [42], [51], [52]. However, this sulfate adsorption argument was rejected by Collepardi and co-workers [53] who showed that C_3A was not retarded in presence of Na_2SO_4 .

2. Stage II: The heat flow monitored by calorimetry is low and stationary during this period. Ettringite continues to form but at a lower rate than in Stage I. According to results obtained in dilute suspensions, the sulphate concentration is constant up to the middle of this period and then decreases linearly until complete disappearance. The calcium concentration follows almost the same trend, but it increases or levels up just before the onset of stage III. (see Figure 2.4) [2].

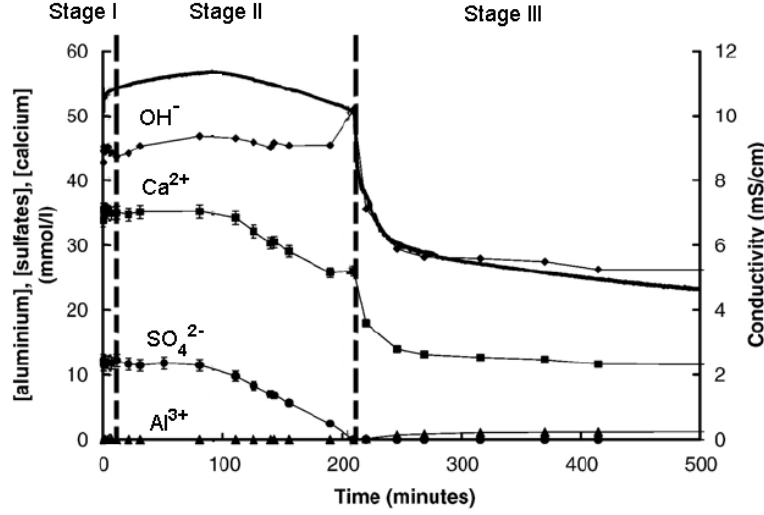


Figure 2.4: Ionic concentrations (aluminium:▲, sulphates: ●, calcium: ■ and calculated hydroxide: ◆) and conductivity evolutions during hydration of 7.4 mmol of C_3A and gypsum (1.5 mmol) in 50 mL of a solution saturated with respect to the Portlandite (L/S=25). Adapted from [2]

3. Stage III: This second sharp exothermic peak, attributed to the dissolution of C_3A , occurs when no more sulfate ions are present in solution [2]. It can also be seen on Figure 2.4 that Al^{3+} concentration starts to be detected in mM range during this third stage and the evolution of the Ca^{+2} concentration between stage II and III exhibits a slight increase before a dramatic drop due to the precipitation of AFm phases (e.g. monosulphoaluminate). At this stage, these AFm phases precipitate and ettringite being the new sulphate source dissolves. Ettringite does not completely disappear as it is generally still observed in mature pastes.

2.2.3 Role of sulfate content

The effect of sulfate content on the C_3A hydration can be seen on Figure 2.5 [2]. As the sulphate content increases, stage II lasts for a longer period as the total consumption of the sulphate into solution would last longer for a larger initial amount of gypsum.

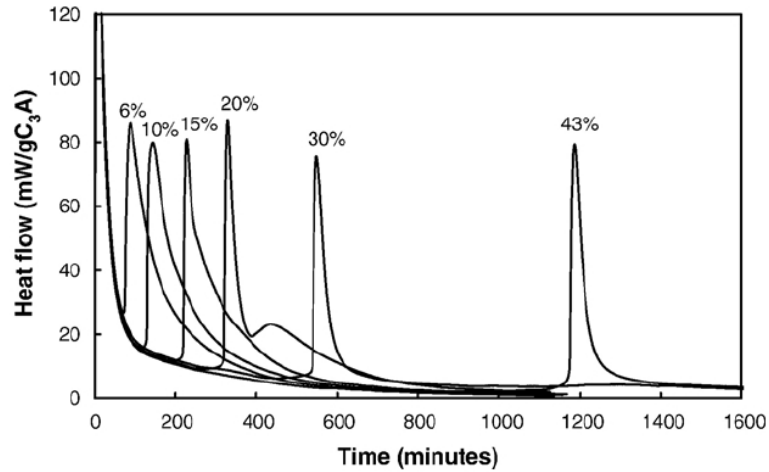


Figure 2.5: Heat evolution rate curves during the hydration of C_3A in solutions saturated with respect to Portlandite ($w/b = 25$) carried out with increasing quantities of gypsum. From [2]

In the case of ordinary Portland cement, gypsum is added to the clinker during the grinding process. Its amount cannot be too high because of durability issues (internal sulfate attack) and it cannot be too low (under-sulfated) otherwise the silicate hydration might be severely delayed as it can be seen on 2.6 [3] and Figure 2.7 (adapted from [4]).

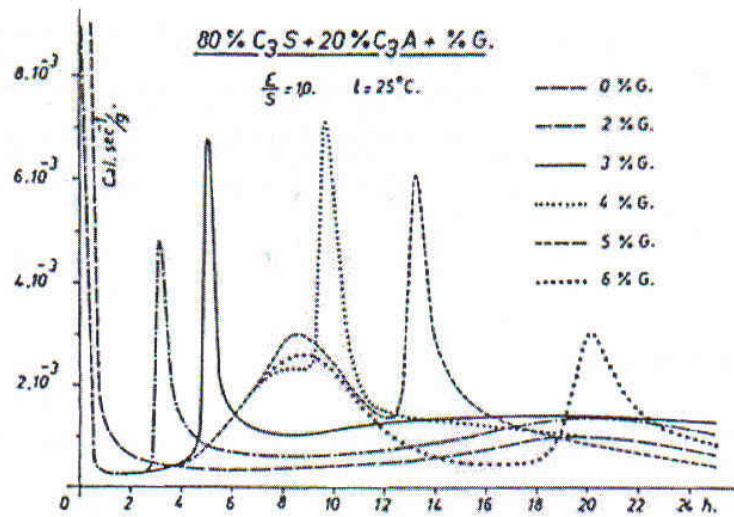


Figure 2.6: Influence of the gypsum content (0%, 2%, 3%, 4%, 5% and 6%) on the heat flow generated by a mass mixture of 80% of C_3S and 20% of C_3A . the water to binder ratio is 1 and the temperature is 25 °C. From [3]

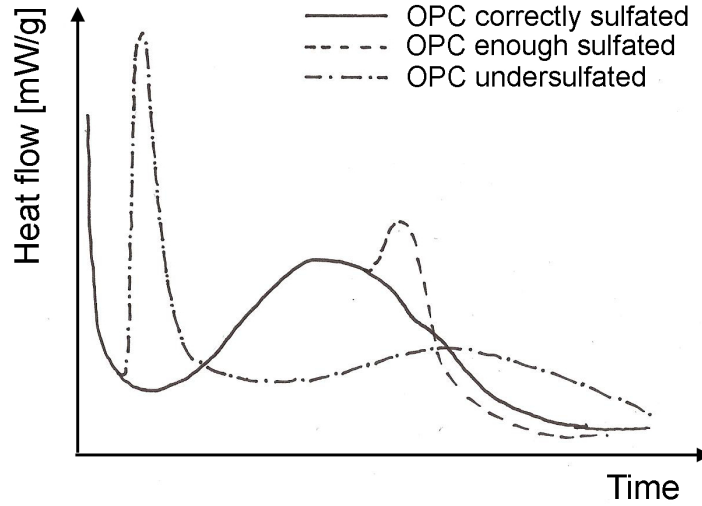
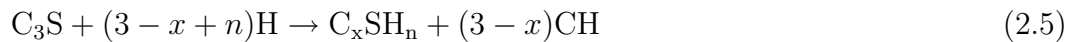


Figure 2.7: Scheme showing the influence of the gypsum content on the heat flow generated by PC having various amount of gypsum addition. Adapted from [4]

As it can be seen on Figure 2.7, if the peak related to the aluminate reaction occurs before the one related to the silicate hydration, this latter is dramatically affected. The reasons for this shutdown are not clear yet. However, if we consider the space filling mechanism introduced by Bishnoi and Scrivener [6], we can suppose that the aluminate hydration in undersulfated conditions produces sufficient hydrates to fullfill almost all the space available. Therefore, when the acceleration period of the silicate hydration takes place, there is not enough space available to precipitate massively CH and C-S-H and this would be the reason for the low heat generated by the silicate reactions. This aspect is also discussed in a later section when the effect of alkali-free accelerator on the cement hydration is presented.

2.3 Early Hydration of Alite

Tricalcium silicate containing minor impurities such as alumina or magnesium oxide (alite) is the principal phase in Portland cement. On reaction with water it forms a calcium silicate hydrate phase of variable composition, C-S-H, and crystalline calcium hydroxide referred as portlandite, CH [5]:



in which n , the water to silicate ratio (H/S), is approximately 4 for saturated pastes. The typical range of values for the CaO to SiO₂ ratio (C/S) for cement pastes varies from 1.2 to 2.1. In the case of pure C₃S pastes however, the C/S ratio of C-S-H is around 1.7-1.8 [48], [54]. Thus the amount of water necessary for the complete reaction of C₃S corresponds to a water to cement ratio (w/c) of 0.42 [48].

The hydration process can be monitored using different techniques, but one of the easiest and most traditional technique to follow the early stages of the reaction remains isothermal calorimetry, which can be a very sensitive technique because the highly exothermic nature of the C_3S hydration [5]. However techniques such as chemical shrinkage, continuous X-ray diffraction with conventional copper anode or synchrotron radiation, SEM, TEM, AFM, ESCA measurements and liquid phase analysis are some of the techniques which have also been used to follow the hydration process of alite. The hydration reaction is usually divided in several time periods or stages corresponding to different regions of the calorimetry curve. They are presented in Figure 2.8 where the heat flow monitored by isothermal calorimetry coupled to the Ca^{2+} concentration evolution in solution are presented (from [5]). According to Gartner and co-workers [5], the typical sequence of the hydration of C_3S in paste is divided in 5 stages:

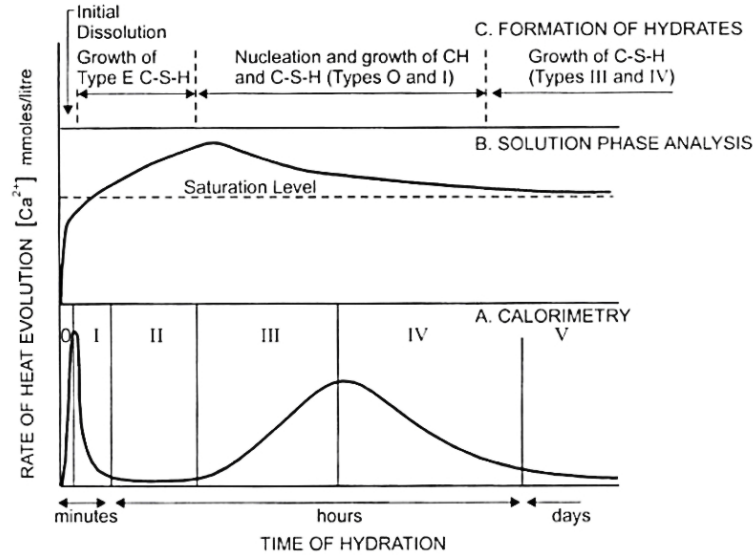


Figure 2.8: Solution phase analysis with the associated heat development monitored by isothermal calorimetry. From [5].

1. Stage 0, Initial fast reaction: On first contact with water, hydrolysis of the anhydrous surface layer release rapidly ions into solution presumably as simple hydrated ionic species: Ca^{2+} , OH^- and $H_2SiO_4^{-2}$ [5]. This initial reaction is highly exothermic and lasts only a few minutes. Barret and co-workers postulated that superficial hydroxylation of the anhydrous surface should occur very rapidly and lead to a slowdown of the reaction [55]. The dissolution is believed to be congruent at this stage as well as for the other stages.
2. Stage I, First deceleration: The surface is though to be altered in such a way as to be less reactive. It is often proposed that a protective coating of metastable hydrate ($C-S-H(m)$) is forming around the anhydrous grains preventing further dissolution. This concept is however different from the one of the superficially hydroxylated layer (C_3S_{sh}) proposed by Barret and co-workers [55]. The different theories proposed to date in order to explain this stage are discussed later.

3. Stage II, Induction period: The rate of reaction is low during this period. Ca^{2+} ions build up in solution, surpassing the theoretical level of saturation for CH, until it reaches a maximum. The reasons for the end of the induction period remain unclear. The total degree of hydration by the beginning of the acceleration period is typically 0.1-2 percent [5].
4. Stage III, Acceleration period: Massive precipitation of hydrates (C-S-H and CH) occurs at this stage and the rate of heat evolution rises again. It is widely believed that nucleation and growth of these hydrates is the rate controlling factor during this stage. However, there is still a lack of knowledge on the growth mechanism of C-S-H. Garraut and Nonat [56] have proposed the aggregation of anisotropic nanoparticles of C-S-H whereas more recently, Bishnoi and Scrivener [6] have proposed that during the acceleration period a loosely packed C-S-H fills a large fraction of the microstructure and the subsequently packing density increases with hydration. Assuming this growth model and using the modelling platform μic , Bishnoi and Scrivener were able to model properly part of the acceleration period but more importantly, the transition between the acceleration period and the second deceleration period.
5. Stage IV, Second deceleration period: The rate of reaction decreases continuously during this period. This trend has generally been attributed to the onset of a “diffusion regime” across a dense layer of C-S-H formed around the anhydrous grain. However, comparison of experimental results from Costoya [26] with simulations of different mechanisms using μic have shown that neither the nucleation and growth mechanism nor the diffusion controlled mechanism can explain this deceleration. The best fits were found assuming the densification process of the initially loosely packed C-S-H (see Figure 2.9)[6].

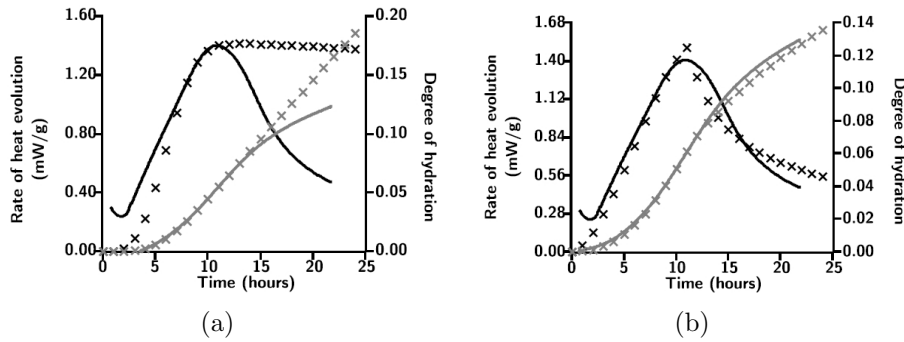


Figure 2.9: Simulation vs experimental data of alite particles having a narrow particle size distribution centred around $38 \mu\text{m}$. (a) Simulation using the nucleation and growth mechanism and (b) using the “densification” process. Black data are the heat flow of alite hydration and grey data, the associated degree of hydration. Plain curves are experimental data. From [6]

6. Stage V, Final slow reaction: At this stage, there is gradual densification of the microstructure and the heat flow becomes really low. The calcium concentration in the pore solution is believed to remain at CH saturation. The

factor controlling reaction are not yet known but it is generally assumed that transport process is the limiting factor.

Several major reviews on mechanisms of hydration have been published [48], [5], [57], [58]. Even though the phase transformations during the first 24 hours are well documented, reactions at very early ages are still a subject of controversy, particularly regarding the so called induction or “dormant” period where the rate of reaction slows down dramatically after a short burst of rapid reaction on contact with water. It is often stated in literature that the hydration of cementitious materials is a dissolution-precipitation process as originally proposed by Le Châtelier [59], but very few publications have given much consideration to the role of alite dissolution [31], [38], [55], [60], .

Without the presence of retarding admixtures, a distinct induction period - i.e. prolonged period of low heat output, may not be clearly identifiable [5], nevertheless the initial slowdown in reaction of tricalcium silicate after the addition of water, and the time before onset of the acceleration period still need to be explained. Many theories, summarised in Table 2.1, have been proposed to explain these phenomena.

In the next section we present in more detail the different theories on the early hydration of cementitious materials and discuss some results from the literature related to this period.

2.3.1 Protective membrane

One of the earliest theories for the first deceleration period is the formation of a protective layer of hydration products on the surface of the reacting grains which would limit the dissolution of the anhydrous phase. Stein and Stevels postulated that “a hydrate is formed fitting closely the C_3S surface”. Hydration reinitiates when this hydrated layer is removed or “converted” and the anhydrous surface again comes in contact with water [61]. For example, Kantro and co-workers [62] as well as Stein and Stevels [61] proposed that the primary hydrate converts into another one fitting the anhydrous surface less closely and more permeable to water. Later, it was proposed that the rupture of the hydration membrane is caused by an osmotic pressure [63], [64], but little further evidence has been found to support this theory.

The study by Gartner and Jennings [7] on solution concentrations provides some of the strongest evidence for the existence of an impermeable hydrate. They identified two distinct trends in the data, which they claimed indicate the existence of two forms of C-S-H, one with higher solubility (SI) being metastable with respect to the other (SII) (Curves B and A respectively on Figure 2.10). They postulated that “the first-formed C-S-H (SI) has protective characteristics responsible for the period of slow reaction and that a solid-state transformation (rather than a transformation involving dissolution and reprecipitation) to a less protective form of C-S-H (SII) occurs when the two phases (C-S-H (SI) and C-S-H (SII)) have the same molar ratio of CaO to SiO_2 , namely 1.7”. However, it has never been possible to observe experimentally such continuous layer. Moreover, such adherent protective layers usually have an epitaxial relationship with the substrate, which is difficult to envisage for such different crystal structure as C_3S and C-S-H.

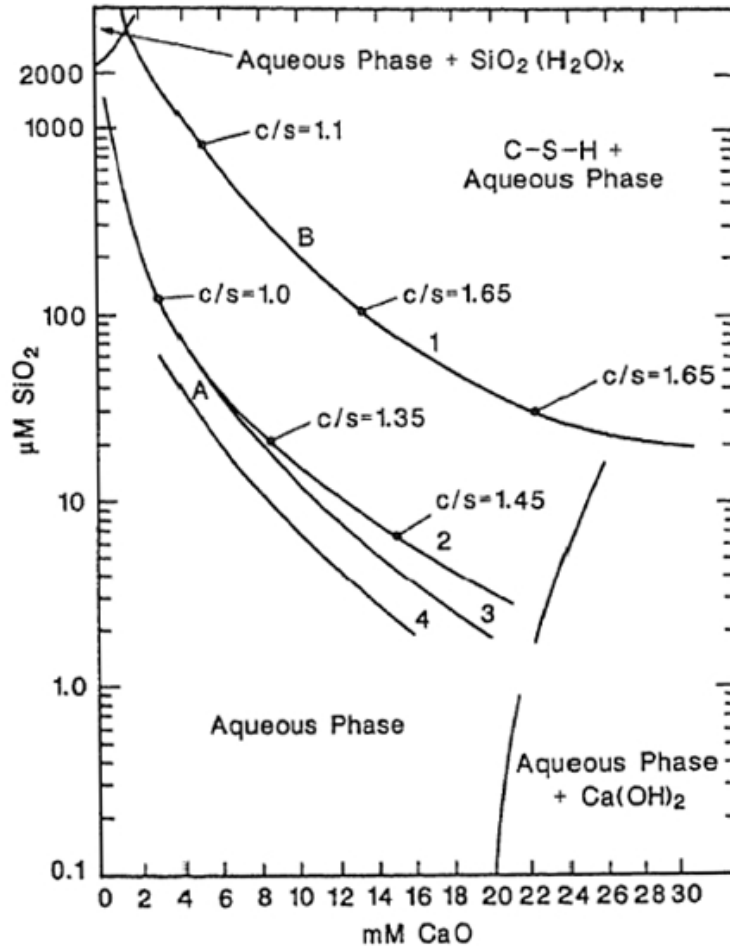


Figure 2.10: Water-rich region of the CaO-SiO₂-H₂O phase diagram showing the solubility curves of two types of C-S-H. Curves A represent three possible solubilities for C-S-H formed by precipitation either from solutions of a calcium salt and sodium silicate or from solutions of Ca(OH)₂ and silicic acid. Curve B represents the solubility of a C-S-H formed from a hydrating C₃S. From [7].

2.3.2 Double layer theory

An alternative theory to that of a protective layer invokes the formation of an electrical double layer with a build up of Ca²⁺ ions close to the surface which inhibit further dissolution [58]. Tadros imagined that the formation of a double layer required incongruent dissolution with Ca²⁺ and OH⁻ moving rapidly into solution to give a charged SiO₂-rich surface layer [65]. Subsequent re-adsorption of the Ca²⁺ on the now negatively charged surface creates an electrical double layer and a positive zeta potential. This view would be in accordance with ESCA studies showing an initial drop of the C/S ratio of the hydrated C₃S surface leading to the formation of a calcium depleted layer.

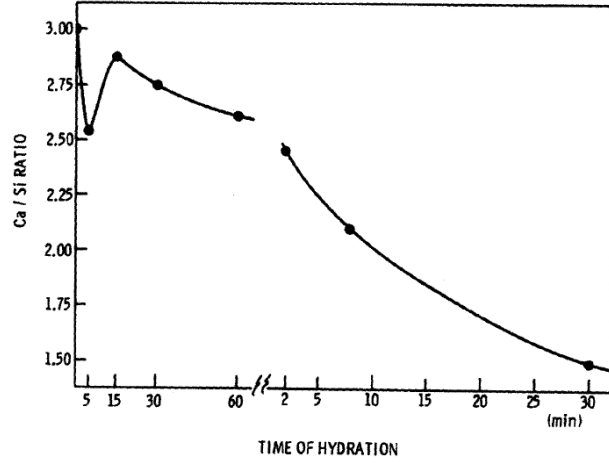


Figure 2.11: Change in C/S ratio of a hydrated C_3S surface as a function of hydration time. From [8]

According to this theory, the acceleration period is triggered by the precipitation of phases which consume Ca^{2+} ions from solution and leads to a gradual breakdown of the double layer [57].

The electrical double layer theory is well recognised in other domains related to surface-solution interfaces to explain the ionic environment in the vicinity of a charged surface. A schematic representation is presented in Figure 2.30. (see [40], [66], [67], [25]). Solid particles surfaces can develop electric charge in three principal ways [22]:

1. The charge may arise from chemical surface reactions of ionisable functional groups: $-OH$, $-COOH$, $-OPO_3H_2$, $-SH$ for example. Therefore, the charge of these particles becomes dependent on the degree of ionisation (proton transfer) and consequently on the pH of the medium.
2. Surface charge at the phase boundary may be caused by lattice imperfections at the solid surface and by isomorphous replacement within the lattice. For example, if in an array of solid SiO_2 tetrahedra an Si atom is replaced by an Al atom, a negatively charged framework is established. Similarly, isomorphous replacement of the Al atom by Mg atoms in networks of aluminium oxide octahedra leads to negatively charged lattice. Clays are representative examples where such atomic substitution causes the charge at the phase boundary.
3. A surface charge may be established by adsorption of a hydrophobic species or a surfactant ion.

Thus, different types of surface charge contribute to the net total particle charge denoted σ_P . According to the Gouy-Chapman theory, the surface charge density σ_P ($C.m^{-2}$) is related to the potential at the surface $\psi(V)$:

$$\sigma_P = \sqrt{8RT\epsilon\epsilon_0 C} \cdot 10^3 \sinh\left(\frac{Z\psi F}{2RT}\right) \quad (2.6)$$

where R is the gas constant, T the absolute temperature, ϵ the dielectric constant of water, ϵ_0 the vacuum permittivity, c the molar electrolyte concentration, Z the ionic charge, ψ the surface potential and F the farad. The double layer thickness is defined by the Debye length κ :

$$\kappa = \left(\frac{2IF^2 \cdot 10^3}{\epsilon\epsilon_0RT} \right) \quad (2.7)$$

where I is the ionic strength.

However, the Gouy-Chapman treatment runs into difficulties for small values of κ as the charge potential becomes high. The local concentration of ions near the surface become far too large due to the assumption of point charges and by neglecting the ionic diameter. It was then suggested that the surface could be divided into two parts: one consisting of a compact layer of ions adsorbed on the surface (the Stern layer) and the second consisting of a diffuse double layer see Figure 2.12.

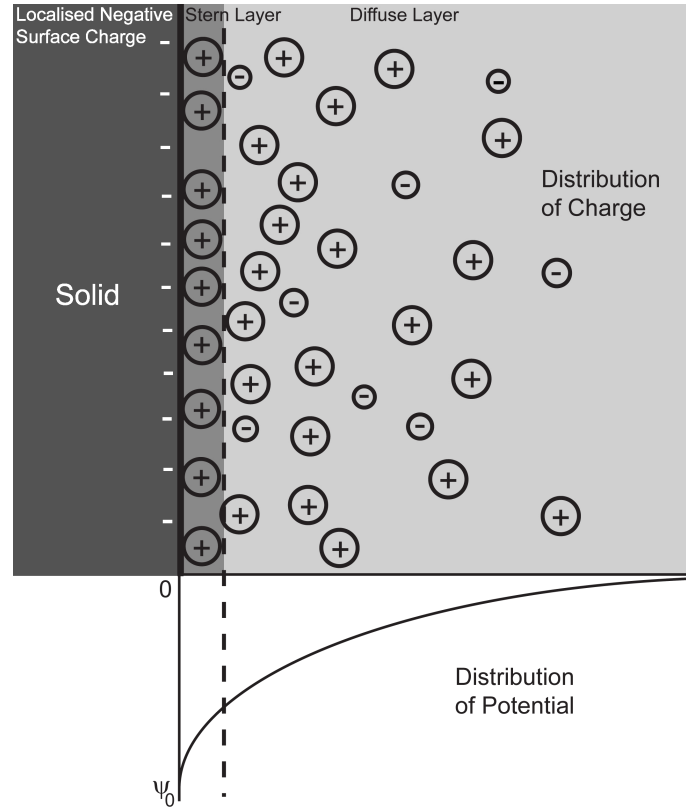


Figure 2.12: Schematic representation of the charge distribution close to a negatively charged surface and the associated potential evolution. Adapted from [davis:1990]

The description of the model presented above is only one of the existing model. For more details about the subject, the readers are invited to consult [22], [68], [69].

2.3.3 Nucleation and growth

Other theories postulate that the length of the induction period is governed by the delayed nucleation and growth of hydrates - either CH or C-S-H [60], [70], [71], [72]. The theories claiming that the nucleation of CH is rate determining suggest that this hydrate is not precipitated, even after the saturation of the solution with respect to this phase, due to a poisoning of the nuclei by silicate ions [65]. When the concentration of CH becomes high enough to overcome the poisoning effect of adsorbed silicate ions, CH starts to precipitate. Young and co-workers [73] confirmed by analysis of the liquid phase composition that the induction period ends when calcium concentration in solution reaches the maximum. The calcium ion concentration reaches generally 1.5 to 2 times the saturation of Portlandite before the onset of the acceleration period [9] (see Figure 2.13). However the decrease in saturation of CH at the end of the induction period could just be a consequence (rather than the cause) of the onset of the acceleration period. Contrary to expectation, attempts at provoking the end of the induction period by seeding with CH have no effect on the duration of the induction period [71]. Furthermore, in dilute solutions the rapid onset of C-S-H formation occurs significantly before CH precipitation [32].

Others have argued that the rate of reaction during both the induction and acceleration periods is controlled by nucleation and growth of C-S-H nuclei [10], [71], [72]. From this point of view, the induction period ends when growth of C-S-H nuclei starts. However, there is a substantial evidence for the precipitation of C-S-H minutes, if not seconds, after the addition of water [8], [39]. Garrault and Nonat claim that the nuclei form at the very beginning of the hydration reaction and argue that there is no true induction period but a continual increase in the rate of C-S-H formation. However, most of their studies relate to hydration monitored by electrical conductivity of dilute suspensions undersaturated or saturated with respect to lime (see Figure 2.14). As discussed later the mechanisms operating in this case may differ significantly from those in pastes at more practical water to cement ratios.

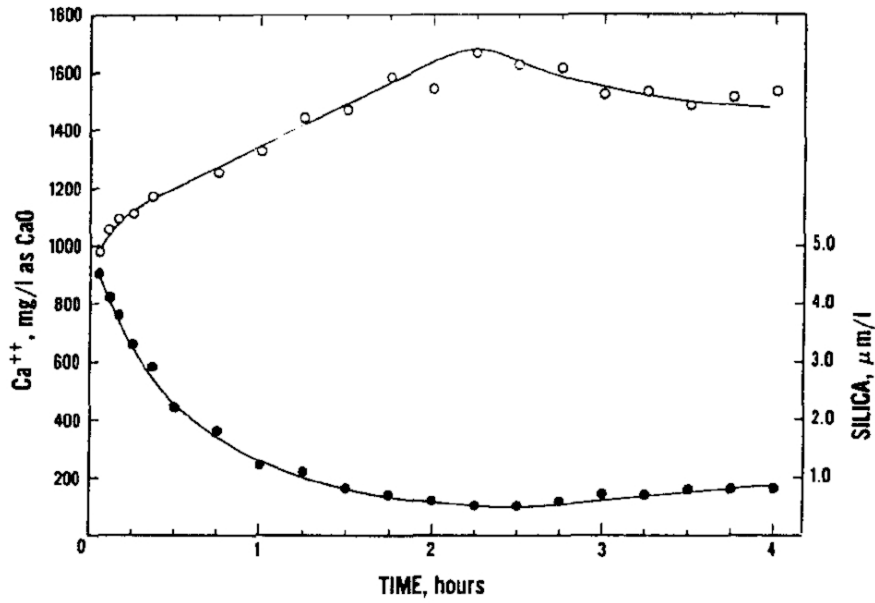


Figure 2.13: Calcium ion and silica concentrations in solution during the first 4 hours of hydration at a w/C_3S ratio of 0.7. From [9]

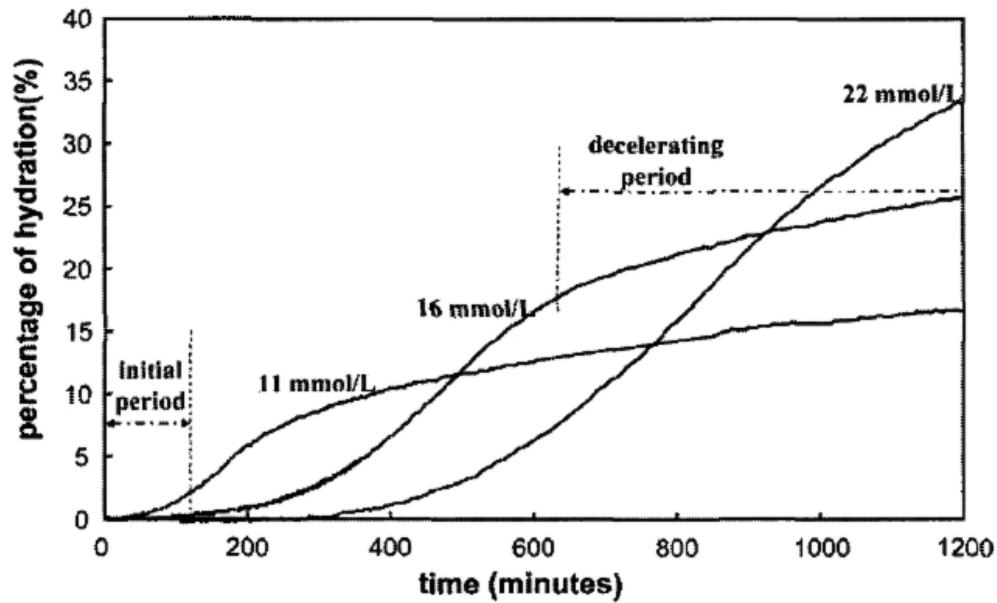


Figure 2.14: Variation with lime concentration of the percentage of hydration against time during the hydration of Ca_3SiO_5 grains, $l/s=50$. The characteristic periods are indicated for the curve obtained at 16 mmol/L. From [10]

The kinetics of hydration varies with the lime concentration in solution (Figure 2.14) [10]: the lower the lime concentration, the shorter the initial period (i.e. higher nuclei density); the lower the lime concentration, the lower the degree of reaction corresponding to the onset of the deceleration period. These variations are attributed

to the influence of the nuclei density of C-S-H and their associated growth mode which both depend on lime concentration. However, theories where nucleation is the rate determining factor do not address the question of the rapid slowdown of the reaction in the first few minutes.

A theory developed during the seventies which did not receive as much attention as the other ones presented above claims that the induction period duration depends on the density of crystallographic defects present at the grain surface and nucleation of hydrates is a delayed process [28], [70], [74], [75]. The different authors mainly performed thermal treatments on alite and observed shorter induction period as the quenching process was faster. Fast cooling is supposed to induce more crystallographic defects and their densities was supposed to be inversely proportional correlated to the length of the induction period.

Table 2.1: Causes of the induction period and its termination

Causes	Description	References
Protective membrane	The product of the initial reaction forms a protective layer on the C_3S particles; the induction period ends when this layer is destroyed or rendered more permeable by ageing or phase transformation.	[7], [9], [61], [62], [76], [77], [78]
Semi-permeable membrane	The product of the initial reaction forms a semi-permeable membrane which encloses an inner solution and is destroyed by osmotic pressure.	[64]
Double layer theory	The ions released in solution during the initial reaction inhibit further dissolution of the C_3S particles by lowering locally the undersaturation. The induction period ends when supersaturation with respect to hydrates is achieved and massive nucleation and growth occur.	[58], [65]
Crystallographic defects	The length of the induction period is related to the density of crystallographic defects. The induction period ends when supersaturation with respect to hydrates is achieved and massive nucleation and growth occur.	[28], [70], [74], [75]
Nucleation of CH	The induction period occurs because CH nuclei are poisoned by silicates and cannot grow. The induction period ends when the level of supersaturation is sufficient to overcome this effect.	[65], [73]
Nucleation of C-S-H	The rate of reaction in the induction period is controlled by nucleation and growth of the C-S-H formed initially; the induction period ends when growth begins.	[60], [70], [71], [72]

2.4 Crystal dissolution

Historically, the science of crystal growth has advanced much more than that of crystal dissolution [17]. The early work on mineral dissolution concentrated on the changes in the chemical composition of solutions in contact with various minerals [79]. The various hypotheses that have been advanced to account for one or another set of experimental observation have been classified by Petrovic [80] into three broad categories:

1. The armouring precipitate hypothesis [81], [82], [83], [84], where diffusion through the interstices of a coherent amorphous or crystalline surface precipitate limits the rate of hydrolysis.
2. The surface reaction hypothesis [44], [85], [86], [87], [88], where the rate is controlled by reactions at the mineral/aqueous solution interface.
3. The leached layer hypothesis [89], [90], [91], where diffusion through a leached shell surrounding the mineral is believed to be the rate controlling factor.

It soon became apparent that understanding the reaction mechanisms could only come about by detailed studies of the surface chemistry [79]. The chemistry of the surface layer of reacted feldspars was studied by ESCA by Petrovic and co-workers [92]. This study emphasised the control of processes at the surface on the rate as opposed to the idea of diffusion either through an extensive leached layer or a surface precipitate layer [Berner et al., 1980]. As extensive SEM work began to be carried out, numerous papers found the formation of crystallographically controlled etch pits to be a prominent and ubiquitous feature of mineral surfaces (e.g. Holdren and Berner, 1979 [93], Berner and Holdren [94], Berner et al., 1980 [95]; Schott et al., 1981 [96], Berner and Schott, 1982 [97], van der Hoek, 1983[98]). The existence of these etch pits was concordant with the idea that the processes at the surface of certain minerals controlled the kinetics of dissolution and that diffusion played a secondary role [44], [99]. In the following sections, the different mechanisms of dissolution as well as their dependence with the saturation state of the solution are presented.

2.4.1 Surface and crystallographic defects

Before introducing the concepts and mechanisms of crystal dissolution, a brief description of surface properties and crystallographic defects encountered in crystals is presented. Numerous types of defects are present in crystals such as point defects, dislocations, twinning, grain boundaries or cracks [99]. These defects can be the result of crystal growth or of subsequent process such as grinding. Defects are important and often responsible for numerous crystal properties [13]. On the other hand, properties of materials at or near surface or interfaces are likely to be different as part of their coordination environment is either missing or different than it would be in the bulk [100]. We will mainly focus here on the description of surface properties and dislocations as well as the effect of grinding procedure.

Surface properties

Definition

A surface is the exterior boundary of a condensed phase in a vacuum or gaseous environment. An interface is the boundary between two condensed phases [100]. Surface or interfacial area increases, relative to volume, as particle or grain size decreases. Surface area can be measured in many ways. The most common method used today utilises the interpretation of adsorption densities of gases (often N₂) and is known as the BET method, named from its originators, Brunauer, Emmet and Teller [101].

Surface energy

The surface energy, γ , is usually defined as the work needed to create new surfaces. If G is the Gibbs free energy, γ is defined as:

$$\gamma \equiv \left(\frac{\delta G}{\delta A} \right)_{p, T, n} \quad (2.8)$$

The subscripts p , T and n specify that pressure, temperature and composition remain constant. This energy has unit of mJ.m^{-2} which is equivalent to erg.cm^{-2} . The surface energy has many implication as it will also be shown in the following sections but for more details, the readers are invited to read [22], [100]. In this section, a special attention will be given to the effect of adsorption on surface free energy. From equation 2.8, the Gibbs equation, also called the Gibbs isotherm can be derived [22]:

$$\Gamma_i = -\frac{1}{RT} \left(\frac{\delta \gamma}{\delta \ln a_i} \right)_{p, T} \quad (2.9)$$

with Γ_i is the surface concentration in mol.m^{-2} or more specifically the surface excess which represents the difference between the total moles of the i^{th} component in a system and the moles of the i^{th} component in a particular phase, R the gas constant, T the temperature, γ the surface energy and a_i the activity of species i . This equation relates the extent of adsorption at an interface to the change in surface energy and qualitatively, predicts that a substance which reduces the surface energy will be adsorbed at the surface [22]. Figure 2.15 illustrates schematically the influence of water interacting with quartz surfaces and its effect on the surface free energy.

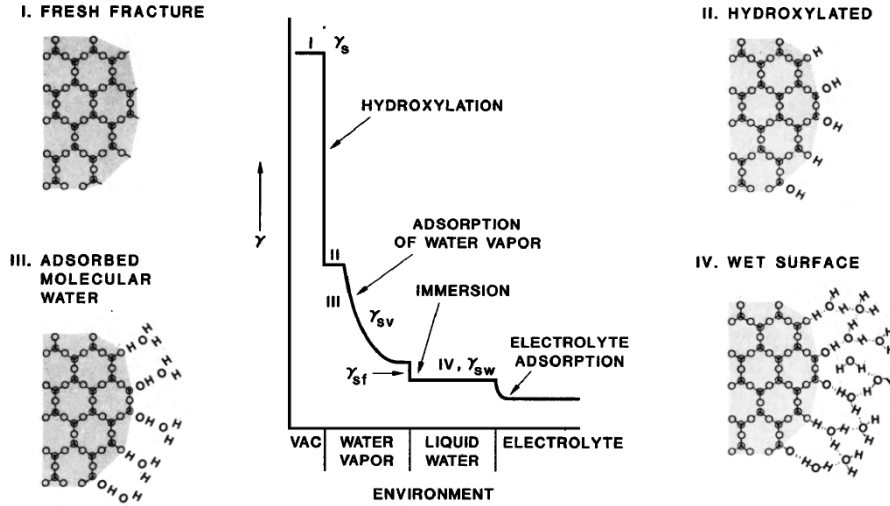


Figure 2.15: Interactions of water with quartz surfaces and associated surface energy changes (schematic). From [11]

More recently, atomistic simulation techniques have been used to calculate surface structure of different minerals such as calcite, wollastonite and many others [43], [102], [103]. All these studies show that the surface free energy of these minerals decreases with a partial hydroxylation of their surface depending on the crystallographic orientation of each plane, as it can be observed on the following table (see Table 2.2, adapted from [43]).

Table 2.2: Surface energy and adsorption energies for water and hydroxyl on low-energy pure wollastonite surfaces [43].

	Surface energy [Jm^{-2}] ^a			Adsorption energy [kJmol^{-1}] ^b	
Surface	SE_P	SE_W	SE_H	AE_W	AE_H
{100}	0.72	0.44	0.69	-87.4	-426.23
{001}	1.42	1.18	0.46	-85.34	-232.41
{100}	1.33	1.22	1.76	-93.23	-418.27

^a SE_P , SE_W and SE_H denote the surface energy for pure wollastonite surfaces and wollastonite surfaces that contain water and hydroxyl respectively. ^b AE_W and AE_H denote the adsorption energy for wollastonite surfaces that contain water and hydroxyl, respectively.

Adsorption phenomena at the surface are important when an anhydrous interface is put in contact with a solution and can greatly affects parameters such as the surface energy and the reactivity.

Surface reactivity

Reactivity is one of the most important chemical properties of any material, and because reactions of a solid with another material must take place starting on the surface of that solid, understanding surface reactivity is of fundamental importance [104]. Chemical and physical properties of a bulk material are different from the chemical and physical properties of its surface as atoms at the surface (the top atomic layer) reside in a different environment than atoms just below the surface (the near-surface), whose environment in turn is different from atoms representative of the bulk. The surface reactivity of a solid is ultimately dependent on three surface characteristics [104]:

1. Chemical composition; surface composition are not representative of the bulk and are laterally inhomogeneous. Modification of the surface composition can occur via attachment (sorption), exchange or detachment (desorption) reactions, or some combination of these. In addition, these reactions rarely happen uniformly across the surface. Certain attaching species will react preferentially at certain sites such as steps, kinks or at perpendicular atomic site on a flat surface (see Figure for a schematic description of these specific sites.) Moreover, the compositional modification of the surface may not be only restricted to the surface but in some cases extend into the mineral up to considerable depth (thousands of Angstroms or more).
2. Atomic structure; as for the chemical composition of a surface, the atomic structure of the top few monolayers is not representative of the bulk structure. In the majority of cases, surface atoms will relax to obtain a lower energy arrangement. Depending if the surface atoms are under- or over-bonded compared to the bulk atoms, the spacing between the upper few atomic layers (generally confined to the top 5 monolayers) will decrease or increase respectively. Furthermore, if enough thermal energy is available, there is a possibility that the surface will atomically reconstruct, resulting in an entirely different atomic arrangement at the surface.
3. Fine-scale morphology, or microtopography. Surfaces are very rarely flat over large areas. Surface micro-cracks and other defects such as vacancies or dislocations are common. Atomic and molecular-scale roughness is a key factor in mineral surface reactivity as surface atoms are less coordinated. These sites on the edges of steps, kinks and other discontinuous feature have more flexibility in potential reaction configurations.

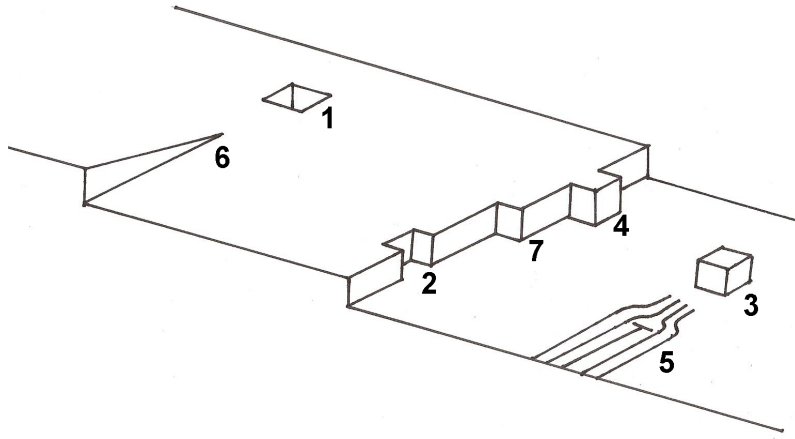


Figure 2.16: Scheme illustrating some of the defects which may occur at a free surface. The examples shown are (1) a vacancy on a terrace, (2) a vacancy at a step, (3) an adatom on a terrace, (4) an adatom at a ledge or step, (5) an edge dislocation-surface intersection, (6) a screw dislocation-surface intersection and (7) a kink site. Note that in the removal of an atom at a kink site, the kink is regenerated. Adapted from [12]

Figure 2.16 illustrates some of the surface features important for either adsorption, growth or dissolution. A loosely adsorbed atom (or molecule), such as species 3 in Figure 2.16, is commonly termed an adatom. The counterpart to adatoms are vacancy defects (species 1 in Figure 2.16). Impurity ions can also play an essential role in surface dynamics and can lead to either catalytic or inhibitory effects on the kinetics (e.g., the effect of phosphate ions on calcite growth [23], see Figure 2.32). The effect of impurities is discussed in a separate section in this chapter. Another important defect is the surface step where atoms attached to it are much more stable than simple adatoms because there are more bonds formed with the surface atoms. The propagation of steps is basic to orderly crystal growth or dissolution [105]. The central focus of step growth occurs at sites, such as number 2 in Figure 2.16, which have half the number of bonds present as in the bulk phase. Such sites are special because they self-generate (i.e., an atom arriving or detaching at such sites creates a new similar site without any change in surface area); they are given the name kinks [105]. Two other defects that can greatly affect growth or dissolution are the outcropping of edge or screw dislocations at the surface (Figure 2.16, features 5 and 6). These outcrops provide high energy sites as well as self-generating steps. These defects are described in more details in the next section.

Dislocations

A dislocation is a line defect in crystal defined by two parameters: the Burgers vector \vec{b} and the line vector $\vec{\xi}$. When the Burgers vector is colinear with the line vector ($\alpha=0$), this is a screw dislocation (Figure 2.17 (a)) and when the two vectors are perpendicular ($\alpha=90$), this is an edge dislocation (Figure 2.17 (b)). Mixed dislocations have the angle α ranging between 0 to 90.

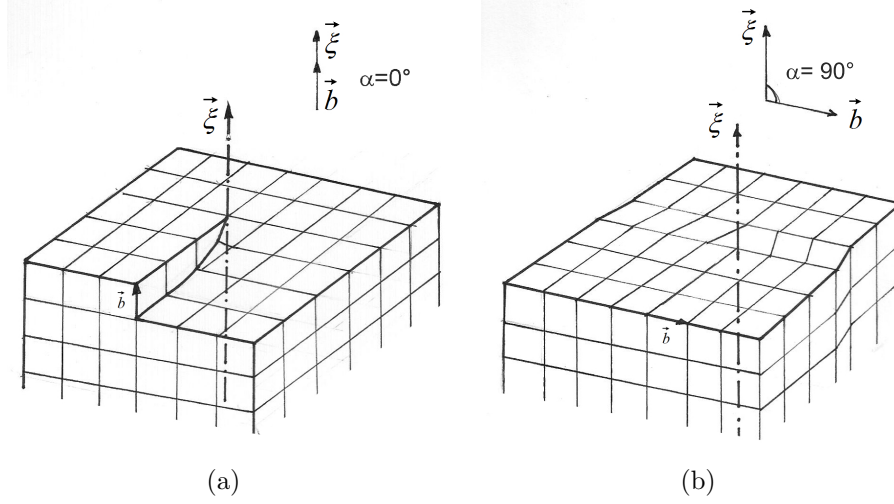


Figure 2.17: Schematic representation of a crystallographic lattice with (a) a screw dislocation, (b) an edge dislocation. The vector \vec{b} is the Burgers vector and $\vec{\xi}$ is the line vector of the dislocation.

Following studies in metal and alloys, dislocations in ceramics have been the object of many investigations during the last quarter of the twentieth century [13]. However, most ceramic materials have low symmetry crystal structures with large unit cells, producing a number of consequences regarding dislocations. The Burgers vector can be as large as 1 to 2 nm [13], with correspondingly several extra half-planes inserted for edge dislocations (Figure 2.18). The local lattice distortion can be associated to the elastic energy approximation:

$$E_{\text{dislocation}} = \frac{\alpha G \vec{b}^2}{4\pi} \ln \frac{R}{r_0} \quad (2.10)$$

per length of dislocation; with G , the shear modulus, \vec{b} the Burgers vector of the dislocation, r_0 the radius of the dislocation core, R the external radius of the stress field of the dislocation and $\alpha=1/(1-\nu)$ for a clean edge dislocation and $\alpha=1$ for a clean screw dislocation (where ν is Poisson's ratio) [106]. The following simple formula is generally applied as R has only little importance and exceed greatly the radius of the core dislocation, r_0 , which is generally equal to $2\|\vec{b}\|$ [106]:

$$E_{\text{dislocation}} \approx \alpha G \vec{b}^2 \quad (2.11)$$

As the dislocation energy has a square and a linear dependence with respectively the length of Burgers vector and the shear modulus, the elastic energy of dislocations in ceramic can be very large compare to metals due to generally higher shear moduli and longer Burgers vectors.

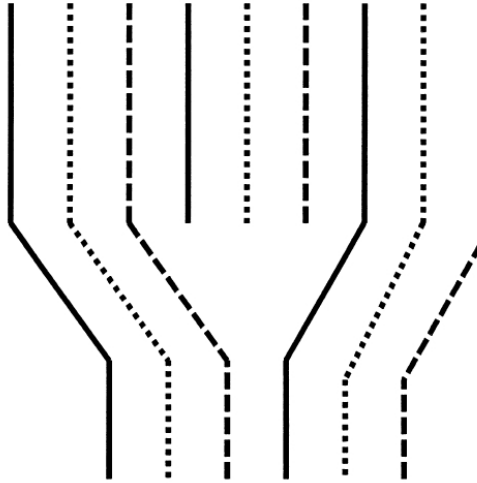


Figure 2.18: Schematic representation of a perfect edge dislocation lying in the prism plane of sapphire, with a Burgers vector of the type $\langle \bar{1}010 \rangle$. The crystal is represented by the stacking of three different layers. From [13]

Effect of grinding

Dislocations in alite may emanate from the growth and cooling process in presence or not of impurities during the clinkerisation and also during the grinding procedure.

Concerning the grinding process, studies performed on quartz and different type of silicates show that generation of defects can be resolved into a multitude of individual events belonging into two competing processes [107]:

1. Fracture under the tensile component of the stress at the crack tip, which in its pure form produces angular fragments without significant subsurface damage.
2. Localised plastic deformation, which occurs within domains subjected to substantial compressive and shear stress by creation and motion of dislocations and accordingly results in significant subsurface damage.

Note that these changes depend both on the severity of grinding and on the fluid surrounding the fragments, if there is one. Artifacts related to the second process induce distortion of the lattice without breakage of the bonds. Severe grinding can increase the amorphous amount of the starting material. Mori and co-workers [14] ball-milled tricalcium silicate up to 30 hours in order to study the influence of grinding on the crystallographic structure of C_3S (Figure 2.19) and its influence on hydration (Figure 2.20).

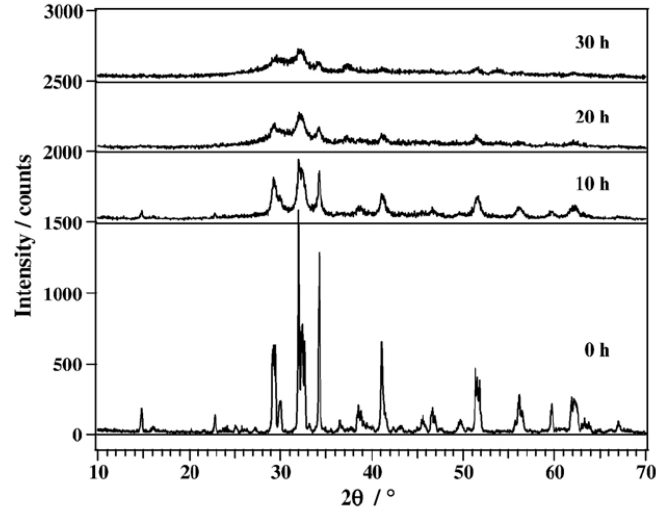


Figure 2.19: X-ray diffraction patterns of C_3S after 0h (unmilled), 10h, 20h and 30h of milling. From [14].

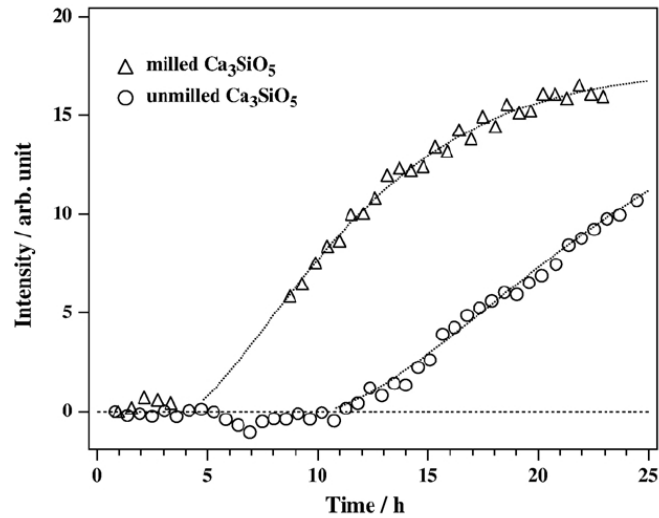


Figure 2.20: Time dependence of intensities for the 101 reflection of $Ca(OD)_2$ for the hydrated unmilled and hydrated milled Ca_3SiO_5 . Experimental data are represented by unfilled symbols. From [14].

It can be seen on Figure 2.19 that extensive milling induces a large content of amorphous materials. Therefore, substantial compressive and shear stresses can arise from this process and should also significantly increase the dislocation density. They then followed the hydration process of a milled and unmilled samples by TOF-NPD (Time-of-flight neutron powder diffraction). Heavy water, D_2O , was used instead of water in order to suppress the incoherent hydrogen scattering but still enable the comparison between the two samples. The milled one show a strong enhancement in reactivity compare to the unmilled one (Figure 2.20) [14].

2.4.2 Role of crystallographic defects and solution saturation on crystal dissolution

Dissolution of crystal has been shown to take place at specific sites characterised by an excess of surface energy due to local lattice distortion [18], [17].

Dove and co-workers showed that mechanisms analogous to those used in classical growth theory can explain the dissolution behaviour of many minerals (quartz, feldspar, olivine, gibbsite, calcite, etc.) and even protein crystals [16],[108], [109]. Dissolution can be simply described as the inverse of nucleation and growth, as suggested by Cabrera and Levine for calcite in 1956 [110]. There are three main mechanisms of dissolution presented in Figure 2.21: formation of 2D vacancy islands, etch pit formation at dislocations and step retreat at pre-existing roughnesses. The first two have defined activation energies, ΔG_{crit}^n and ΔG_{crit} ($\Delta G_{\text{crit}}^n \geq \Delta G_{\text{crit}}$).

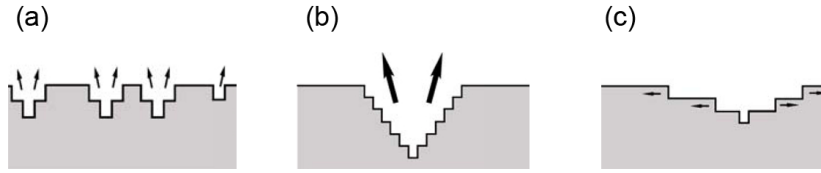


Figure 2.21: Dissolution mechanisms: (a) two-dimensional vacancy islands: nucleation of small pits at perfect surfaces with or without the help of impurities; (b) etch pit: formation at the outcrops of a dislocation with the surface; and (c) step retreat taking place at pre-existing roughness. Mechanisms (a) and (b) are fast dissolution processes occurring at far from equilibrium conditions. (c) is a slow dissolution mechanism occurring at close to equilibrium conditions.

The energy to overcome these activation energy barriers is provided by the undersaturation of the solution (NB. the undersaturation is also referred to as $\ln(S)$ in some publications).

$$\sigma = \frac{\Delta\mu}{kT} = \frac{\Delta G^*}{RT} = \ln \left(\frac{Q}{K_{\text{SP}}} \right) = \ln(S) \quad (2.12)$$

where σ is the undersaturation coefficient, ΔG^* the free energy difference between the solution and the solid phase for dissolution into solution of activity product Q , $\Delta\mu$ the difference in chemical potential, k the Boltzmann constant, R the gas constant, T the temperature, Q the ratio of the activity products to reactant species raised to the power of their stoichiometric coefficient, K_{SP} the mineral solubility product, and S is defined as the saturation index [40], [108], [111].

Depending on the undersaturation, three regimes of dissolution are delimited by two activation energies. For very large undersaturations two-dimensional pits can nucleate on surfaces without the presence of dislocations (Figure 2.21(a) and Figure 2.24, mechanisms (a) and (a')). Teng [15] was able to observe experimentally these

two-dimensional pits using an in situ fluid cell AFM on a cleaved calcite surface at saturation conditions very far from equilibrium ($S = 0.007$, see Figure 2.22). However, as with the homogeneous nucleation of precipitates, the activation energy for this mechanism is high so this regime is not expected to operate much in cementitious systems, apart possibly for very short time and when using ultra-pure water.

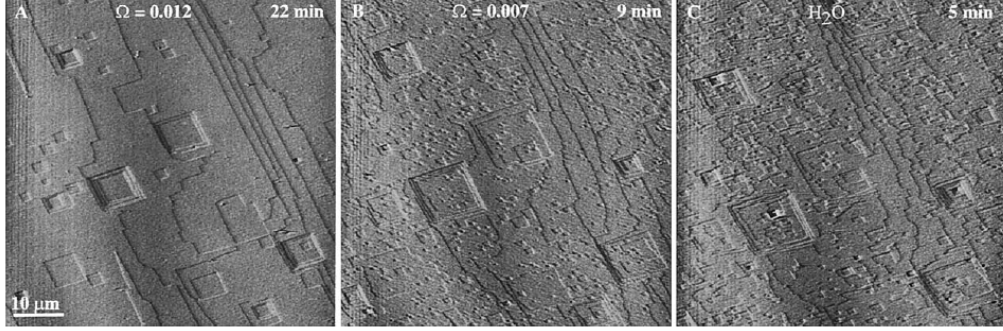


Figure 2.22: In situ AFM images of a dissolving $10\bar{1}4$ surface showing the abrupt leap in pit density when the saturation index decreases from (A) $S = 0.012$ to (B) $S = 0.007$ and the resemblance of the surface morphologies at (B) $S = 0.007$ and in (C) distilled, deionised water. From [15].

Dove and co-workers [16] have established a general expression for the free energy barrier for nucleation of a two-dimensional pit on a plain surface, ΔG_{crit}^n :

$$\Delta G_{\text{crit}}^n = \frac{\pi\gamma^2\Omega h}{N_A\Delta\mu} = \frac{\pi\gamma^2\Omega h}{\Delta G^*} \quad (2.13)$$

where h the step height, γ is the solid-liquid interfacial energy, Ω the molar volume, N_A the Avogadro number, $\Delta\mu$ and ΔG^* are the same parameter defined in equation 2.12.

The surface energy may be modified by the presence of defects or impurities, which increase this value significantly compared to the surface free energy of a perfect crystal [17], [40].

As the undersaturation decreases, the activation barrier ΔG_{crit}^n increases and it is eventually no longer possible to nucleate etch pits on plain surfaces. On the other hand, etch pits can continue to form where dislocations intersect the surface. The second free energy barrier concerns this process ΔG_{crit} and is defined by:

$$\Delta G_{\text{crit}} = \Delta G_{\text{crit}}^n \sqrt{1 - \xi} \quad (2.14)$$

with ξ is defined as:

$$\xi = \frac{N_A G \vec{b}^2 \alpha}{2\pi^2 \gamma^2 \Omega} \Delta\mu \quad (2.15)$$

where γ is the solid-liquid interfacial energy, Ω the molar volume in the crystal, N_A the Avogadro number, G is the shear modulus, \vec{b} the Burgers vector of the dislocation, and $\alpha=1/(1-\nu)$ for a clean edge dislocation and $\alpha=1$ for a clean screw dislocation (where ν is Poisson's ratio):

$\Delta G_{\text{crit}} \rightarrow 0$ when $\Delta\mu \rightarrow \frac{2\pi^2 \gamma^2 \Omega}{N_A G \vec{b}^2 \alpha}$, which therefore defines the critical undersaturation above which etch pit formation is spontaneous at dislocations:

$$\sigma_{\text{crit}} = \frac{\Delta\mu_{\text{crit}}}{kT} = \frac{\Delta G_{\text{crit}}^*}{RT} = \ln\left(\frac{Q_{\text{crit}}}{K_{\text{SP}}}\right) = -\frac{2\pi^2 \gamma^2 \Omega}{RT G \vec{b}^2 \alpha} \quad (2.16)$$

(Complete details can be found in [40])

When the ionic activity is high and the undersaturation becomes lower than σ_{crit} , the formation of etch pits at dislocations is no more spontaneous. The activation barrier increases as the undersaturation decreases and the formation of new etch pits at dislocations rapidly stops. There is then a transition to a slow dissolution process controlled by step retreat at pre-existing steps (Figure 2.21(c) and Figure 2.24, mechanism (c)). The density of steps, and therefore the rate of dissolution in this regime, will depend on the number of etch pits created previously. It should be noted that step retreat takes place regardless of the undersaturation, but since its rate is slow, its contribution to the overall dissolution rate is small at larger undersaturations.

Figure 2.23 shows how these two energy barriers vary as a function of the undersaturation and indicates the delimitation of the three dissolution regimes. The degree of undersaturation therefore defines which dissolution mechanism prevails. In part I, II and III, it is respectively the step retreat, the etch pit formation at dislocations and the formation of 2D vacancy islands that are the rate controlling mechanisms of the overall dissolution.

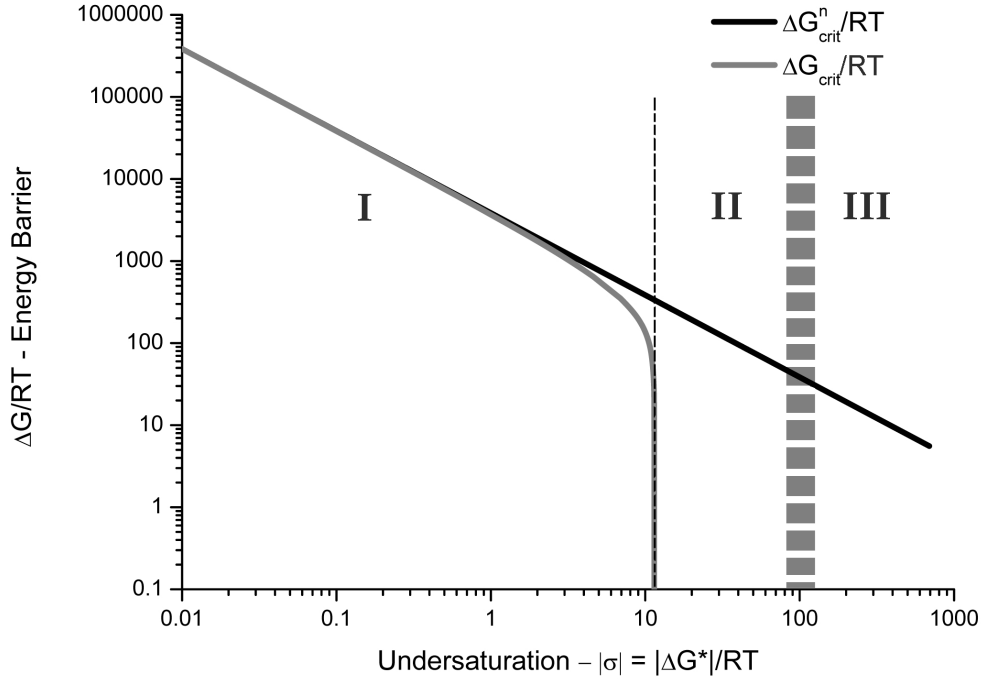


Figure 2.23: Dependence of the two activation energy barriers ΔG_{crit}^n (2D vacancy islands) and ΔG_{crit} (etch pit) in function of the undersaturation for an albite crystal having $\gamma = 0.05 \text{ mJ.m}^{-2}$, $\Omega = 100 \text{ cm}^3.\text{mol}^{-1}$, $\|\vec{b}\| = 7 \text{ \AA}$ and $G = 30 \text{ GPa}$. Values from [Burch et al., 2003]. In part I, II and III, it is respectively the step retreat, the etch pit formation at dislocations and the formation of 2D vacancy islands that become the rate determining mechanisms.

Owing to variations in the size of the Burgers vector \vec{b} and in the solid-liquid interfacial energy, different crystal faces will behave differently during etch pit formation and the number of etch pits will vary according to the types and number of dislocations present [79].

The principal features discussed above are illustrated in Figure 2.24 for surfaces of quartz (100) under different undersaturation conditions [16].

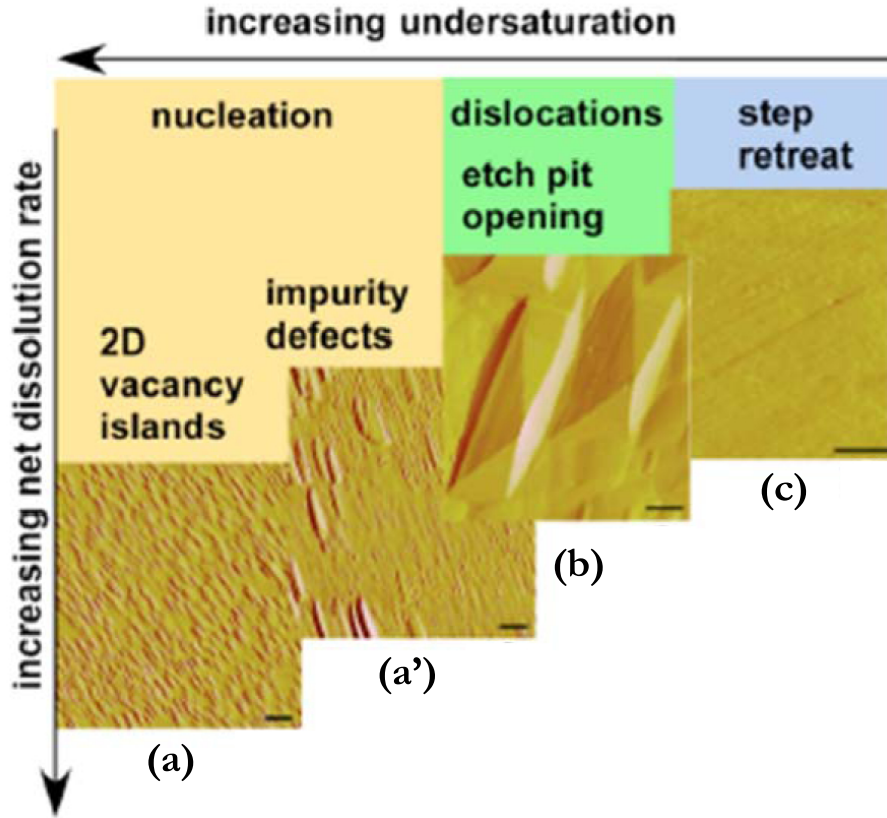


Figure 2.24: AFM images of quartz (100) surfaces produced from different solution chemistries illustrate dissolution process that occur across driving force and solution chemistry after equivalent extents of reaction. (a) When $S = 0.10$ and the solution contains 0.0167 M CaCl_2 , the surface is covered with a high density of small pits with flat bottoms and with steep flanks. (a') At an intermediate driving force of $S = 0.65$ in a salt solution of 0.0167 M CaCl_2 , a mixture of larger and smaller flat bottom pits form across the surface. (b) When $S = 0.10$ in H_2O , surface are dominated by large etch pits with sloping sides that converge at dislocation sources. Pits are separated by relatively flat regions on the surface. (c) At a low driving force of $S = 0.90$ in 0.0167 M CaCl_2 , surfaces shows only straight edges steps with no evidence of pitting. The associated equations between the different processes are equation 2.13 for the transition 2D vacancy islands-impurity defects and dislocations-etch pit opening and equation 2.14 for the dislocations-etch pit opening and the step retreat process. Adapted from [16].

Experimental results for the dissolution rate of various minerals as a function of undersaturation (from [17]) are shown in Figure 2.25. It can be observed that there are two regimes of dissolution, corresponding to the regime in which the undersaturation of the solution is low enough ($\sigma RT \ll \Delta G_{\text{crit}}^*$) to cancel the activation energy for formation of etch pits at dislocations, followed by a sharp decrease at undersaturations still quite far from equilibrium where only step retreat can occur. (The regime of homogeneous formation of etch pits is not observed in these plots). Most of these minerals show large values of ΔG_{crit}^* - from 2 to several kJ.mol^{-1} . Therefore, slow dissolution rates are observed not only close to equilibrium, but quite far from it. Phenomenologically this drastic slow down in dissolution rate is similar to what is seen for alite. This observation led us to carry out some new experiments and

re-examine published data on the early stages of alite and C_3S reaction (see next Chapter).

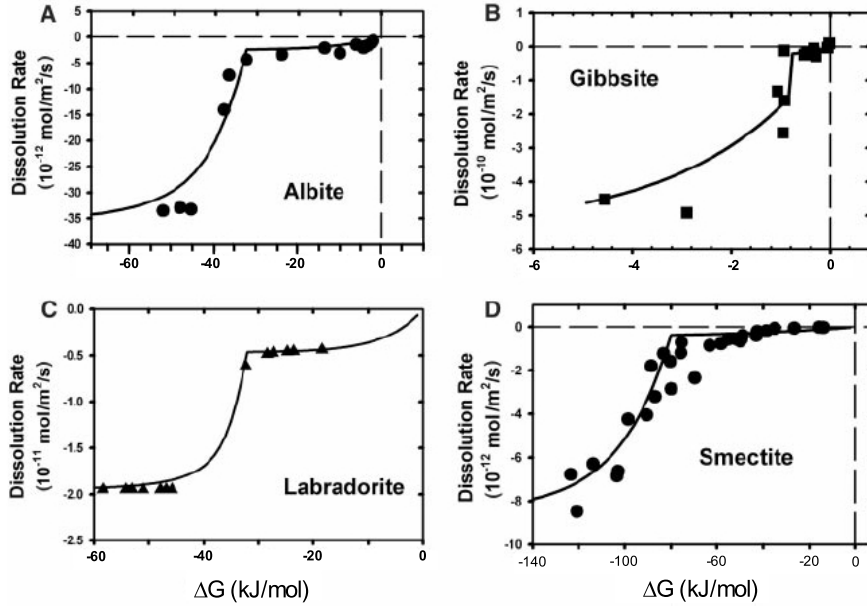


Figure 2.25: Comparison of the full dissolution theory (see Equation (5)) with experimental data. (A) Albite at pH 8.8 and 80°C. (B) Gibbsite at pH 3 and 80°C. (C) Labradorite at pH 3 and 25°C. (D) Smectite at pH 3 and 80°C. (From [17]).

2.4.3 Relation between dislocation density and rate of dissolution

Many studies have tried to correlate the dissolution rate with the density of crystallographic defects. Two possible routes have been tried: either an increase of the defect density under plastic deformation or a decrease of the defect density by thermal treatment. However, due to the number of different defects that can be encountered in crystals, parallel processes of dissolution can take place as shown schematically on Figure 2.26. It is therefore difficult to correlate the measured dissolution rate with a specific density of defects such as dislocations.

What determines measured dissolution rate with parallel processes?

Fastest process is normally rate-determining, unless its contribution to total dissolved concentration is insignificant.

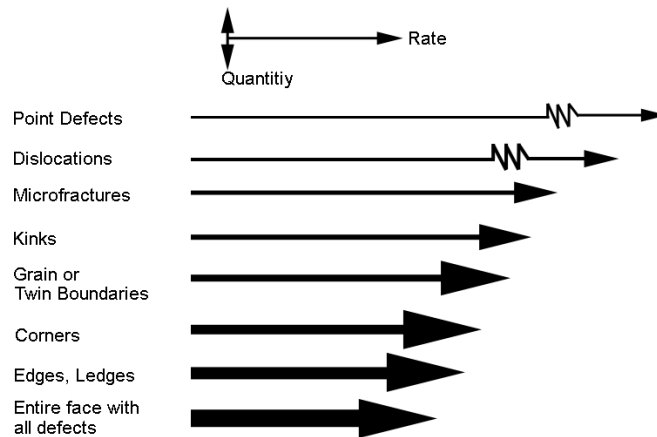


Figure 2.26: Highly schematic illustration of the parallel processes involved in crystal dissolution. The horizontal length of each arrow indicates the relative rate of each process (actual rates can differ by many orders of magnitude). The vertical thickness of each arrow represents the relative quantity of material dissolved and delivered to aqueous solution by that process. Thus, while point and linear defects react most rapidly, they deliver less dissolved material to solution than slower dissolution of faces and pits occurring at edges, ledges and corners. From [18].

Effect of shock loading on the rate of dissolution

Studies on dissolution kinetics of experimentally shocked silicate minerals suggest that the surface dislocations produced by shock treatment are not the primary sites for dissolution reactions. This technique enables to increase the defect density by several orders of magnitude. This would be much more difficult using a mechanical process such as grinding even if this latter is also known to induce crystallographic defects. The difference in observed dissolution rates between shocked and unshocked minerals appears to have a weak correlation with the increase in the density of dislocations on the mineral surface [19]. They found that increasing the density of dislocations by several orders of magnitude with shock-loading causes a relatively small increase in dissolution rate for labradorite, oligoclase and hornblende. However the rate of dissolution increases by a factor 2. Similar results were obtained by Casey et al. [20] on shocked rutile.

It is however important to note that the distribution of dislocations was really heterogeneous. This could have as a result a decrease of their associated stress field as the elastic stress fields of a dislocation tend to cancel out when dislocations are close to each other [15]. Hence, etch pits should form faster at isolated dislocations than at clustered ones if elastic strain energy is responsible for pit formation.

Dislocation density as well as the associated rate of dissolution between untreated and treated minerals are presented on Table 2.3.

As pointed out by Eggleston et al. [21], the rate of dissolution observed during

the first few hours of their experiments is much higher for their shocked powders than for their unshocked one (see Figure 2.27).

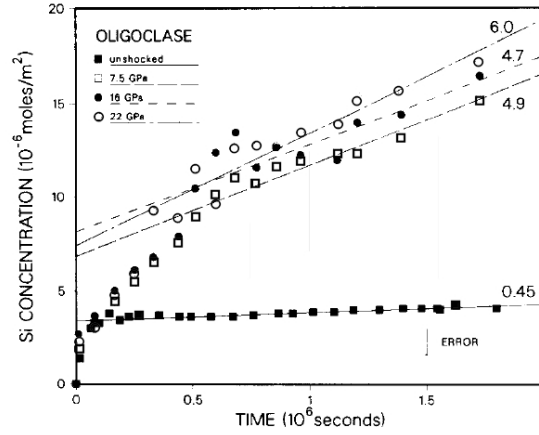


Figure 2.27: Si concentration history for the dissolution of oligoclase in four conditions: unshocked and recovered from three shock-loading experiments. Values of Si dissolution rates corresponding to steady-state slope of curves are provided in units of $10^{-12} \text{ mol.m}^{-2}.\text{s}^{-1}$. Data were obtained from experimental runs performed at 25°C and pH 4.0. From [19].

Two different propositions can be found in the literature in order to understand this behaviour. It has been proposed that the initial dissolution rate is more sensitive to the concentration of defects outcrops than the long-term rate are. But more importantly, as suggested by Teng and co-workers [112], a common approach in laboratory studies of mineral dissolution is to ignore the dependence of dissolution on saturation state by directly carrying out experiments in distilled water or solutions only with controlled acidity or ionic strength. This implies that dissolution is often occurring at far-from equilibrium conditions. It is therefore possible in some cases that the saturation states in studies conducted under these conditions are above the corresponding ΔG_{crit}^n values of the minerals concerned. Therefore, unassisted pit nucleation is probably playing a dominant role in controlling the dissolution kinetics and any increase in dissolution rates resulting from a dislocation density increase will be overwhelmed by the spontaneous pit formation on the dissolving surfaces. Almost all the studies previously mentioned, that reported a weak, if existent, dependence of dissolution rate on dislocation density, were conducted in solutions with uncontrolled saturation states. It is therefore likely that experimental conditions in these studies were such that $|\Delta G^*| > \Delta G_{\text{crit}}^n$ and two-dimensional pit nucleation controlled the dissolution kinetics. Blum et al. [79] and MacInnis and Brantley [113] both suggested that pit formation in defect free regions in highly undersaturated solutions provides an extra step source that overwhelms the contributions of dislocations to dissolution rate. Therefore, a valuable correlation between dislocation density and rate of dissolution remains to be found.

Table 2.3: Variation in dislocation densities and associated rate of dissolution for different minerals

Mineral	Dislocation density (cm^{-2})	Specific dissolution rate for Si^a , Ti^b and Ca^c ($10^{-12} \text{ mol.m}^{-2}.\text{s}^{-1}$)	Reference
Labradorite unshocked	$\leq 10^6$	6.7 ± 0.4^a	[19]
Labradorite shocked	$10^8 - 10^9$	17 ± 1.8^a	[19]
Oligoclase unshocked	–	0.45 ± 0.04^a	[19]
Oligoclase shocked	–	6 ± 1.2^a	[19]
Horblende unshocked	–	1.2 ± 0.5^a	[19]
Horblende shocked	–	4.5 ± 0.7^a	[19]
Rutile unshocked	10^6	$1.9 \cdot 10^{-3} \pm 0.14^b$	[20]
Rutlie shocked	10^{11}	$4.3 \cdot 10^{-3} \pm 0.14^b$	[20]
Calcite unstrained	10^6	$2.8 \cdot 10^{2c}$	[18]
Calcite strained	10^{11}	$4.15 \cdot 10^{2c}$	[18]

Effect of annealing and ageing on the rate of dissolution

In their study looking at the influence of defect density on the rate of dissolution of rutile, Casey and co-workers also performed a series of annealing treatment at different temperatures on their shocked powders. The rate of dissolution decreases linearly as the annealing temperature increases (see Figure 2.28). Here again, no direct correlation are found between the reduction in defect density and the decrease in the rate of dissolution. Though the density of defects does have an impact on the dissolution rate, it seems really difficult to find a direct correlation between the measured rate and the density of dislocation for different reasons:

1. Parallel processes are taking place as shown schematically on Figure 2.26. Therefore it becomes difficult to exactly know the contribution of each process to the average rate of dissolution.
2. The saturation state of the solution is not always taken into account as pointed out by Teng [15] and mechanisms of homogeneous nucleation of 2D vacancy

islands on plain surface might have been overlooked.

3. Dislocations across a crystal are not uniformly distributed as pointed out by Casey and co-workers [20] and generally tend to minimise their energy configuration [106]. Therefore, even if the density of dislocations increases, due to their spatial distribution across the crystal, the associated energy (see Equation 2.10) will not be proportional to the total number of dislocations.

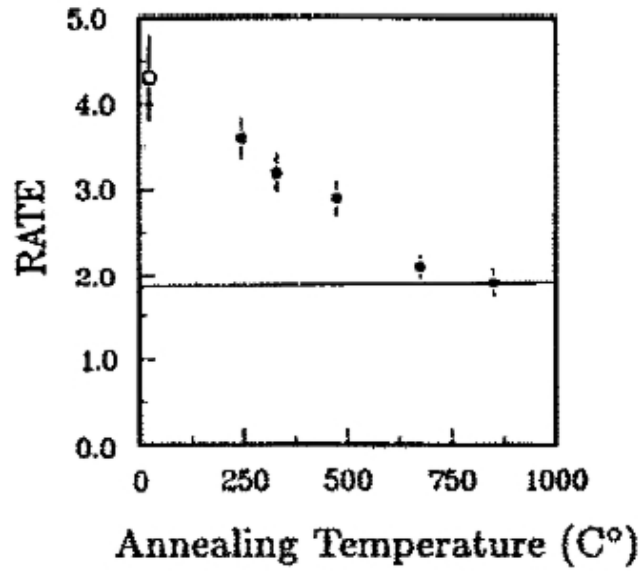


Figure 2.28: Dissolution rate data versus annealing temperature. Units of rate are titanium moles $\text{cm}^{-2}.\text{s}^{-1}.10^{-15}$. The error bars identify the 99 percent confidence interval of the regression slope. The horizontal line corresponds to the dissolution rate of the unshocked starting material. The open circle is the shocked and unannealed sample. From [20]

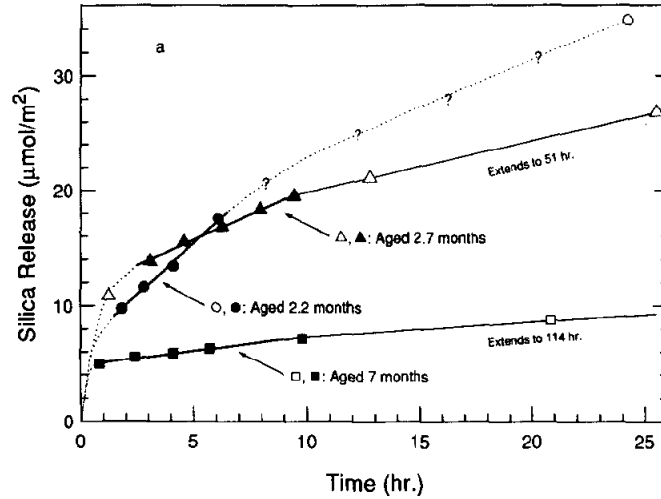


Figure 2.29: Experimental results for the release of silica during dissolution of diopside powders as a function of age. Data for the unwashed powder aged 2.2, 2.7, and 7.0 months. Filled and open symbols are used to calculate rates of dissolution for various stages. From [21]

Eggelston and co-workers [21] observed a reduction in their measured rate of dissolution of diopside as their powders were more aged (see Figure 2.29). Structural distortion may be affected by ageing if thermal energy available at room temperature is sufficient to cause the slow relaxation of such strain. Using these data for the reduction in the number of defects caused by one hour of annealing at various temperatures, which roughly parallels the reduction in lattice strains and dislocation density, Eggelston and co-workers did a simple Arrhenius calculation which suggests that a similar reduction in defect density could be caused by several months of ageing at room temperature, assuming that the same mechanisms pertain. These results suggest that diopside surfaces created by grinding gradually relax toward a less-reactive state under room temperature conditions.

Loss of reactivity has already been observed for OPC stocked in sealed conditions (prehydration is unlikely to happen) for several months [114]. It is possible that cementitious phases undergo the same surface relaxation process.

2.4.4 Effect of impurities on dissolution

Impurities may interfere in different manners with the dissolving materials. The understanding of the dynamics of the dissolution processes and their retardation (inhibition) requires a precise description of the reaction leading to the transfer of the chemical species between the mineral and the aqueous solution and an understanding of the structure and chemical bonding at the water mineral interface [22].

One model to study these specific interactions is the surface coordination model. Its basic concepts are the surface functional groups formed on all inorganic solids; the surface functional group of greatest abundance on hydrous minerals being the hydroxyl group. The mineral surface may be looked at as a metal complex with aquo, oxygen, hydroxo or other ligands as shown on Figure 2.30 [22].

These impurities, being complexed on the dissolving surface, can modify the rate of dissolution of different minerals. For instance, Al^{3+} may inhibit the dissolution rate of feldspar [12], [115] and strongly inhibit silica dissolution [116], [117]; and phosphate has a strong inhibitory effect on the growth and dissolution of calcite [23], [118], [119].

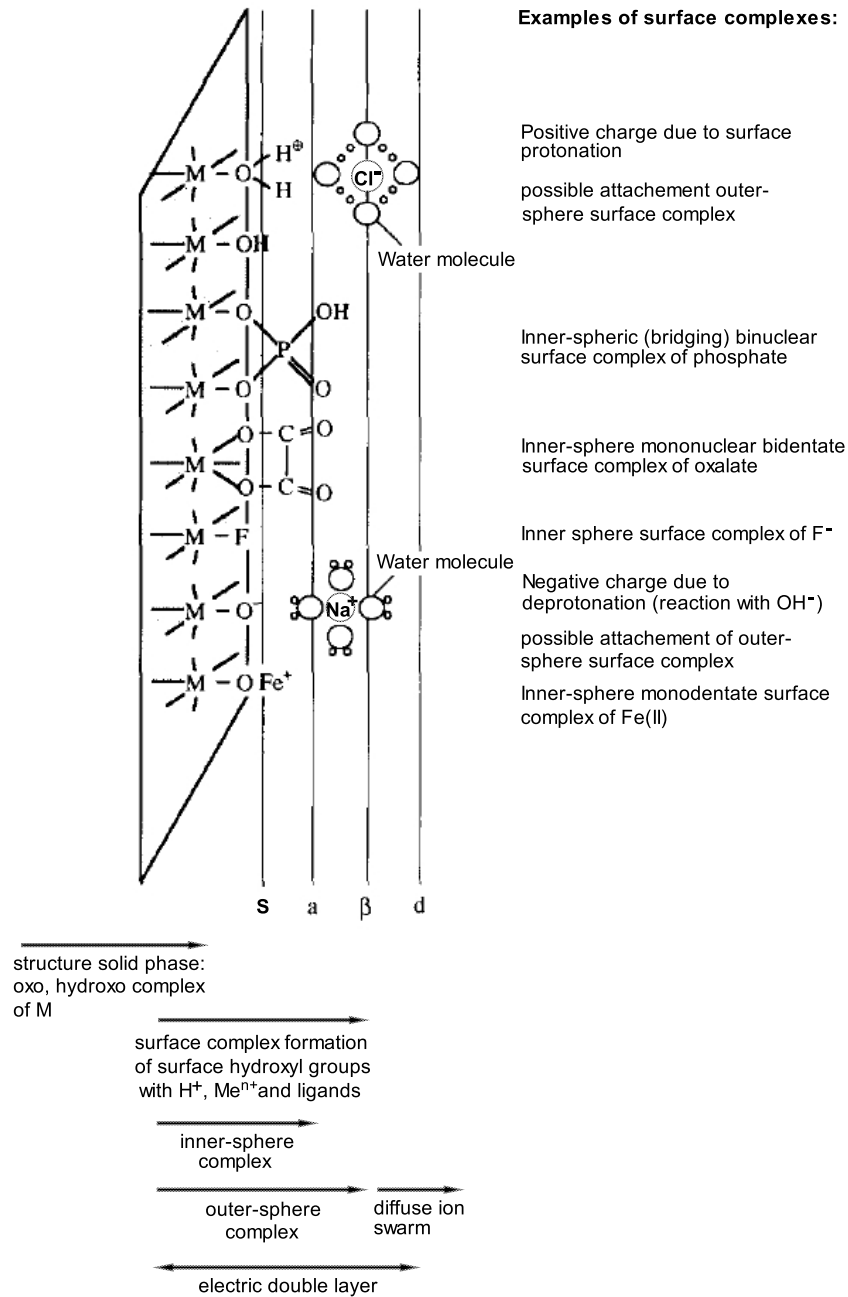


Figure 2.30: Schematic representation of the hydrous oxide surface, showing planes associated with surface hydroxyl groups (S), inner-sphere complexes (a), outer-sphere complexes (β) and the diffuse ion swarm (d). In case of an inner-sphere complex with a ligand (e.g., F^- , HPO_4^{2-}) the surface hydroxyl groups are replaced by the ligand (ligand exchange). From [22]

In the case of dissolution inhibitory impurities, Lasaga proposed that impurity

molecules are not mobile once they are adsorbed on the surface of a mineral [12]]. Therefore, if a retreating (or growing) step encounters such an immobile impurity, the step attempts to continue around the impurity. This would lead to a curvature in the step which is energetically unfavorable (see Figure 2.31 and Figure 2.32). This can also create a bunch of steps and subsequently decrease the kink density. The combination of these two effects can lead to a strong inhibition of the dissolution rate.

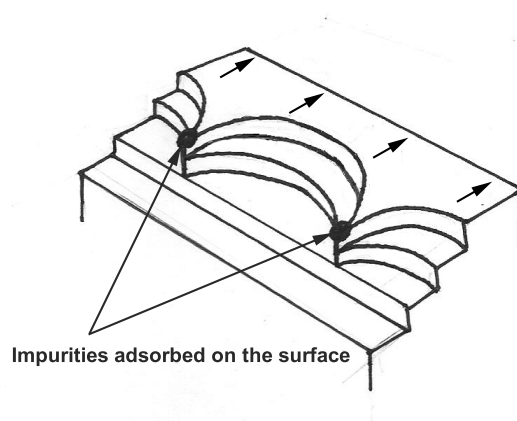


Figure 2.31: Schematic representation on the influence of adsorbed impurities on the shape of retreating step.

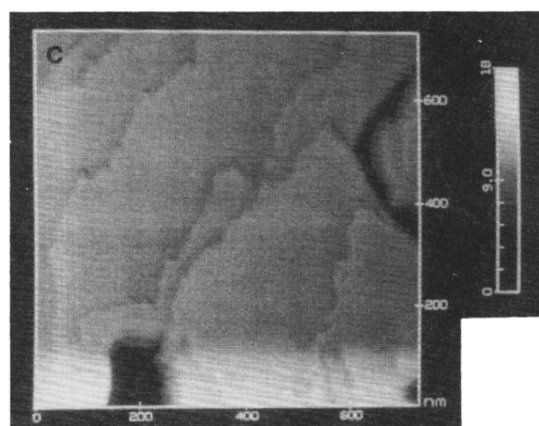


Figure 2.32: AFM image of phosphate poisoning on calcite growth in solution. In the presence of phosphate, step advance is dramatically reduced, steps become jagged and eventually growth stops all together. From [23]

This adsorption will have therefore a direct effect on the kinetics of dissolution (or growth). In addition to that, adsorption of impurities can also vary the solid-liquid interfacial energy, γ , and the crystal solubility, K_{SP} [40], [109].

However, some impurities have a complete different effect as they can catalyse the dissolution rate of certain minerals. Alkalies such as Na^+ and K^+ can catalyse the

dissolution rate of quartz in hydrothermal solutions [24], [120] and CaCl_2 increases rates and probabilities of pit formation of quartz [16], [108]. Dove and co-workers extensively studied the role of alkali and alkaline earth cations on the dissolution rate of quartz [24], [117], [120], [121]. At near-neutral pH the rate-enhancing trend increases in the order: “pure water” < Mg^{2+} < $\text{Ca}^{2+} \approx \text{Li}^+ \approx \text{Na}^+ \approx \text{K}^+ < \text{Ba}^{2+}$ [117]. It is observed that small concentrations of electrolytes increase the dissolution rate, some by as much as 1.5 orders of magnitude above the values measured for deionised water. The effect is greatest for solutions of NaCl and KCl where reaction rates increase with increasing electrolyte concentrations up to 0.05 molal and become constant at higher molalities. Smaller rate increases are observed for LiCl and MgCl_2 solutions. Increased reactivity of the surface in the presence of adsorbed cations on quartz is also demonstrated by ab initio molecular orbital calculations of possible surface intermediate species, which show that the presence of certain cations increase the Si–O–Me angle helping therefore the disruption of Si–O bond (Figure 2.33) [24]. Though these ions had an important impact on the rate of dissolution of quartz, they did not show the same trend on other silicate minerals [24].

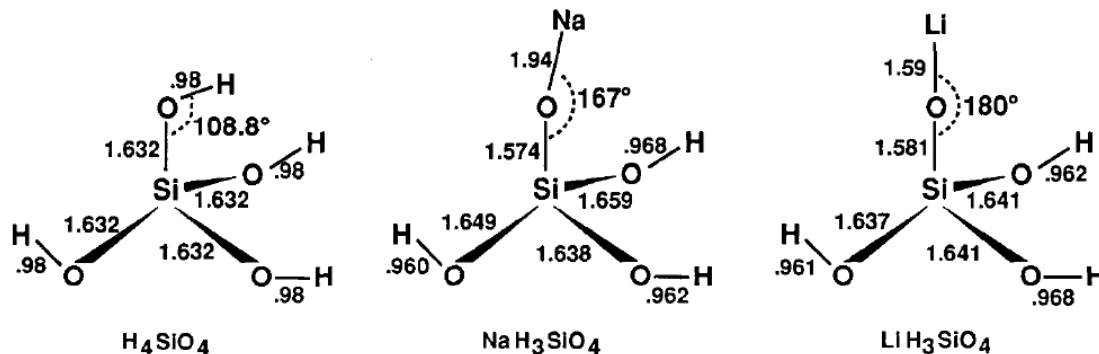


Figure 2.33: Optimized bond lengths and angles for the static molecular models of H_4SiO_4 , NaH_3SiO_4 and LiH_3SiO_4 . From [24].

Spagnoli and co-workers studied the effect of CaCl_2 on calcite dissolution by molecular dynamics simulation [25]. The free energy profile of the dissolution of a calcium ion as a function of distance from the surface was obtained by running a series of MD simulations where the ion is constrained at different heights above the surface. As the ionic strength of the electrolyte increases, the free energy of dissolution decreases (see Figure 2.34). The results also suggested that the chloride ions were located in distinct regions of the solution, corresponding to areas of high water concentration with areas of low, and almost zero, concentration between them [25]. This would be in accordance with the schematic representation of Figure 2.30.

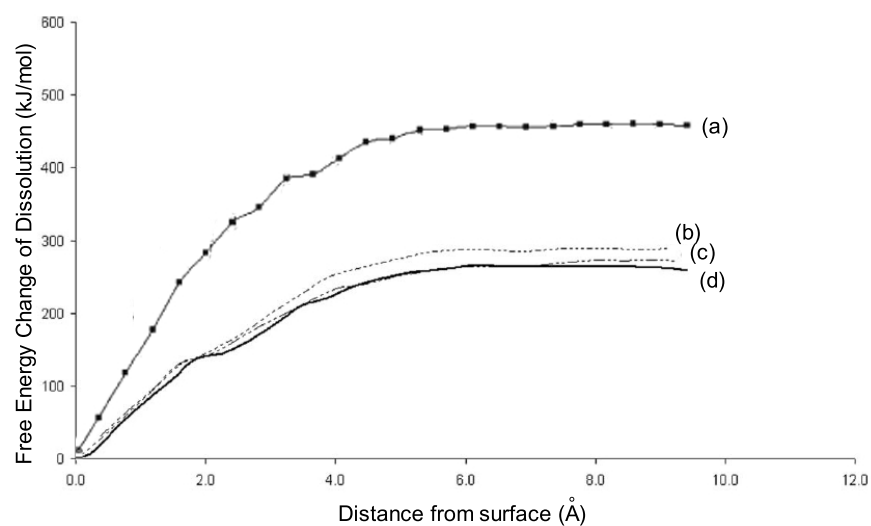


Figure 2.34: Free energy change of dissolving a calcium ion into (a) water, (b) 0.59 M, (c) 2.38 M and (d) 3.58 M salt water. Adapted from [25]

Chapter 3

Assesement of Dissolution Theory to Alite Early Hydration

In this chapter, different experiments related to the early hydration period are reviewed, especially those concerning the induction period. These results are discussed bearing in mind the concepts of crystal dissolution presented in the previous chapter. Additional experiments have also been undertaken on alite in order to see the effect of solution saturation state on the surface evolution as well as the effect of thermal treatments (annealing) to observe their impact on the reactivity. Finally a new mechanism for the early hydration of alite is proposed and discussed compared to previous theories explaining the induction period.

3.1 Influence of Alite Crystal Structure on its Early Hydration Kinetics

3.1.1 Surface observation of coarse anhydrous alite

In order to investigate the relevance of the dissolution theory to the early dissolution process of alite, studies were made on alite synthesised in laboratory. Alite was obtained by mixing calcium carbonate (precipitated GR for analysis, Merck), silica (highly dispersed extra pure, Merck), magnesium oxide (GR for analysis, Merck) and alumina (anhydrous γ -alumina, Merck) with deionised water in a ball mill for 24 hours and by firing the dry pelletised product at 1600°C for 10 hours. Magnesium oxide and alumina were added in order to favour grain growth and to stabilise the monoclinic structure of alite. The fired pellets are then quenched in air [26] and ball milled or only fractured to give fresh surfaces. The following images (Figure 3.1) are taken in the secondary electron mode at an accelerating voltage of 2 kV on freshly fractured surface in order to show representative features of our starting material. All samples remain uncoated in order to preserve the fine details of the surface morphology. Figure 3.1(a) and (b) are low magnification images. The average fractured surface appears granular at these scales with the presence of inter and trans-granular fracture features present either rough or cleaved surfaces (Figure 3.1(c) and (d)). The size of the apparent crystals is around 20 μm . Large pores are also present due to

the sintering process of alite which is not optimised to produce a denser polycrystal. At higher magnification, inter-granular or cleaved surfaces present a smooth plain surface with the presence of steps arising from the fracture process (Figure 3.1(c) and (e)) whereas transgranular fracture may show some layered features related to the crystallographic structure of alite (Figure 3.1(d) and (f)).

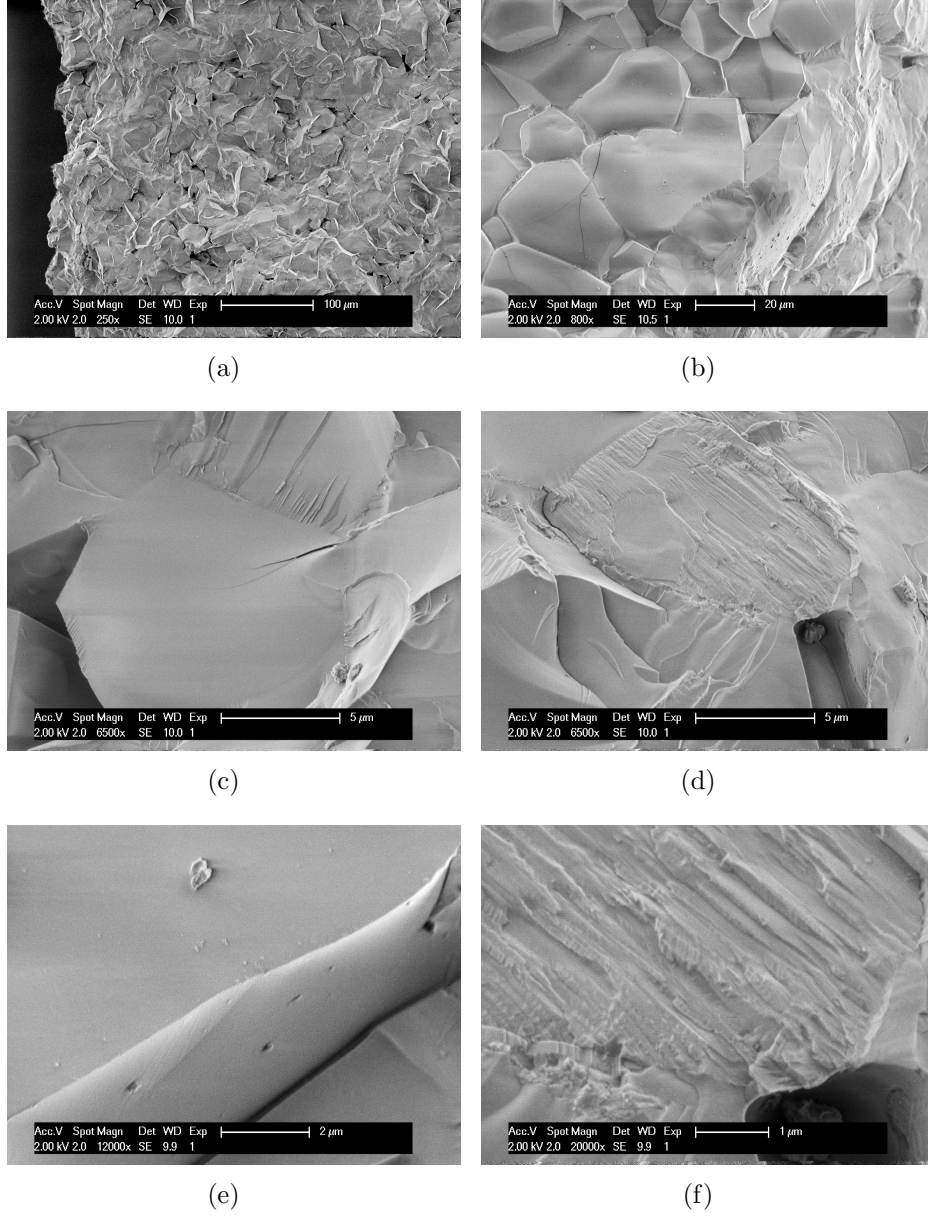


Figure 3.1: SEM micrographs of anhydrous surface of coarse alite samples.

3.1.2 Induction period and crystallographic defects

In order to study the influence of crystallographic defects on the early reactions of alite with water, alite of broad particle size distribution (see Figure 3.2(a)) has been thermally treated at 200°C and 750°C for 6 hours. The annealing process is a common thermal treatment used principally in metallurgy in order to remove the internal

stresses by thermal activation and therefore decrease the density of crystallographic defects. It can be seen on Figure 3.2(a) that the particle size distribution is not much affected by the different thermal treatments even though the treated samples appear to be less agglomerated than the reference one, which is probably an artifact of sample preparation. The XRD results show that only the sample treated at 750°C changes from polymorph MIII to TI (see Figure 3.2(b)). The samples were then mixed mechanically at 500rpm during 2 minutes at a w/c ratio of 0.4.

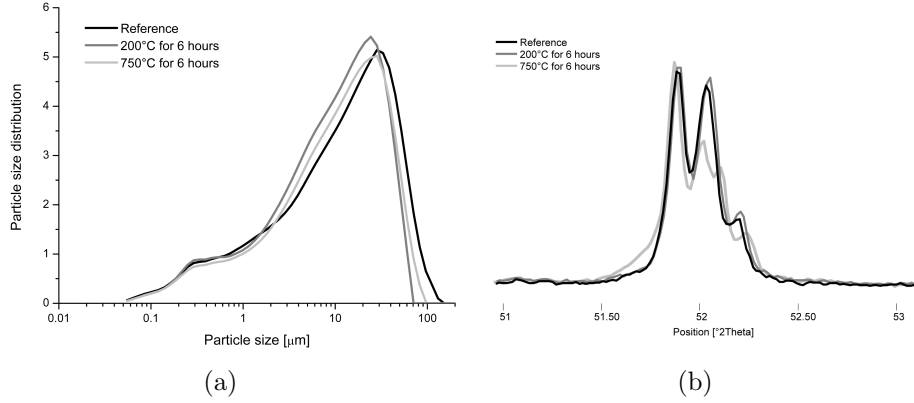


Figure 3.2: (a) Particle size distributions of reference and thermally treated (200° and 750°C for 6 hours) alite used for this experiment and (b) associated XRD pattern showing the change from polymorph MIII to TI for the sample treated at 750°C.

Figure 3.3 shows the associated isothermal calorimetry curves for the different samples. It can be seen that during the induction period (Figure 3.3(a)), the annealed samples have a lower heat flow compared to the quenched alite (reference), which means that less chemical activity is taking place. Regarding the dissolution theory, this result could be interpreted as lesser dissolution occurring when the sample has been annealed at higher temperature. Over 24 hours of hydration (Figure 3.3(b)), the sample annealed at 750°C shows the highest peak rate of reaction, but the sample annealed at 200°C which also presents a lower heat flow at early age remains at a lower rate of reaction compared to the reference. In these experiments the effect of particle size distribution may scatter the results.

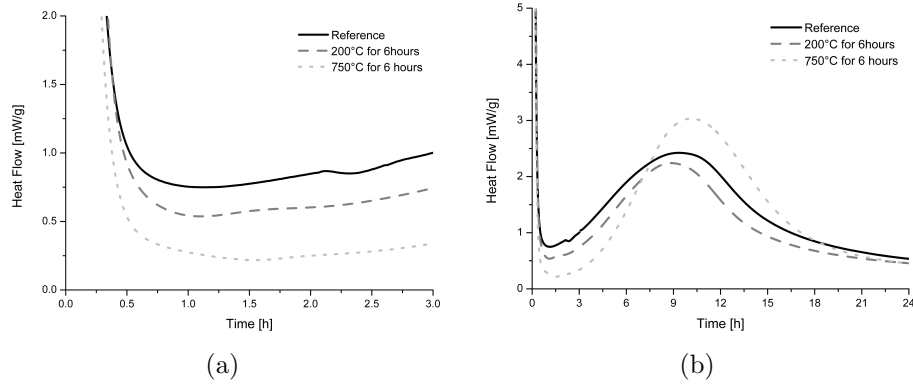


Figure 3.3: Isothermal calorimetry curves of alite quenched in air, quenched in air and subsequently annealed at 200°C or 750°C for 6 hours. (a) Induction period and (b) hydration over 24 hours.

Therefore, in order to avoid the effect of large particle size distributions, narrow particle size distributions were chosen to avoid dispersion of the reactivity due to different particle sizes. Narrow particle size distributions of quenched alite were thermally treated at 650°C for 6 hours. The particle size distributions were centred around values of d_{V50} of 38, 61 and 82 μm the particle size distribution is shown in Figure 3.4 [26].

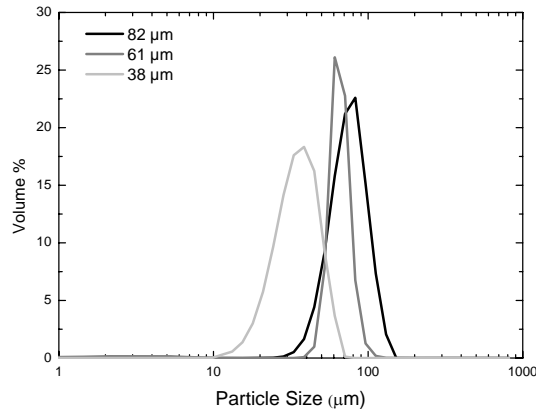


Figure 3.4: Particle size distribution of alite used in this study [26].

The annealing temperature of 650°C is one at which recovery - annealing of defects and a decrease in the number of dislocations - is also expected to occur. The treated samples changed from polymorph MIII to TI as demonstrated by the X-ray diffraction patterns in Figure 3.5, which is consistent with the results presented before and a decrease in defect density. The particle size distribution was also not affected by this heat treatment.

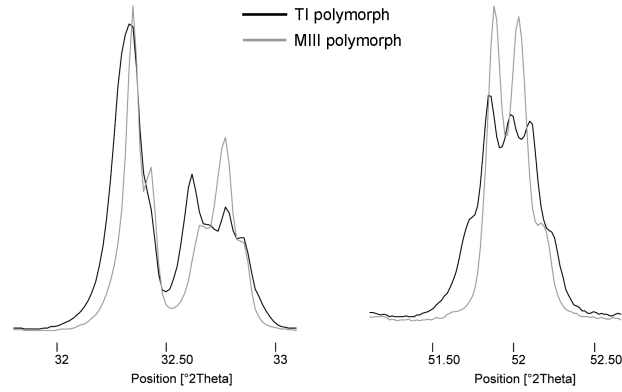


Figure 3.5: Diffraction pattern of the reference alite in grey showing the MIII polymorph and the thermally treated sample in black showing Tl polymorph.

The heat of hydration was followed by isothermal calorimetry at 20°C, with a water to cement ratio of 0.4. The samples were mixed by hand due to the limited amount of powder available. Figure 3.6 shows the heat evolution of the quenched and thermally treated samples. Figure 3.6(a), in which the samples were mixed inside the calorimeter (in situ measurement), shows that the first heat peak is much smaller for the thermally treated sample than for the control. In Figure 3.6(b) the samples were mixed externally by hand before insertion into the calorimeter. The sharp initial heat peak is followed by a period of low chemical activity which is prolonged for several hours for the thermally treated specimens, with a definite, almost flat, induction period. However, the acceleration and deceleration parts of the curves are very similar for both treated and untreated samples, which suggests that the same mechanisms and rate laws apply to both the quenched and the heat treated samples at this stage.

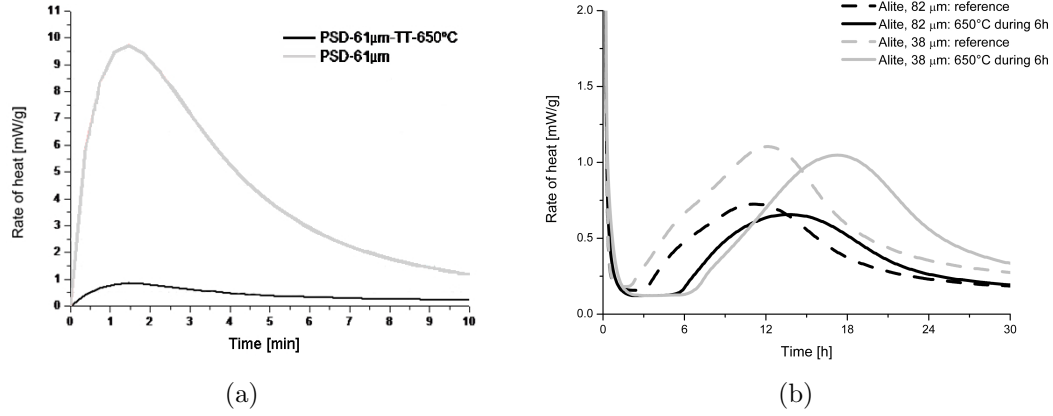


Figure 3.6: Heat evolution of alite untreated (reference) and treated at 650° for 6 hours of narrow particle size distribution. (a) 61 μm during the first dissolution period (in-situ measurement), the grey curve is the reference sample and the black one is the thermally treated sample and, (b) 38 μm and 82 μm for the main peak of hydration. Dashed curves are the reference samples and the plain curves are the thermally treated samples. All measurements were performed at 20°C and the water to cement ratio was kept at 0.4.

These experiments show that the early dissolution behaviour is dramatically affected by the defect density of the crystals and that this affects the time needed to reach the acceleration period. According to the theory of dissolution, a low density of crystallographic defects will lead to a low number of etch pits. Therefore when dissolution becomes limited to the step retreat process (as the solution concentration increases) the surface is less rough due to the low number of etch pits so there are less steps. Therefore, dissolution proceeds at a lower rate compared to the quenched alite.

3.2 Morphological Studies of Early Hydrated Alite

3.2.1 Surface study of coarse alite in normal alite paste

Coarse alite samples were prepared by the same procedure as explained previously. A fracture sample of approximately 5 x 5 x 5 mm was mixed by hand for 2 minutes in an alite paste having a w/c ratio of 0.4 and hydrated during a determined period of time (10 min, 3, 5 and 7 hours, see Figure 3.7). Hydration was stopped by a freeze-drying technique and the samples were then studied by SEM and focus ion beam (FIB). This latter technique coupled with a 3D reconstruction software enables to reconstruct the surface in 3 dimensions with a spatial resolution of about 5 nm. As it can be observed on the corresponding calorimetry curve, Figure 3.7, the different times were chosen in order to study the surface transformation during the induction period.

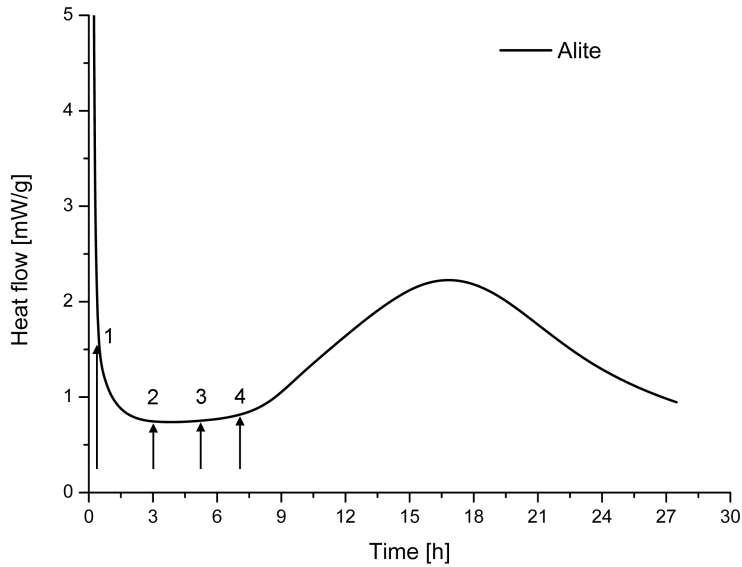


Figure 3.7: Calorimetry curve of an alite paste mixed 2 minutes by hand mixing. Number 1, 2, 3 and 4 (10 minutes, 3, 5 and 7 hours respectively) represent times where surface investigation were performed.

After 10 minutes of hydration, the surface appears smooth with the formation of pits located at the intersection of grain boundaries. However, these features might be related to remaining porosity due to the sintering process. Locally, it is possible to observe small crystals of CH. After 3 hours of hydration, the surface is still smooth. Due to the limited resolution of the SEM images, one cannot exclude that small etch pits could have already opened up but remain too small to be observed yet. Since the sample is also mixed with particles of smaller sizes having a much higher surface area, the coarse sample of alite should have a smaller contribution to the overall dissolution and might even be prevented from rapid dissolution as its surrounding solution might be saturated due to the faster hydration of smaller particles. In addition to that, the surface of the coarse sample should present fewer crystallographic defects as it was not mechanically ground and consequently, the surface reactivity of the coarse sample would be lower than the particles one. It is only after 5 hours that etch pits on plain surface are visible which suggest that saturation of the solution changes at the end of the induction period due to the precipitation of hydrates. The surface is rougher as it can be seen on Figure 3.8(e) and (f). At 7 hours, which corresponds to the end of the induction period according to the associated calorimetry curve (Figure 3.7), the surface morphology of the alite surface is similar as after 5 hours of hydration but with deeper etch pits. It is also possible to see more hydration products forming at the surface. Tiny acicular needles of what seems to be C-S-H are visible on some surfaces (Figure 3.8(g) and (h)).

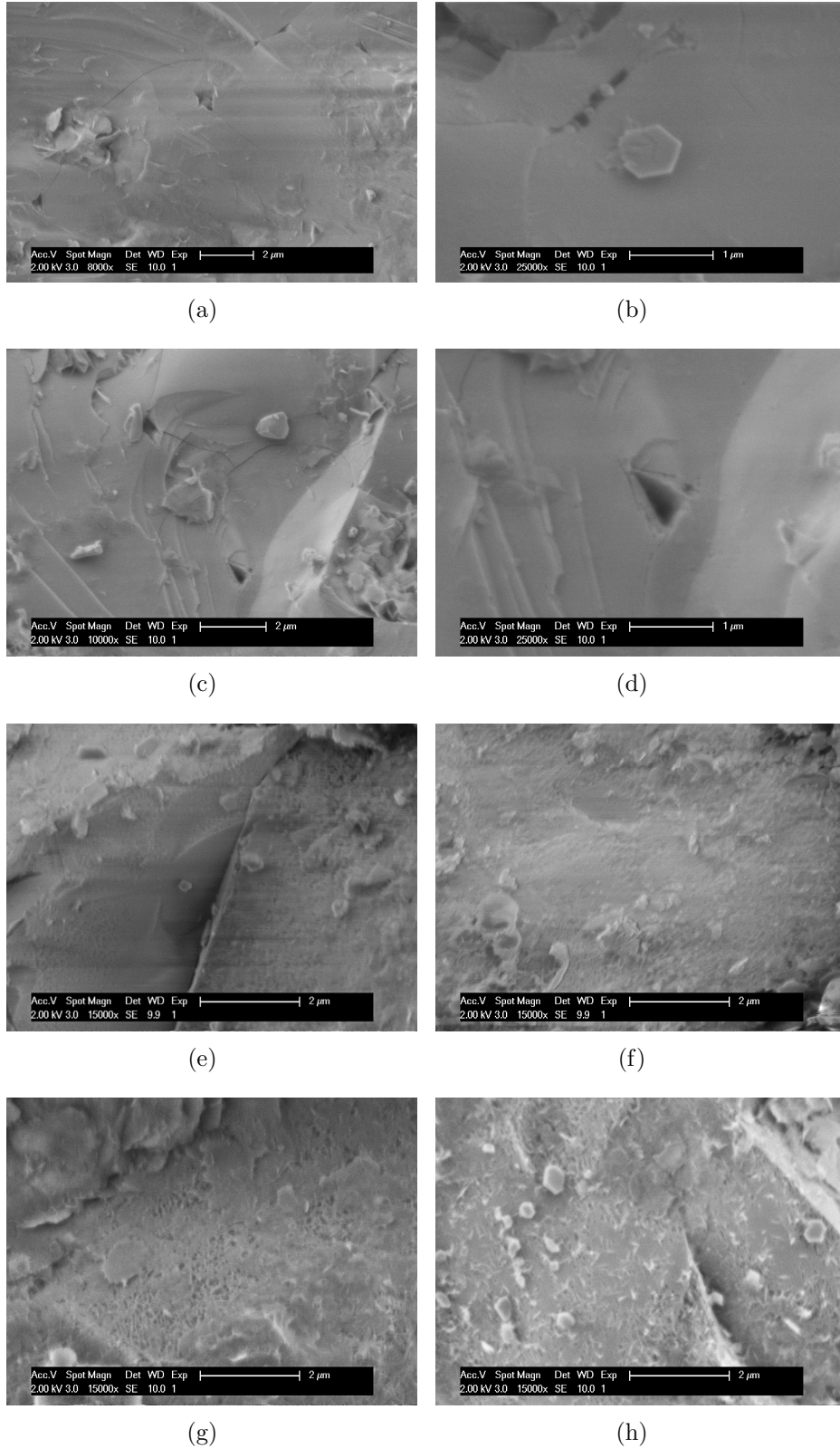


Figure 3.8: SEM micrographs of surface of coarse alite samples hydrated after, (a) and (b) 10 minutes, (c) and (d) 3 hours, (e) and (f) 5 hours and (g) and (h) 7 hours of hydration.

FIB observations were conducted on the sample hydrated for 7 hours. The surface

was first coated with gold and subsequently with platinum where the measure is performed. This platinum coating attenuates the ions beams (gallium ions at an accelerating voltage of 30kV) and preserves the sample from a too rapid degradation. The results are shown in Figure 3.9. In this reconstruction of the surface the pits can be observed in 3 dimensions. Their size vary between 50 nm and 200 nm and their depth is roughly estimated to 50 nm. No visible protective membrane was observed at the surface. As the resolution of the coupled SEM is 3 nm at an accelerating voltage of 2kV, only membrane with thickness less than 3 nm could exist but due to the coating, this membrane could have been destroyed.

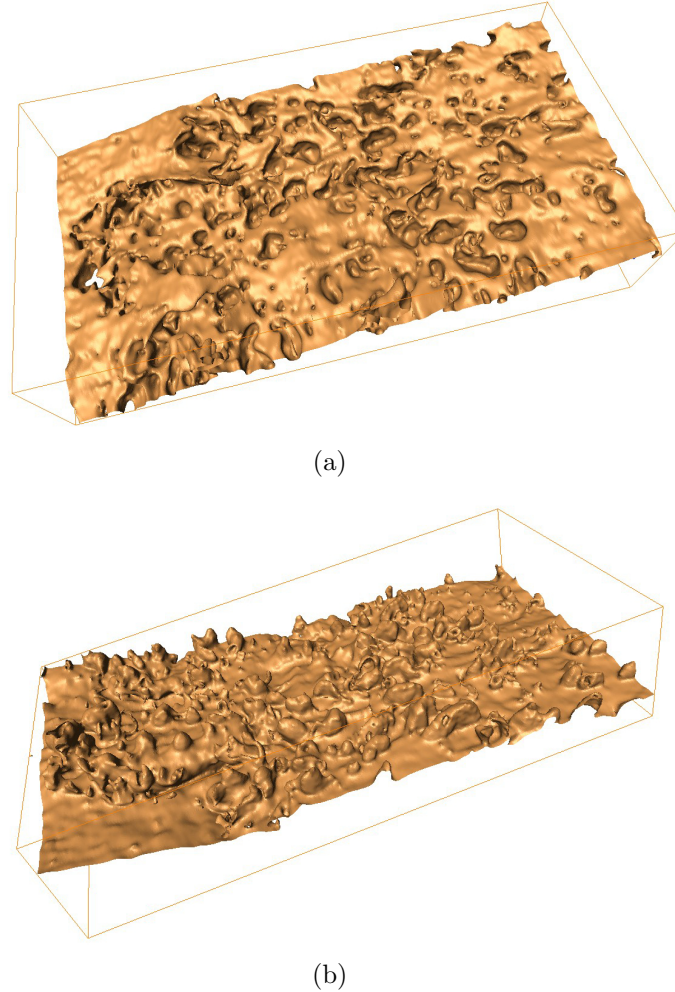


Figure 3.9: FIB reconstruction of (a) an alite surface hydrated in paste for 7 hours and (b) the bottom view image. The dimension of the box are $1.75 \mu\text{m} \times 1 \mu\text{m} \times 400 \text{ nm}$.

3.2.2 Effect of solution saturation state

The theory of dissolution presented previously indicates that the state of saturation of the solution should be of great importance. Therefore, the samples having a size of approximately $5 \times 5 \times 5 \text{ mm}$ were immersed in two different solutions (around 3.5 ml): deionised water and saturated lime solution for 2 and 30 minutes. The water to cement ratio is calculated to be higher than 1000. The samples were not coated

for examination in the SEM; the pictures (Figure 3.10) were taken in the secondary electron mode at an accelerating voltage of 3 kV.

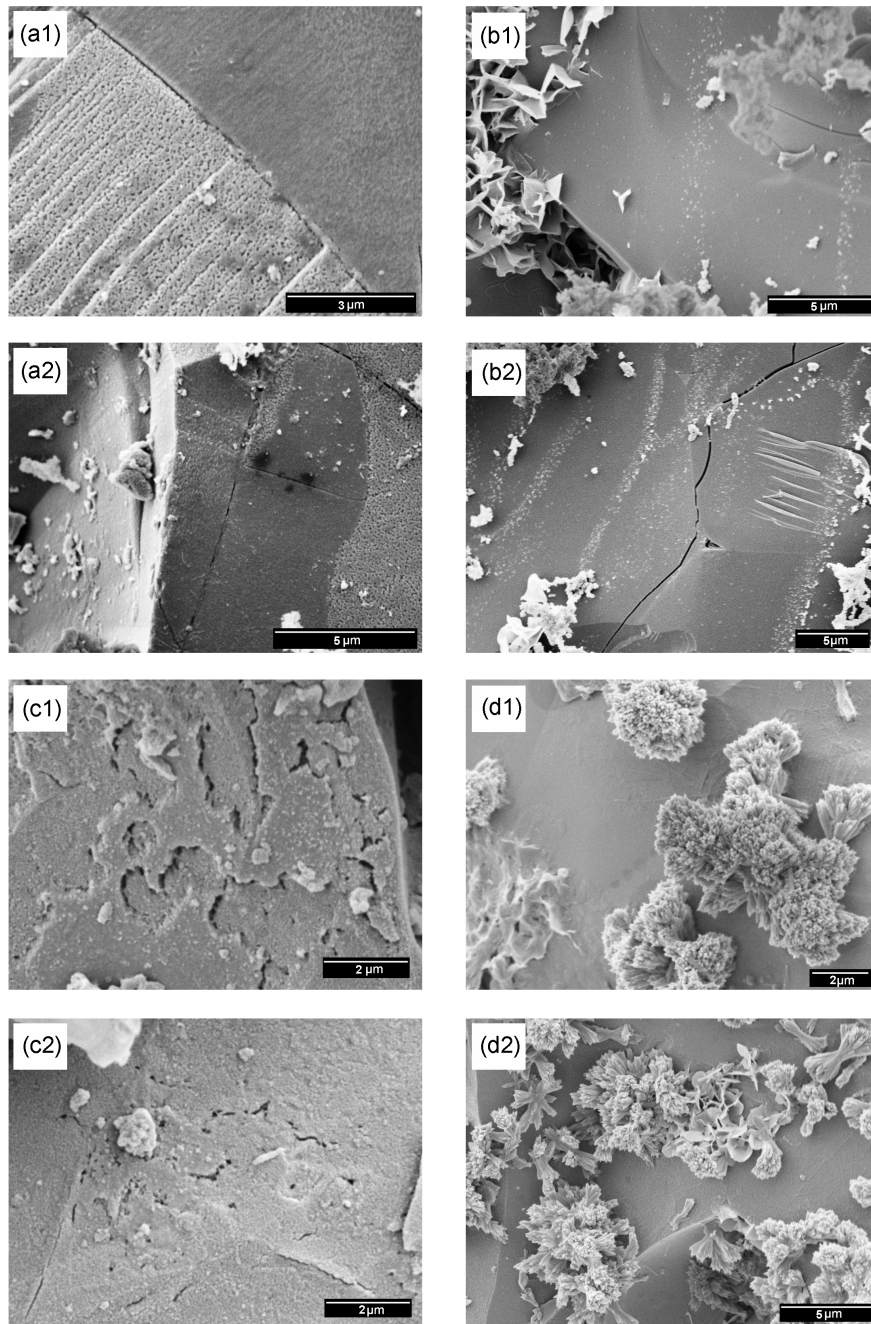


Figure 3.10: SEM micrographs of alite immersed during 2 minutes in (a) deionised water, (b) saturated lime solution, and 30 minutes in (c) deionised water and (d) saturated lime solution.

After only 2 minutes samples immersed in water show extensive surface pitting. There is also a marked difference in Figure 3.10(a) between the crystal in the top right of the picture and the one in the bottom left. This is a consequence of the crystallographic orientation of the grains, which would have different interfacial

energies, different dislocation densities and therefore different energy barriers for the nucleation of pits. It is also pertinent to note that the clear definition of these etch pits suggests that there is no hydrate layer covering the surface. After 30 minutes of hydration (Figure 3.10(c)) one can observe that the surface has been severely corroded with height differences reaching several hundreds of nanometers.

In the case where the alite was hydrated in saturated lime solution, the surface does not undergo such extensive dissolution. After 2 minutes, Portlandite and other hydrates have precipitated, maybe during specimen drying or at places where supersaturation is locally reached (Figure 3.10(b)). After 30 minutes (Figure 3.10(d)), C-S-H with a “sheaf of wheat” morphology [122], [123], is observed. However, at both times most of the surface appears smooth and unattacked. This strongly suggests that under saturated lime conditions, the predominant regime of dissolution is step retreat since the formation of etch pits on plain surfaces is not observed for these samples.

These observations confirm that the concentration of the solution plays an important role in the dissolution process of alite as seen in studies of other minerals and explained in the previous chapter.

In fact, examination of the literature indicates other studies in which the effect of solution concentration on dissolution rate is apparent. For example, Barret and Ménétrier [60] analysed filtrates obtained by passing a limited amount of solvent (distilled water or lime solution at various lime concentrations) through C_3S spread on a millipore filter. They showed that the lime concentration increase in solution (ΔC) was always smaller when the lime concentration in the solvent was high.

3.3 Previous evidence of the role of crystallographic defects on the reaction of cementitious materials

In fact, the role of defects in the early hydration processes of cementitious materials was already noted by previous researchers [28], [70], [74], [75]. Maycock and co-workers [75] and Odler and Schüppstuhl [74] studied the effect of quenching rate on the reactions of alite and found that faster quenching, likely to induce more crystal defects, resulted in shorter induction periods. Fierens and Verhaegen [70] cooled tricalcium silicate at different rates from 1600°C to 1300°C before quenching. Besides calorimetry (Figure 3.11), they used thermoluminescence to follow the changes during the early reaction [27], [124]. Thermoluminescence gives an indication about the presence of crystallographic defects in the structure by excitation with plasma, γ ray, or UV sources followed by relaxation upon heating, leading to the emission of light [125]. Two populations of defects were identified, whose amount increased with higher cooling rates. One of these populations of defect progressively disappeared during early hydration. Furthermore, the length of the induction period was found to be inversely proportional to the original magnitude of this thermoluminescence peak. (The changes in the calorimetry curve are different to those reported above due to the fact that a broad range of particle sizes is present.)

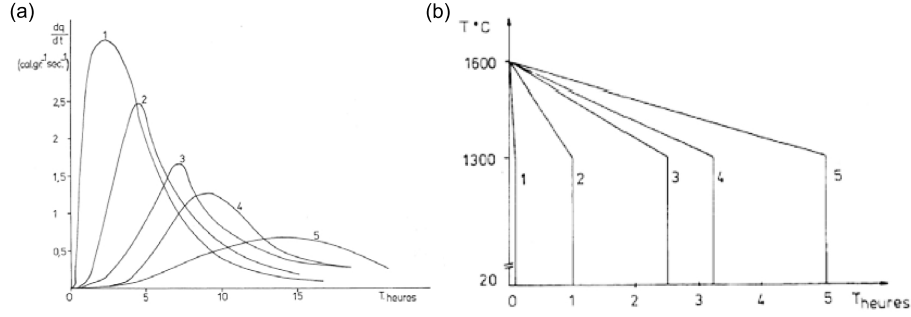


Figure 3.11: (a) Calorimetry curves of tricalcium silicate thermally treated showing the effect of crystallographic defects on the length of the induction period resulting from different thermal treatment. (b) Associated thermal treatments. From [27].

Dislocations and planar defects were observed by TEM in alite thermally treated at 700°C by Hudson and Groves [126], although the density of dislocations was too low to be measured by TEM. Dislocation densities below 10^6 cm^{-2} are near the limit of resolution of TEM method for determining dislocation densities [19]. It is however not excessive to assume that surfaces of quenched alite should be intersected by numerous line defects. Dislocations in alite would arise from the growth and cooling process, possibly affected by the presence of impurities, and during the grinding processes.

Sakurai and co-workers [28] etched alite with a solution of 0.4% HF with 0.6% HNO_3 in ethyl alcohol in order to reveal defects, grain boundaries, etc. Their SEM images reproduced in Figure 3.12 show that etching begins at grain boundaries and etch pits are formed that they associated with the emergence of dislocations.

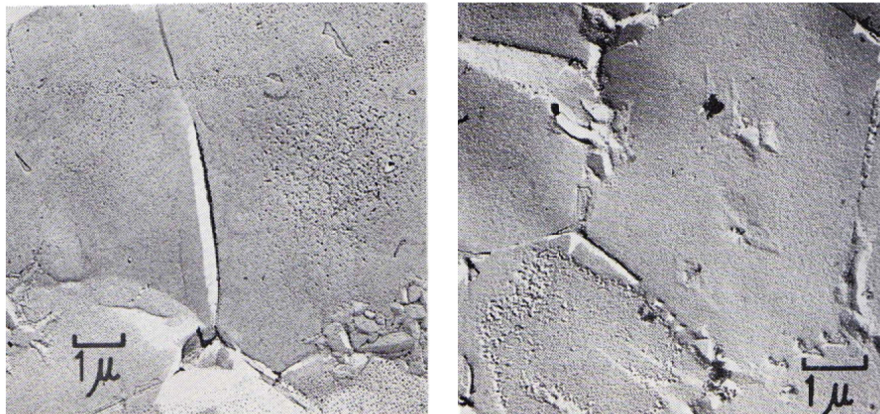


Figure 3.12: SEM micrographs of C_3S samples with 1.1% wt. Cr_2O_3 after 1 minute in etchant (0.4% HF with 0.6% HNO_3 in ethyl alcohol) [28].

Ménétrier and co-workers [8] observed by SEM a non-uniform attack of the C_3S surface exposed to water before growth of hydrates occurred (Figure 3.13).

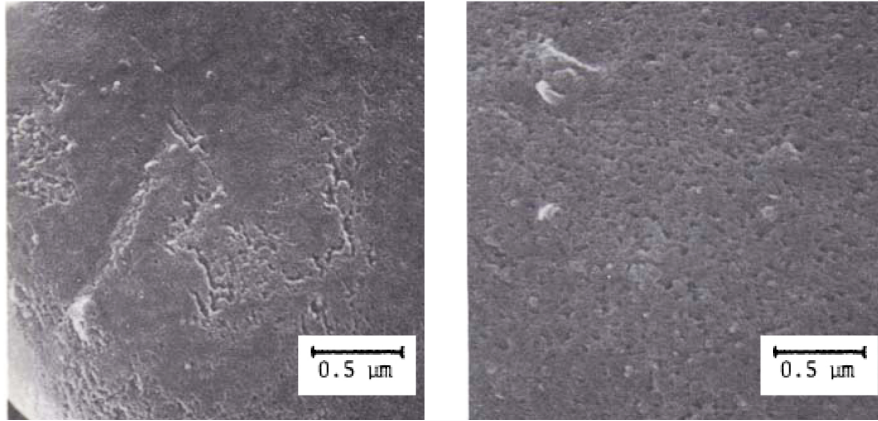


Figure 3.13: High-resolution SEM micrographs of hydrated C_3S surface at $w/c = 1.0$ [8].

Etch pits have also been observed recently by Makar and Chan [29] for commercial Portland cements hydrating at a water to cement ratio of 0.5 (Figure 3.14).

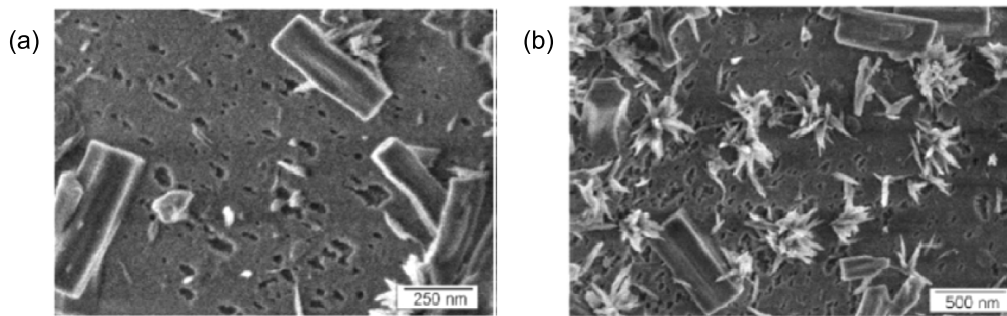


Figure 3.14: Morphology of ordinary Portland cement at different times of hydration ($w/c = 0.5$). (a) After 180 minutes of hydration and (b) after 240 minutes. From [29].

By atomic force microscopy, Garrault and Nonat [10] observed preferential dissolution, forming parallel steps, during the early hydration of a polished section of alite in saturated lime solution. This could correspond to a slow dissolution process by step retreat occurring at the low undersaturation provided by the saturated lime solution they used. Similar studies by di Murro [30] show the evolution of the surface as a function of time, Figure 3.15. These images were interpreted as showing nucleation and growth of C-S-H and CH. However, re-examination of these images suggests that they in fact show surface dissolution with the formation of steps as arrowed in Figure 17, (b). It can also be observed that dissolution of the surface does not occur evenly, demonstrating the importance of the crystallographic orientation.

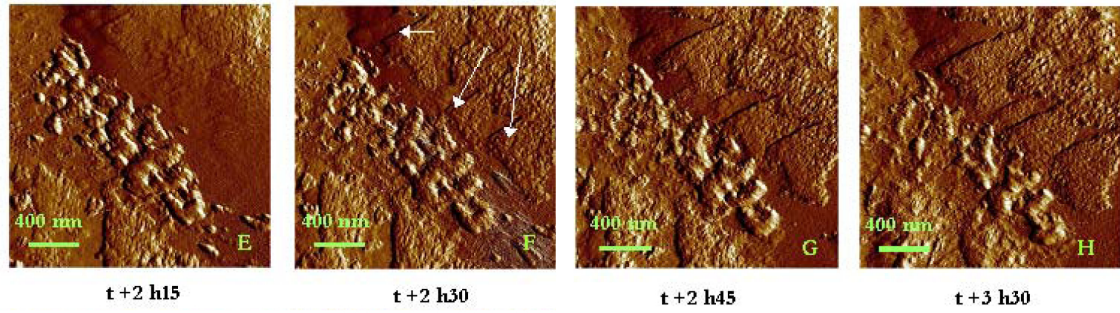


Figure 3.15: Topographic observation by AFM of alite surface hydrating in a saturated lime solution (deflection mode). From image E-F-G-H it is possible to observe the dissolution of specific crystallographic planes. It can also be observed that the presumed C-S-H appearing in the 1st preferential area (image B) as well as the one in the 2nd area are dissolving with time (AFM images from [30])

3.3.1 Effect of calcium hydroxide addition

Brown and co-workers noticed that hydration of pure C_3S in saturated lime solution with a water to binder ratio of 0.6 is retarded compared to hydration with demineralised water [9]. This shows again the importance of the initial saturation state of the solution, its effect on the first dissolution process and its later effect on the induction period.

In their article on the induction period, Odler and Dörr observed that the initial hydration was stimulated by adding prehydrated paste and by lowering the calcium concentration with oxalic acid [71]. They suggested that calcium concentration below Portlandite saturation in the pore solution was accompanied with a fast dissolution process and that the presence of stable hydrates would shorten the induction period and accelerate the initial hydration. In these two experiments they observed that products rapidly consuming calcium ions would avoid the slow dissolution process (or delay its onset) by keeping high undersaturation. They also concluded that added crystalline Portlandite was not acting as a nucleating agent since the duration of the induction period was not shortened. Crystalline Portlandite, instead of acting as a nucleating agent, would rather dissolve in the initial conditions of undersaturation that follow water addition. This is not the case for C-S-H present in the prehydrated paste because of its lower solubility compared to Portlandite.

In their study by flame adsorption spectrometry on filtrates obtained by passing a limited amount of solvent (distilled water or lime solution at various lime concentration) through C_3S spread on a millipore filter, Barret and Ménétrier observed that although the ratio of the lime concentration increase in the filtrate to the filtrate silica concentration ($[\Delta C/S]$) was very similar for each solvent, the lime concentration increase was always smaller when the lime concentration in the solvent was high [60]. These results reflect here also the limitation of the dissolution process due to a decrease of the undersaturation coefficient as the calcium concentration in solution increases. Dissolution experiments undertaken by Nicoleau [31] of highly dilute suspensions in different solutions are presented in Figure 3.16. It is again very clear

that the saturation state of the solution affects dramatically the rate of dissolution of C_3S . The curves are not linear during the entire experiments due to the fact that the experiments are undertaken in a closed system and therefore the solution is not renewed leading to a build up of ions in solution. This has for consequence to lower the undersaturation and decrease the dissolution rate over time.

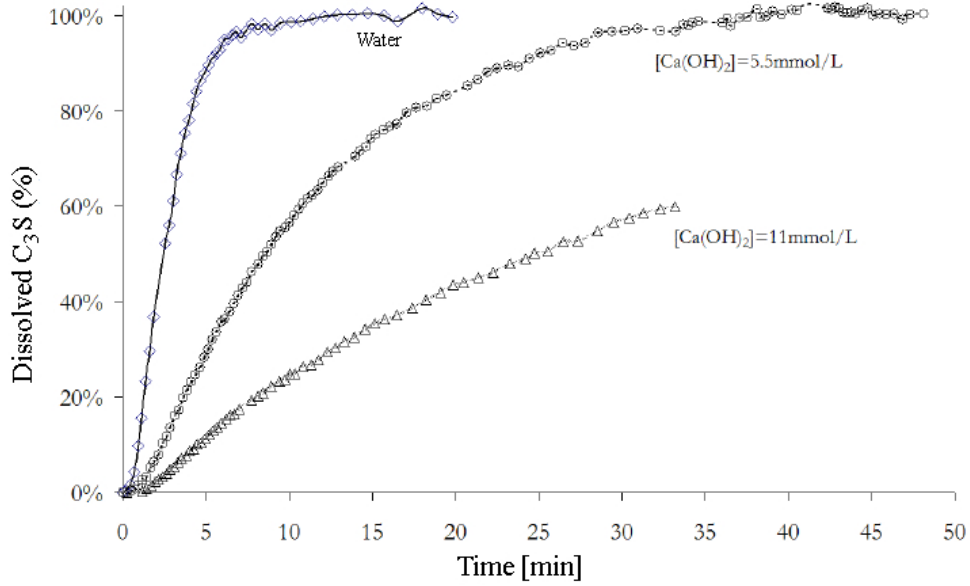


Figure 3.16: Dissolution of 1.5 mg of C_3S in 200 mL of calcium hydroxide solution of 0, 5.5 and 11 mM. Speed of mixing is kept constant for all experiments. From [31].

On Figure 3.17, it can be seen that the intensity of the first peak of dissolution is completely different between the two cases showing again the effect of the initial saturation state of the solution. Less dissolution is taking place in the saturated lime conditions.

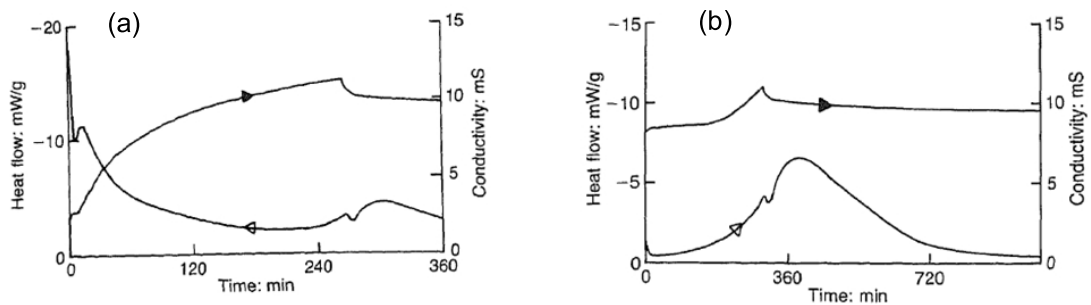


Figure 3.17: Heat evolution and electrical conductivity curves plotted against hydration time for C_3S hydration (a) in water at a $w/c=18$ and (b) in a 22 mM lime solution at $w/c=16$, from [32].

One should keep in mind that if the aqueous phase is a concentrated lime solution, the surface topography at the nanometer scale is expected to be different during the

induction period since initial conditions of undersaturation are not the same. Dilute suspensions in deionised water cannot be representative for the process happening in paste and comparisons between paste and dilute suspension in saturated lime conditions should be analysed carefully. The duration of each dissolution mechanism is not the same which will induce some differences at the atomic and nanoscale level. Application of the dissolution theory to dilute suspension does not contradict previous conclusions but the missing interpretation of the dissolution process leads to a direct extrapolation of the hydration mechanism from diluted suspension to paste which in a first approximation doesn't appear so straightforward since the topography of the anhydrous phase will undergo different transformation depending on each different condition. For instance, Figure 3.18 compares the effect of Portlandite addition to a suspension of C_3S when it is present since the beginning (reference) or added 10 minutes later [33]. The hydration is monitored by conductivity measurement and the $w/c=70$. It is observed that the delayed addition of CH shortens slightly the induction period. The interpretation proposed was that CH dissolves rapidly leading to a rapid increase of the conductivity and in this case, CH acts as seeds which enhance the kinetics of hydration. However, it can be proposed that before the addition of CH, the C_3S particles undergo fast dissolution and the surface is severely corroded due to the high undersaturation conditions. After the addition of CH, the undersaturation is lowered and the dissolution mechanism occurs by step retreat at pre-existing roughness. Therefore, the surface roughness would be much more important in the case of the delayed addition of CH compare to the reference one and this difference in surface microtopography can explain the shortening of the induction period.

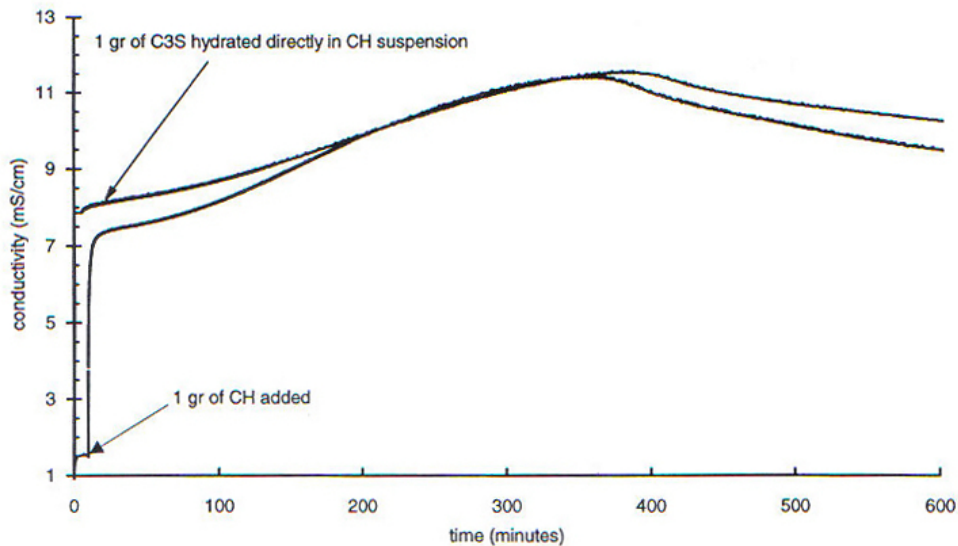


Figure 3.18: Delayed addition experiment of CH during the hydration of C_3S at $w/c=70$. From [33].

3.3.2 Effect of free lime addition

It has been noticed that an addition of 2.5% of free lime by weight of C_3S retards the hydration process but that higher amounts accelerate it [76]. These phenomena interpreted from the dissolution point of view, would lead to the following explanation: the rate of dissolution of free lime being higher than for C_3S , a large quantity of calcium ions would rapidly pass into solution and lower the undersaturation with respect to the anhydrous phases. This will prevent fast dissolution of alite and etch pit formation. This would consequently increase the duration of the induction period as the pre-existing roughness serves as a source for the step retreat mechanism during the period of low chemical activity. However, the initially high concentration of calcium ions will reduce the energy barrier for hydrates to nucleate, which explains why the induction period is only slightly retarded. At larger concentrations of free lime, supersaturation with respect to Portlandite and C-S-H would be reached even more rapidly for the same reason mentioned earlier, without important dissolution of the alite.

3.4 Effect of inorganic addition

Inorganic salts that have a marked effect on the kinetics of hydration are generally classified as either ‘accelerators’ or ‘retarders’, depending on how they affect the time of set [5]. Kantro [34] performed a large series of calorimetry tests at 27°C on alite mixed with different salt solutions in order to test the effect of specific cations and anions. For the chlorides of alkali and alkaline earth metals, the order of effectiveness of the cations was:

$$Ca^{2+} > Mg^{2+} \sim Sr^{2+} > Rb^+ \sim K^+ \sim Li^+ \sim Cs^+ > Ba^{2+} \sim Na^+ > H_2O \quad (3.1)$$

They also found a series for anions using soluble salts of calcium and the order of effectiveness was:

$$Cl^- \sim Br^- > SCN^- > I^- > (NO_3)^- > (ClO_4)^- > H_2O \quad (3.2)$$

It is however difficult to correlate the radius and the charge with the effectiveness of acceleration even though it seems that alkaline earth metals appear more efficient than alkalis. It has been proposed to correlate these series with the Hofmeister series [5], [123]. However, the order of effectiveness does not follow the same order and it seems therefore difficult to make a direct comparison. Kantro [34] also showed that the quantity of admixture is also important as it generally increases the accelerating or retarding effect. An example is given on Figure 3.19 where the amount of $MgCl_2$ affects dramatically the first peak of dissolution, the induction period and the rate of reaction during the acceleration period.

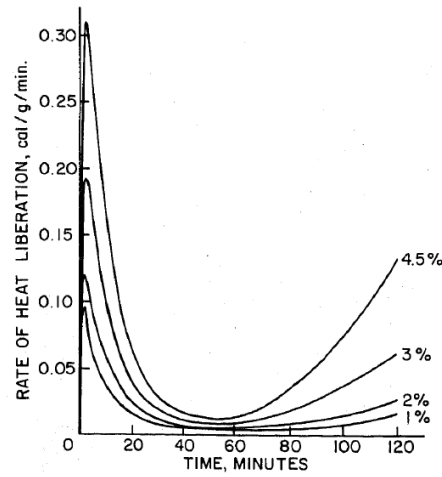


Figure 3.19: Heat flow of alite at early age with different amount of MgCl_2 . From [34].

Brown and coworkers [35] also studied the effect of different salts on the hydration of C_3S . Their main results are presented on Figure 3.20. It can be seen that in this series of measurements, the only effective accelerator is calcium chloride whereas anhydrite (CS), calcium hydroxide and sodium hydroxide turn out to have a slightly retarding effect. However, in the case of anhydrite addition, there is a crossover appearing at around the middle of the acceleration period and the maximum heat flow reached about the same intensity as in the case of calcium chloride.

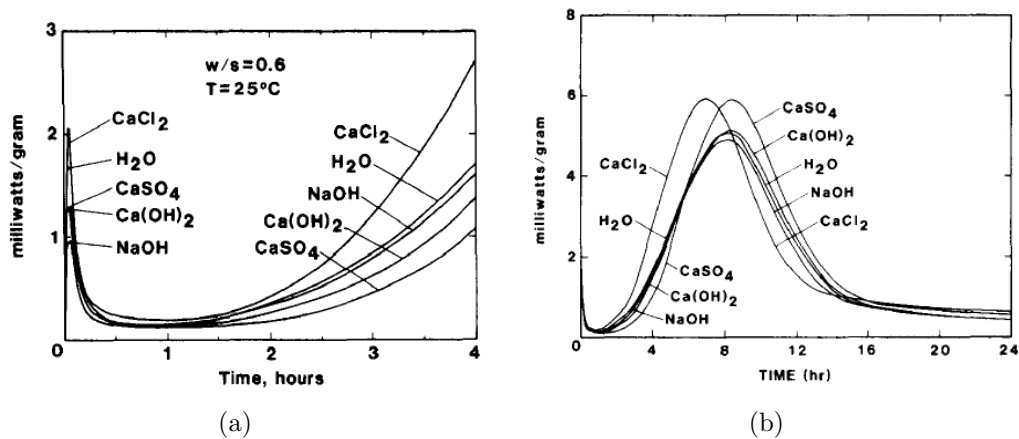


Figure 3.20: Rates of heat evolution from hydrating C_3S with organics salts at a $w/c = 0.4$ for (a) 4 hours of hydration and (b) 24 hours of hydration. From [35].

These results imply that certain ions can effectively catalyse or inhibit the early reaction of hydration but also the rate of formation of hydrates during the acceleration period. Even though certain of these inorganic salts additions such as calcium chloride have been extensively studied [34], [35], [123] no mechanisms have been validated to explain their effect on the hydration kinetics. It is therefore the purpose of the following sections to try and see if dissolution theory is also able to

give some indications on the possible effect of these mineral addition on the kinetics of early hydration of alite.

Effect of calcium chloride

Calcium chloride is one of the most widely recognised and efficient accelerators of hydration, setting and early strength development in cementitious systems [123]. Despite numerous studies on this subject, the mechanisms responsible for its acceleration still remain poorly understood. The two main effects reported in the literature are [5], [123]:

1. A shortening of the induction period, and
2. An enhancement of the rate of hydrate formation during the acceleration period.

(see also Figure 3.20)

Juenger and co-workers [123] used X-ray transmission microscopy to study the hydration of cementitious grains in the presence or not of calcium chloride. These experiments were undertaken in dilute suspension saturated with lime and gypsum. Their observations lead them to conclude that the accelerative power of CaCl_2 may come from its ability to flocculate hydrophilic colloids such as C-S-H. This idea was already proposed by Brown and coworkers in 1985 [35]. However, this proposition would only explain the enhancement of the rate of hydrate formation during the acceleration period but not the shortening of the induction period.

For many different minerals such as quartz or BaSO_4 , it has been reported that chloride ions enhance the rate of dissolution by promoting the formation of etch pits or by forming kink sites along the edge of an edge pit [16], [127]. However, there is also a great dependence with the type of cations forming the chloride salt [117], [121].

In order to see if the effect was the same for cementitious systems, a coarse sample of alite has been dipped into a solution of 2% of calcium chloride for 30 minutes. The results are presented on Figure 3.21. It can be seen that the surface of alite is deeply pitted and etch pits follow specific crystallographic orientations forming large striations on the surface. It seems therefore that the same conclusions can be applied to alite concerning the effect of chloride ions on the dissolution process, which are an enhancement of the dissolution rate and the promotion of etch pits formation. Here again, the dissolution theory provides a rational explanation for the reason of a shorter induction period in the presence of calcium chloride. However, the mechanism at the atomic scale still remain to be elucidated.

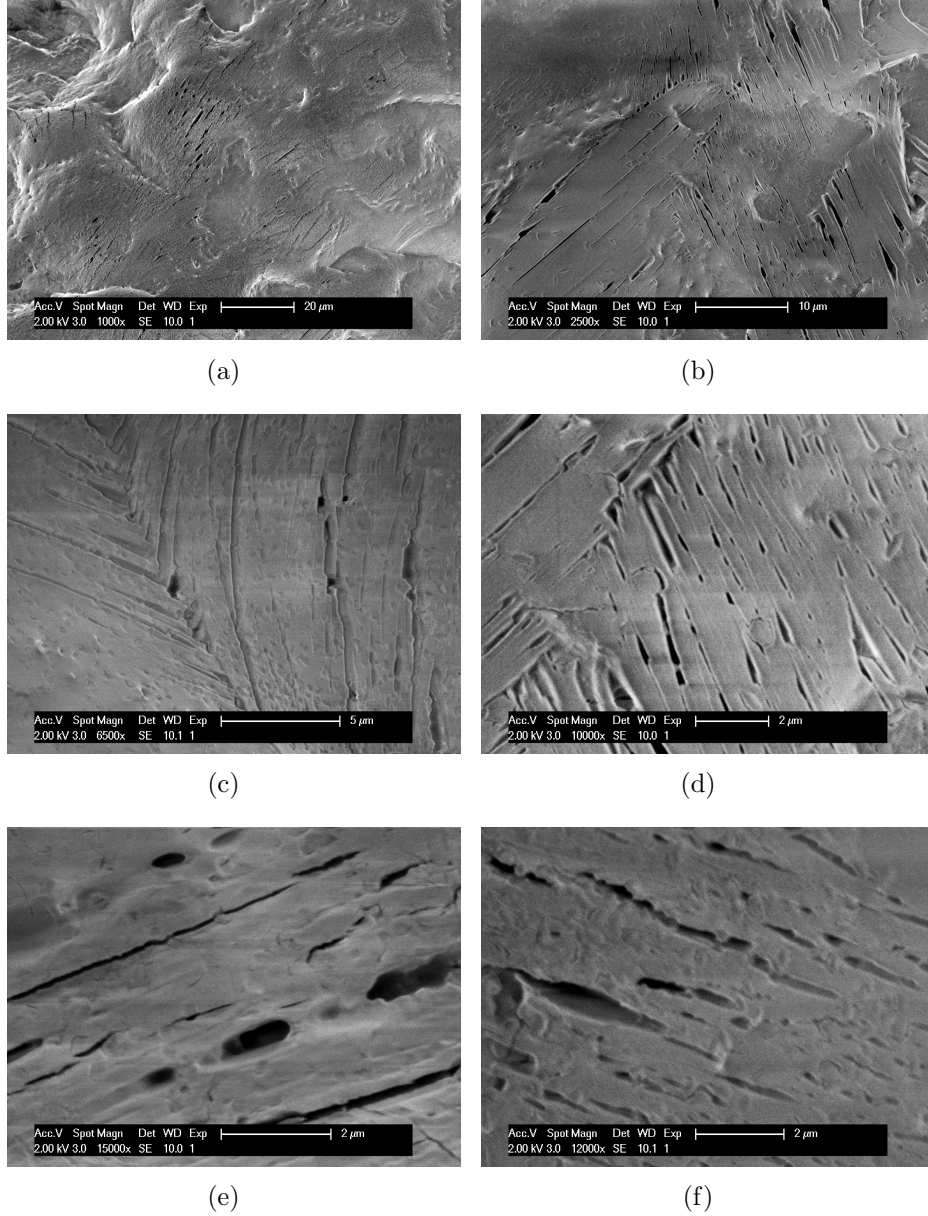


Figure 3.21: SEM micrographs of surfaces of coarse alite samples dipped into a 2 CaCl_2 solution for 30 minutes.

3.5 Discussion

3.5.1 Large difference from solubility limit of C_3S

One of the main objection to theories which do not invoke the formation of a protective layer is the difficulty to account for the large discrepancy between the calculated ion activity product of about 10^{-18} measured experimentally in solution (using calcium and silicate concentrations of 10-20 mM and 50-200 μM respectively at a pH 12) and the expected equilibrium value K_{SP} of around 3 [128]. This was highlighted by Gartner and Jennings [7] who showed on a chemical potential diagram

the large difference in solubility between tricalcium silicate and C-S-H formed at early age (see Figure 3.22).

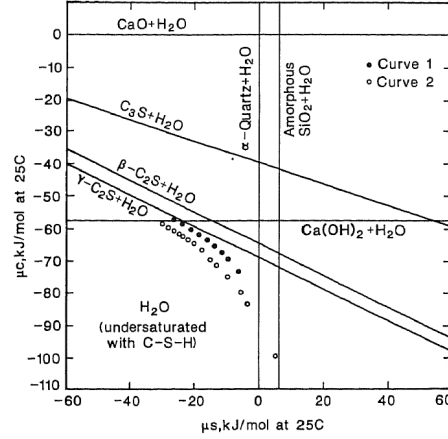


Figure 3.22: (a) Chemical potential phase diagram showing the chemical potential solubility isotherms for various compounds of interest in the CaO-SiO₂-H₂O system, relative to the oxides in their standard states at 298.15 K. Points above and to the right of a phase boundary represent supersaturation with respect to the solid. The slope of a line at any point represents the CaO:SiO₂ ratio according to $R_S^C = -d\mu_s / -d\mu_c$. The precision is roughly $\pm 2n$ kJ/mol for compounds containing n oxides (e.g., ± 8 kJ/mol for C₃S). From [7].

Using solubility product of 3 in equation 2.12 would give an undersaturation coefficient of about -38 to -43 for saturated lime conditions, where it is already observed experimentally that etch pits do not form. This value is larger than the typical values of other minerals at the onset of slow dissolution of around 11 discussed earlier. Figure 3.23 shows the variation in the dissolution regimes as a function of surface energy, compared to the data for albite shown in Figure 2.24. An alite-water interfacial energy of around 1.06 J/m² would be needed for etch pit formation at defects to cease at undersaturations of below about 43. The surface energy of alite in water is not known and cannot be measured, due to its strong reactivity. This value seems high compared to the estimated alite-vapour surface energy of 1.5 J/m² [129]. However, it is possible that there is not much relaxation of the alite surface, due to the initial fast reaction.

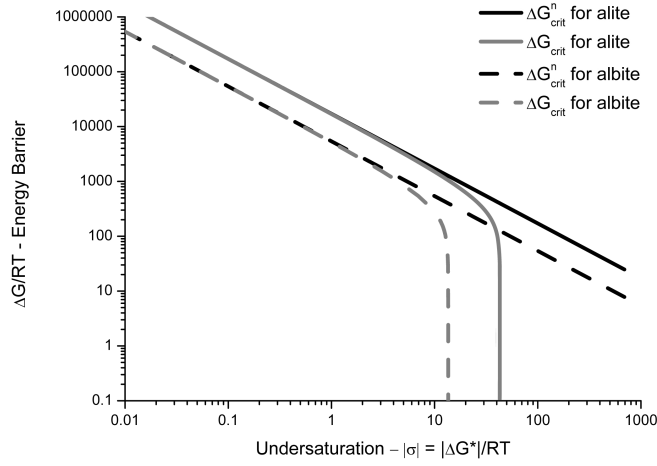


Figure 3.23: Dependence of the activation energy barriers for the nucleation of 2D-vacancy islands (ΔG_{crit}^n) and etch pit formation (ΔG_{crit}) with different assumed solid-liquid interfacial energies; $\gamma = 500 \text{ mJ.m}^{-2}$ for albite and $\gamma = 1060 \text{ mJ.m}^{-2}$ for alite. The other parameters are kept the same as in Figure 3 except for the molar volume, which is equal to $70 \text{ cm}^3.\text{mol}^{-1}$ for alite. The intersection between the abscissa and the plain curves give the values of $|\Delta G_{\text{crit}}^*/RT$ above which etch pits can form at dislocations.

3.5.2 NMR studies of early hydration of C_3S

Cross-polarisation NMR studies of tricalcium silicate hydration [36] have shown that monomeric hydrated silicates are formed at early age of hydration. It is only after the end of the induction period that hydrated silicate dimers were detected. From the quantity of hydrated monomer it was calculated that if these belong to a protective layer, the average thickness would be around 40 nm. Rodger and co-workers [36] also performed the same type of measurements on systems with calcium chloride and sucrose additions. In the case of calcium chloride, the formation of this metastable C-S-H was much more rapid but the induction period was shorter, whereas in the case of sucrose, the formation of the metastable C-S-H was much lower but resulting in a very long induction period (see Figure 3.24). Therefore it appears that this primary hydrates are poorly related with the duration of the induction period.

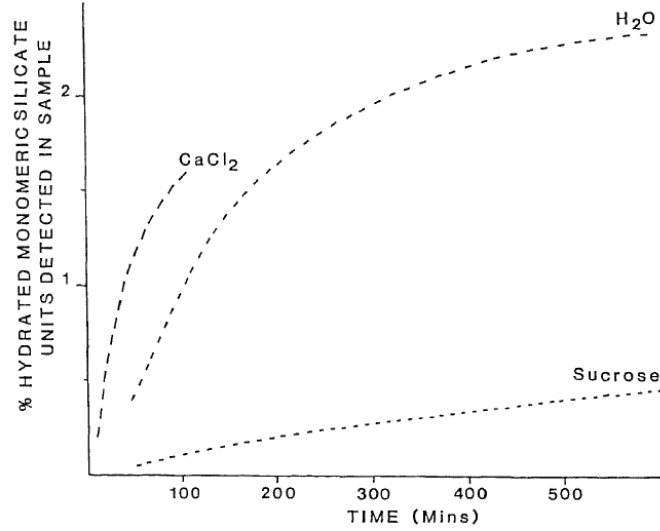


Figure 3.24: Graph showing the formation of hydrated monomeric silicate species as determined by CP NMR during the hydration of C_3S in the absence and presence of admixtures. Adapted from [36].

Even if primary hydrates have been detected after a few minutes of hydration by NMR, this technique cannot provide any information on the spatial distribution of these hydrates. Recently Zingg and co-workers observed hydration products after 24 minutes of hydration by FIB [39]. However, on their micrographs these hydrates did not form a continuous layer on the surface (Figure 3.27).

3.5.3 Calculations of dissolution rate

Transition state theory (TST) also called the activated complex theory (ACT) is often used to predict the rates of reactions of mineral-fluid interactions [65]. The application of TST to overall reactions requires two critical assumptions to be made concerning the nature of the overall reaction. First, a single rate-limiting reaction step must exist. This step involves the irreversible breakdown of an activated complex to form dissolved or precipitated products. Second, the rate-limiting step must be identified as an elementary reaction or a series of elementary reactions such as adsorption or hydrolysis of ions. TST predicts an exponential dependence of the reaction rate on $\Delta G_r^*/RT$, where ΔG_r^* is the Gibbs free energy of the overall reaction given by [37]:

$$f(\Delta G_r^*) = A \left[1 - e^{-\frac{n\Delta G_r^*}{RT}} \right] \quad (3.3)$$

Where A and n are general constants. It has been shown that TST cannot be used to predict rates near equilibrium conditions from those determined at high undersaturation conditions [37]. The reason for this is that TST is not able to catch the non-linearity due to the transition between dislocation-controlled to step retreat

dissolution mechanisms as illustrated for the case of albite in Figure 3.25.

Figure 3.25 shows the comparison of TST predictions (see Equation (7)) with experimental data for albite, [37]. Equation 3.3 is applied for the case of albite where the dissolution rate at high levels of undersaturation was determined as $-33.2 \cdot 10^{-12} \text{ mol.m}^{-2}.\text{s}^{-1}$. The dashed, dark grey and black lines in Figure 3.25 correspond, respectively, to values of $n=0.1, 0.5$ and 1.0 . It can be seen that it is not possible with transition state theory to correctly model rates of dissolution when the solution is close to equilibrium conditions using parameters determined from far equilibrium conditions.

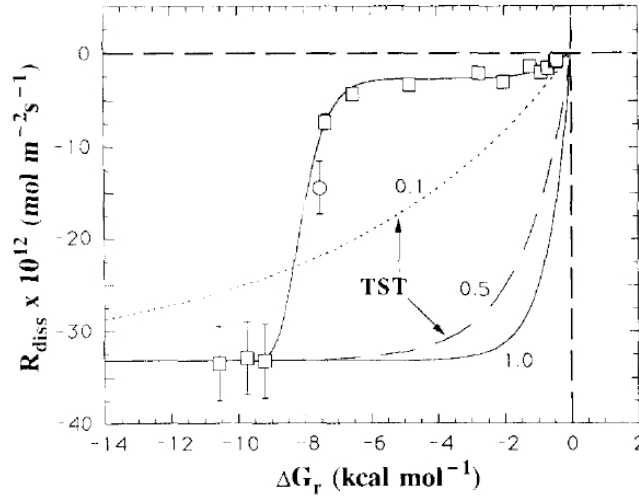


Figure 3.25: Comparison of the full dissolution theory (Equation 3.4) with experimental data and transition state theory (Equation 3.3). Albite at pH 8.8 and 80°C. (From [37]). The dotted dashed, black lines correspond, respectively, to values of $n=0.1, 0.5$ and 1.0 in Equation (6).

It is worth noting that through Equation 3.3, the TST predicts that the dissolution rate should reach a constant value at high undersaturation, which is indeed observed in Figure 3.25. The major prediction of the TST, which is the variation of the rate between low and high undersaturation is however clearly unsatisfactory. This type of conclusion was also reached for C_3S by Bullard [130], who developed a kinetic cellular automaton model that includes transition state kinetics. He found that the data could however be fitted if a metastable C-S-H layer, of which the properties have so far had to be estimated, was incorporated into the model [130]. More recently he reported that the same data could be almost equally well fitted if the C_3S surface is assumed to have a much lower solubility [131].

However, there are other ways to overcome the limitation of TST and to fit experimental data on a large range of undersaturation conditions, Lasaga proposed this general equation for the rate of dissolution of mineral [65]:

$$\text{Rate} = k_0 \cdot A_{\min} \cdot e^{-E_a/RT} \cdot a_{\text{H}^+}^{n_{\text{H}^+}} \cdot \prod_i a_i^{n_i} \cdot g(I) \cdot f(\Delta G_r) \quad (3.4)$$

where

1. k_0 is the rate constant (Average or instantaneous at $t=0$),
2. A_{\min} is the reactive surface area of the mineral,
3. $e^{-E_a/RT}$ is a term related to the temperature dependence,
4. $a_{H^+}^{n_{H^+}} \cdot \prod_i a_i^{n_i}$ with a_i and a_{H^+} are the activities in solution of species i and H^+ , respectively, n_i and n_{H^+} are the orders of the reaction with respect to these species. This represents pH dependence of the dissolution reactions and other possible catalytic effects on the overall rate,
5. $g(I)$ is a function of the ionic strength. The $g(I)$ term indicates a possible dependence of the rate on the ionic strength (I),
6. $f(\Delta G_r)$ relates the velocity of the dissolving steps from a dislocation core as a function of the change in Gibbs free energy.

Damidot et al. [38] showed that the rate of dissolution of alite varies considerably with pH and calcium ions concentration. They estimated the dissolution rate with equation 3.5 derived from the general one proposed by Lasaga [12] (equation 3.4) but omitting the term $f(\Delta G_r)$.

For this, they fitted the coefficients k_0 and n_i for hydroxides and calcium ions with the experiments in water and 5.75 mmol/L of $Ca(OH)_2$. This led to values of 70 $mmol.m^2.s^{-1}$ for k_0 and to 0.465 and -0.33 for the exponents of the H^+ and $CaOH^+$ activities respectively. Finally they propose that the C_3S dissolution can be written as:

$$\frac{dC_3S}{dt} (mmol.L^{-1}.s^{-1}.m^{-2}) = 70.A. (SI - 1) . [H^+]^{0.465} [CaOH^+]^{-0.33} \quad (3.5)$$

The rate of dissolution was measured to be 10.92 $\mu mol.m^2.s^{-1}$ in deionised water and decreases by almost a factor 5 compared to a 5.75 mM lime solution and by a factor 218 for saturated lime conditions. The latter measurement leads to a rate of dissolution of 0.05 $\mu mol.m^2.s^{-1}$ which is 10 times lower than the calculated value using the above equation (see Table 3.1). Damidot and co-workers [38] attributed this discrepancy to the precipitation of a surface layer on C_3S .

Table 3.1: Average and calculated dissolution rate for pure C_3S in different lime solution after 0.1 second of dissolution $W/S=0.5$ and $SSA=4625 \text{ cm}^2.\text{g}^{-1}$. (Adapted from [38].)

Electrolyte	Water	$\text{Ca}(\text{OH})_2$ 5.75mmol/L	$\text{Ca}(\text{OH})_2$ 22mmol/L
Average rate $\mu\text{mol.m}^2.\text{s}^{-1}$	10.92	2.07	0.05
Average rate $\mu\text{mol.m}^2.\text{s}^{-1}$	10.92	2.01	0.54

However, equation 3.5 does not take into account the $f(\Delta G_r)$ factor. This factor relates the velocity of the dissolving steps from a dislocation core as a function of the change in Gibbs free energy and depends on the ΔG_{crit}^* term (for more details see [17]). Nonlinearity in the rate of dissolution should appear around ΔG_{crit}^* which is the barrier for etch pit to open up and substantial reduction in the rate of dissolution should be noticed as it can be observed on Figure 2.24 and 3.25 [2]. $|\Delta G_{\text{crit}}^*|$ values are rather large for minerals (from 2 to several kJ/mol) [17], [79]. Neglecting this parameter could easily account for the error of one order of magnitude between the rate calculated at higher calcium hydroxide concentration (22 mmol $\text{Ca}(\text{OH})_2$) and the experimental value. Lasaga and Lüttge [17] themselves underline that linear extrapolation of data from regions of high undersaturation to the equilibrium point (i.e, rate=0 at $\Delta G=0$) will substantially overestimate the dissolution rates as close to equilibrium conditions are approached.

3.6 Proposed mechanisms of early hydration of alite

New experiments and a reassessment of previously published results show that, the saturation state of the solution has a critical influence on the rate of reaction of alite. For alite in contact with deionised water, the undersaturation coefficient is initially very large. All the dissolution mechanisms discussed in the previous chapter (2d vacancy island formation, etch pit and step retreat) are active leading to the fast release of ions into solution and a high rate of heat evolution, but also to a rapid increase in the concentration of ions in solution and so a decrease in undersaturation. During this initial period of high undersaturation etch pits could form on plain surfaces (regime III, Figure 2.23), but this period of very large undersaturation will quickly give way to the regime in which etch pits form only at the point of emergence of crystallographic defects with the surface. This corresponds to zone II in Figures 2.23 and 3.26. After a few minutes, as the concentration of ions continues to increase, decreasing therefore the undersaturation below that needed to overcome the activation energy (ΔG_{crit}) for the creation of etch pits; the dissolution slows down as it is limited to step retreat at pre-existing steps. This transition from fast to slow dissolution is symbolised by the arrow 1 in Figure 3.26. This process corresponds

to the onset of the period of low chemical activity, the “induction period”. Thus dissolution theory can explain the onset of the induction period without having to invoke additional mechanisms such as the formation of a protective membrane.

It is interesting to note that the transition to slow dissolution occurs at concentrations around those of saturated calcium hydroxide, as shown schematically in Figure 3.26. For this reason it is not possible to verify the existence of the plateau of slow dissolution as more concentrated solutions will precipitate calcium hydroxide and lower the concentration. In the regime undersaturated with respect to calcium hydroxide, the rate of dissolution varies smoothly as found experimentally by Damidot et al. [38] (Figure 3.26). During the induction period, the solution is progressively enriched in calcium and hydroxides, causing the system to approach the critical supersaturation of Portlandite (arrow 2 in Figure 3.26).

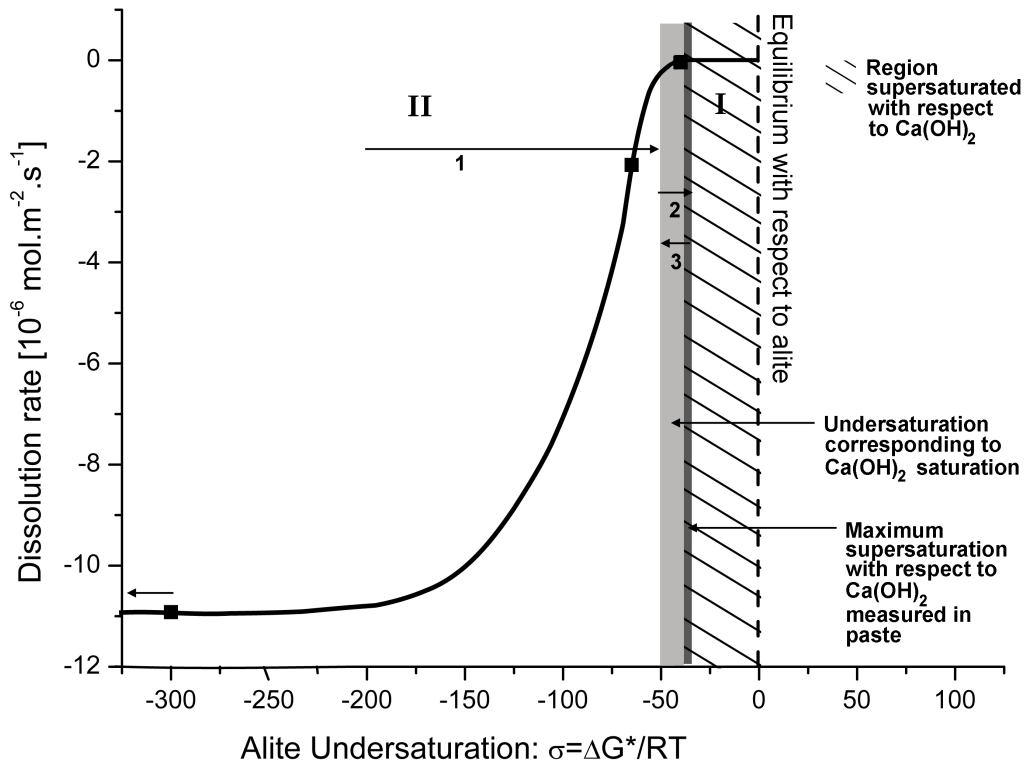


Figure 3.26: Schematic representation of the rate of dissolution of alite as a function of the undersaturation. The black squares represent the experimental data obtained by Damidot and co-workers (see Table 3.1) [38] and the plain curve is the assumed evolution of the rate of dissolution of alite as a function of the undersaturation. The light grey zone corresponds to Portlandite saturation which is assumed to be close to $\Delta G_{crit}^*/RT$ (the width corresponds to the uncertainty in silicate ions concentration). This value delimits the fast dissolution regime controlled by etch pit formation (zone II) and the slow regime of dissolution where only step retreat takes place (zone I). Arrows 1, 2 and 3 show the evolution of the undersaturation during respectively the fast dissolution stage, the induction or “dormant” period and finally the acceleration period.

As the solution quickly becomes saturated with respect to C-S-H, precipitation of this hydrate may occur, but this is not responsible for the onset of the induction

period (strong reduction in rate of heat release). To support this argument, it can be noted that, as observed in the morphological studies presented here (Figures 3.8, 3.9 and 3.10) and also reported by Zingg and co-workers (see Figure 3.27)[39], these primary hydrates do not form any visible continuous layer around the anhydrous grains.

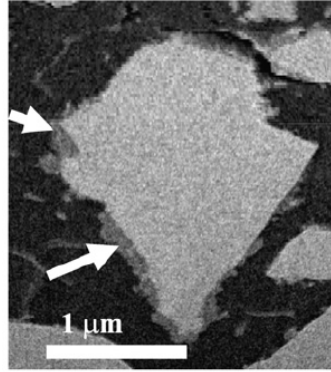


Figure 3.27: Cryo-FIB cross sections where the arrows indicate the discontinuous hydration layer (cement suspension containing 0.2% of polycarboxylate-ether-based superplasticizers, after 24 min of hydration) From [39].

At the end of the induction period the growth of hydrates lowers the concentration of ions in solution (increased undersaturation). This increases alite undersaturation and brings the system back towards undersaturations where alite dissolution may take place in mode II (arrow 3 in figure 3.26). However, at this stage it is most probably the hydrate growth that becomes rate controlling. It appears that the induction period ends when a critical amount of dissolution has occurred as a lower heat output during the induction period corresponds to a longer induction period as seen in our experiments on the annealing of alite, and in studies by Costoya [26] of alites with different particle sizes. However, the exact process which brings the induction period to an end is still unclear. Logically, two possibilities can be suggested: either the precipitation of calcium hydroxide triggers rapid reaction as it acts as a sink for calcium ions and again increases the undersaturation of the solution with respect to alite; or C-S-H starts to grow in a rapid manner (which could be due to enough surface having been created or to the formation of “stable nuclei”).

Figure 21 presents schematically the hydration process at very early ages at a microscopic level.

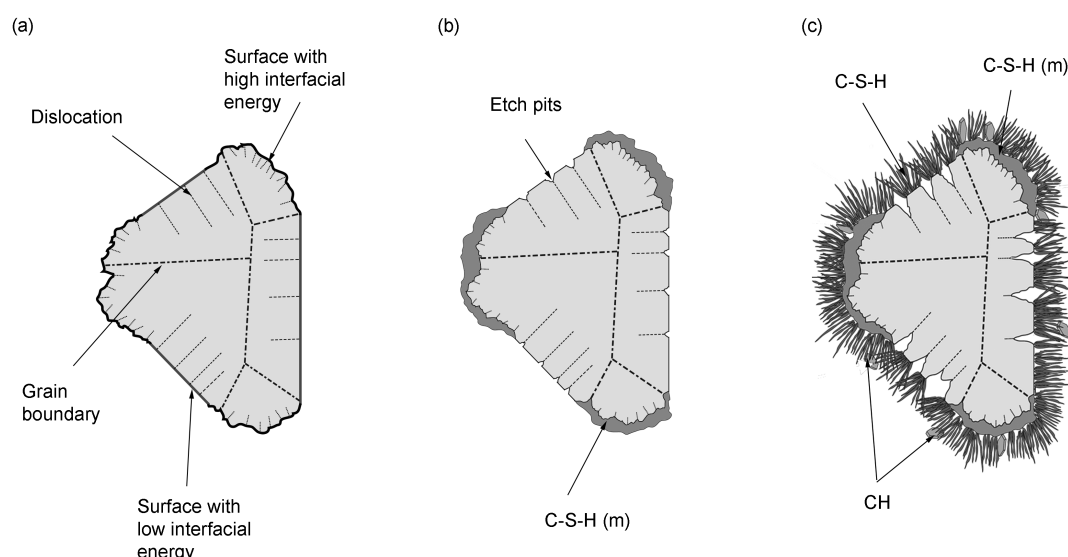


Figure 3.28: Hydration scheme at early age of reaction. (a) An alite grain is represented in cross section. Dislocations and grain boundaries are represented by dashed lines. A simple differentiation is made between areas of high surface energy (in black) and surfaces of lower surface energy (in grey). (b) When the alite grain is put in contact with water, we assume that some primary hydrates will precipitate (metastable C-S-H in dark grey) but not as a continuous membrane. Areas of lower surface energy might remain only partially hydroxylated and will therefore present some etch pitting at the point of emergence of dislocations. (c) Finally, when supersaturation with respect to stable hydrates is reached, stable nuclei of C-S-H and CH start to grow, which marks the end of the induction period and the beginning of the acceleration period. Metastable C-S-H might remain present at least during the first 20 hours as detected by Rodger and co-workers by NMR cross-polarisation [36].

In regard to the above proposed mechanism of alite hydration, it is clear that any change of the critical undersaturation with respect to alite, or of the critical supersaturation with respect to portlandite, can be expected to have a profound impact on alite hydration kinetics.

3.7 Summary

There are two outstanding questions regarding the early hydration of C_3S and alite. The first concerns the very fast deceleration of reactivity that follows the burst in reactivity after contact with water. The second concerns the onset of the acceleration period that follows a period of low chemical reactivity.

In this chapter we show how the dissolution theory developed in the field of geochemistry can explain the initial slowdown in reaction without the need to suppose the formation of a protective membrane. When the level of undersaturation drops below that needed to provide enough energy for the nucleation of etch pits at dislocations, the rate of dissolution becomes slow as atoms may dissolve only from preformed steps.

We provide evidence for this mechanism in the form of new experimental obser-

vations and a re-examination of results in the literature, which show:

1. A very strong dependence of the rate of dissolution on the concentration of the solution.
2. The formation of numerous etch pits on alite surface mixed with deionised water, in contrast to a dominance of smooth surfaces with formation of steps in the case of lime saturated solutions.
3. A strong influence of defect density on the rate of dissolution during the induction period and therefore its length and the variation in density of etch pits as a function of crystallographic orientation.

Experimental data from other minerals exhibit a non linear step change in dissolution rate at levels of undersaturation significantly larger than expected from transition state theory. Comparison of the typical energy barriers for etch pit formation from such minerals to the case of alite indicates that the large difference in concentration between typical hydrating pastes and the equilibrium solubility of alite falls within the magnitude expected for a dissolution limited by the formation of etch pits. Such energy barriers also explain inconsistencies in dissolution rates extrapolated from very high levels of undersaturation.

The mechanism responsible for the onset of the acceleration period remains open, but this appears to occur after a critical amount of dissolution. The precipitation of Portlandite or the onset of rapid growth of C-S-H (which could just be due to the development of a sufficiently large C-S-H surface) are possible causes for the onset of acceleration. The time to reach either event is affected by the change of dissolution rate discussed in this chapter.

The rate of dissolution may also be affected by the presence of certain salts such as in the case of calcium chloride. The implications of these findings in terms of working mechanisms of accelerators and retarders remain to be studied in detail.

Chapter 4

Effect of Mixing on the Early Hydration of Cementitious Systems

Mixing is a crucial step for any concrete application. Poor mixing will result in large inhomogeneities with the persistence of agglomerates [132]. This will reduce the workability and lead to a poor packing of the cement particles resulting in a larger amount of porosity. This can lower mechanical and durable properties.

Many rheological measurements have been done to optimise the mixing process and improve the workability of cement slurries. Control of the viscosity by addition of specific organic molecules has led to an engineering revolution in the mixing and casting processes of cementitious materials and have lead to an enhancement of mechanical properties through the reduction of the excess of water only added to improve the workability. Therefore the impact of hydration on the rheological properties has been the main focus of research rather than relating the influence of mixing or shear rate on the kinetics of hydration.

A specific study focused on the influence of mixing conditions on rheological properties was undertaken by Williams and coworkers [132]. They studied the shear-induced structural breakdown in fresh cement paste through the evaluation of hysteresis loop areas. Fresh cement pastes were mixed for 1 minute at different constant rates, re-homogenised before being subjected to a controlled increase and decrease of shear rates, producing a hysteresis. The resulting area was proportional to the degree of structure remaining after the first mix. Their measurements suggest that inhomogeneities due to the agglomeration of cement particles are significant when the paste is poorly mixed such as hand mixing. In contrary, high shear mixing conditions seem to limit considerably these inhomogeneities and better disperse the cement particles.

Dollimore and Mangabhai [133] reported that increasing mixing time accelerated the reactions of hydration. However, no attempt was made in order to explain the mechanisms responsible for this acceleration of the silicate reaction.

The mechanisms by which the hydration kinetics are affected are still not understood. Therefore the aim of this chapter is to present a systematic study on

the influence of the mixing procedure as well as of the additions of aggregates or admixtures on the kinetics of hydration of pure alite and Portland cement systems. The results obtained are also discussed from the perspective of the dissolution theory.

4.1 Effect of speed of mixing on the hydration kinetics of alite pastes

The evolution of the heat released during the hydration of alite pastes mixed with deionised water ($w/c = 0.4$) at different speeds for two minutes are presented in Figure 4.1. Hand mixing was carried out with a common plastic spatula and mechanical mixing with a steel paddle having six blades with speeds ranging from 200 rpm to 2000 rpm. All mixes were ex-situ.

The mixed quantities were kept to 46 g for pastes and 96 g for mortars ($c/a_{gg} = 0.66$) in order to avoid variations due to mass change. Temperature measurements were made before and after each mixing step in order to assess the effect of the energy input induced during mixing. This effect on the early hydration remains minor as will be shown later. Samples of 10 grams were inserted in the isothermal calorimeter to monitor their kinetics of hydration.

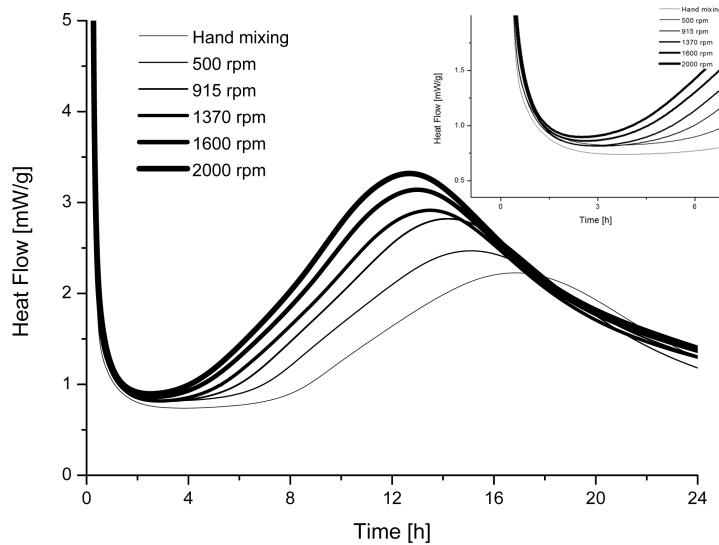


Figure 4.1: Evolution of the kinetics of hydration for an alite paste ($w/c=0.4$) mixed two minutes at various mixing speeds.

The main effects of an increase in mixing speed are a shortening of the induction period and an increase of the heat flow during the acceleration period. The overall dissolution rate should increase during the stages taking place before the onset of the acceleration period as the shearing conditions increase during the mix. Previously we have shown the different dissolution mechanisms that can take place during reaction. To understand the effects that mixing may have it is necessary to examine the process occurring on an atomic scale during dissolution. These can be summarized in four

distinct steps [105]:

1. Transport of atoms through the solvent phase
2. Detachment of atoms from the surface
3. Movement of adsorbed atoms on or into the surface
4. Detachment of atoms from edges or kinks

Processes 2-4, which themselves may involve several elementary steps, are usually labelled surface processes to distinguish them from process 1, the long-range transport of atoms and/or the possible movement through a diffusion boundary layer. The task is then to differentiate surface processes from transport processes and decide which, if any, controls the rate of dissolution. Transport and surface reactions occur normally in series and the slowest process should control the rate of the overall dissolution rate. There are some clues that indicate whether the dominant mode is transport or surface controlled. Experimentally, if the rate of dissolution is surface controlled, there should be nearly no phase gradients between the surrounding medium and the dissolving phase. It is however difficult in aqueous solutions to measure concentration gradients; nevertheless, in this case, a method to determine if the surface reactions control the dissolution reaction is to vary the mixing/stirring rate [40], [105]. Changing the mixing/stirring rate varies the thickness of the stationary boundary layer or the so-called electrical double layer through which the molecules must diffuse from the dissolving surface to the homogeneous bulk solution. Diffusion in the interfacial layer is believed to be slower than in the bulk solution [40]. If the rate is independent of the stirring rate, it is then likely that the reaction rate is surface controlled. A theoretical rule of thumb proposed by Berner [44] states that for aqueous solutions, minerals with low solubility dissolve by surface control whereas high solubility minerals dissolve by transport control. His results are given in Table 4.1.

From the results presented in Figure 4.1, it appears that the overall rate of dissolution is transport controlled, at least to a certain extent. This is also not surprising as we already know that alite is extremely reactive and its solubility constant, K_{SP} , is 3 [128] which would place alite beside $\text{Na}_2\text{CO}_3 \cdot 10 \text{ H}_2\text{O}$ and $\text{MgSO}_4 \cdot 7 \text{ H}_2\text{O}$ in Table 4.1. More interestingly is the fact that during the first dissolution stage of hydration, the surface of alite should be surrounded by a gradient of ions concentration as already proposed by Tardos [65] and Skalny [58].

Table 4.1: Limiting process for various substances arranged in order of solubilities in pure water [44]

Substance	Solubility
Surface reaction control	
KAlSi ₃ O ₈	3.10 ⁻⁷
NaAlSi ₃ O ₈	6.10 ⁻⁷
BaSO ₄	1.10 ⁻⁵
SrCO ₃	3.10 ⁻⁵
CaCO ₃	6.10 ⁻⁵
Ag ₂ CrO ₄	1.10 ⁻⁴
SrSO ₄	9.10 ⁻⁴
Opaline SiO ₂	2.10 ⁻³
Mixed Control	
PbSO ₄	1.10 ⁻⁴
Transport control	
AgCl	1.10 ⁻⁵
Ba(IO ₃) ₂	8.10 ⁻⁴
CaSO ₄ .2 H ₂ O	5.10 ⁻³
NaSO ₄ .10 H ₂ O	2.10 ⁻¹
MgSO ₄ .7 H ₂ O	3.10 ⁰
Na ₂ CO ₃ .10 H ₂ O	3.10 ⁰
KCl	4.10 ⁰
NaCl	5.10 ⁰
MgCl ₂ .6 H ₂ O	5.10 ⁰

The surface reactions are therefore faster than the transport reactions when the solution is highly undersaturated. However, surface reactions progressively become the limiting process at lower undersaturation as the associated mechanism of dissolution takes place by step retreat which is the slowest dissolution mechanism. Note also that stirring of an etchant invariably leads to a change in the morphology of dislocation etch pits [40].

In order to test the validity of this hypothesis, alite was mixed again at different speeds but starting with a solution already saturated with lime. Therefore, no concentration gradient should exist in that particular case and the duration of the induction period should be insensitive to the rate of mixing. The results are presented on Figure 4.2.

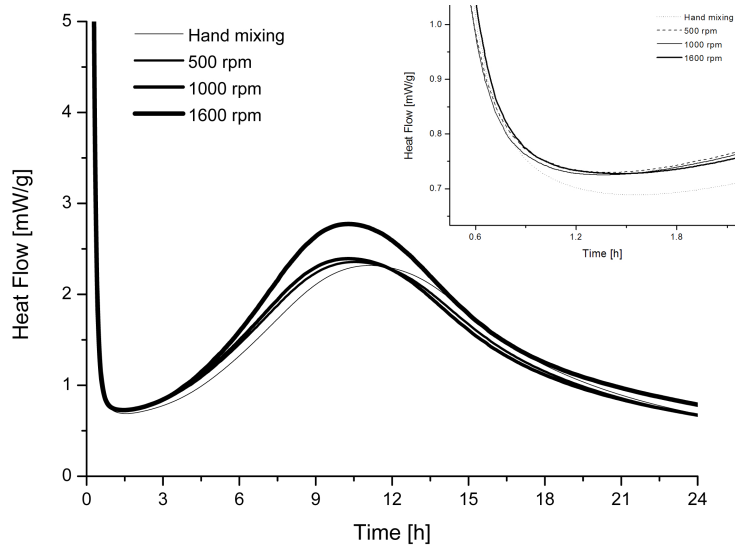


Figure 4.2: Evolution of the kinetics of hydration for an alite paste ($w/c=0.4$) mixed two minutes at various mixing speeds starting with a saturated lime solution.

It can be seen that the rate of mixing does not affect the length of the induction period when the initial solution is already saturated with lime. There is however a slight delay for the hand mixed system which might reflect a poor mixing process resulting in a poor deagglomeration of the alite particles. This would lower the amount of anhydrous surface in contact with water and induce a slightly longer induction period. The induction period is here much shorter than in Figure 4.1. This is not due to an effect of the saturated lime solution but to the fact that the grinding procedure was not kept the same between this alite batch and the other ones and therefore absolute comparison is not possible. However materials were kept the same for each type of experiments which enables a relative comparison.

These results are as expected: at high undersaturation, transport of the chemical species is the rate limiting process as the surface reactions by formation of etch pits at the point of emergence of dislocations are very fast and at lower undersaturation, the slow mechanism of dissolution by step retreat becomes the rate limiting process of the overall rate of dissolution as no more concentration gradient exists.

With these two simple experiments, it is shown that the overall rate of dissolution up to the end of the induction period is limited by two different processes. It is primarily limited by a transport process. As the anhydrous phase quickly dissolves by formation of etch pits at high undersaturation, the concentration at the interface will quickly approach the critical concentration at which the surface reactions will slow down and these latter progressively become the rate limiting factor of dissolution. This change in solution concentration with time will ultimately lead to the step retreat mechanism which is then the rate limiting process. However, when the initial solution is already saturated with lime, etch pits cannot form as the main dissolution mechanism is already the one step retreat.

Therefore, mixing rate influences the overall dissolution rate if transport is the limiting process. This enhancement of dissolution would be due to a reduction of

the thickness of the interfacial layer as suggested by Sangwal [40], schematically presented on Figure 4.3, and diffusion through a thinner boundary layer should enhance the overall dissolution rate.

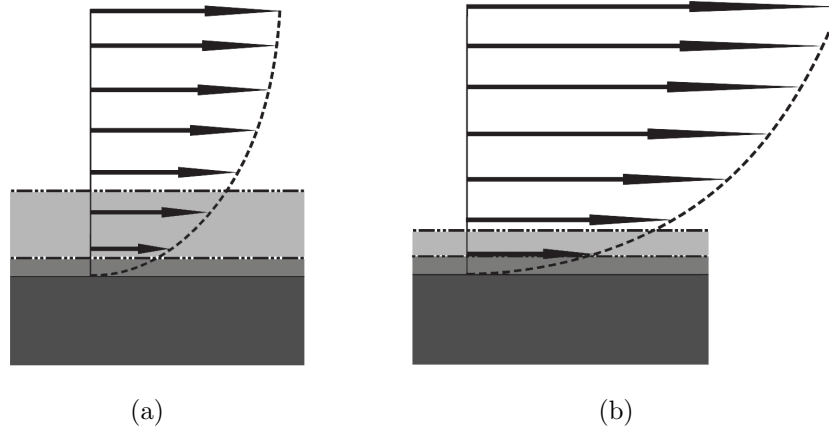


Figure 4.3: Schematic representation of the velocity profile of the surrounding solution close to the surface of a cement grain for a) low shearing conditions and b) high shearing conditions. The dark grey area represents alite and the medium and light greys represent schematically the Stern and diffuse electrical layers respectively. It can be noticed that the double layer becomes thinner for higher shearing conditions according to Sangwal [40].

Based on the theory of early hydration presented in the last chapter, the effect of mixing can be well explained by the dissolution theory. However, the influence of mixing rate on the length of the induction period as well as on the acceleration period has to be explained. It can be observed on Figure 4.1 that the length of the induction period is reduced as the speed of mixing increases and the rate of heat flow during the acceleration period increases with the speed of mixing (see Figures 4.1 and 4.2). Results presented on Figure 4.1 indicates that nucleation and growth of the hydrates is enhanced by a higher initial dissolution rate. However, this process cannot be the only enhancing factor as the rate of dissolution remains the same in saturated lime conditions (see Figure 4.2) but the highest mixing speed still presents a higher rate of heat flow during the acceleration period. Garrault and co-workers [10] have proposed that rate of reaction during the acceleration period may be enhanced by a higher nuclei density of C-S-H. More recently, Thomas and co-workers [41] have shown that small addition of pure C-S-H to pure tricalcium silicate causes a significant acceleration of the early hydration kinetics. They proposed that the C-S-H seeds increase the amount of early hydration by causing product to form in the capillary pore space away from the C_3S surfaces, where it does not interfere with the dissolution of C_3S [41].

When the initial solution is deionised water, a higher initial dissolution rate will homogenise more rapidly the surrounding solution and it can be expected to produce a higher density of nuclei or even promote homogeneous nucleation. In the case of a saturated lime solution, only the last hypothesis might remain valid. It is also possible that the primary hydrates forming very early on may be ripped off the anhydrous surface mechanically and could therefore increase the available surface for

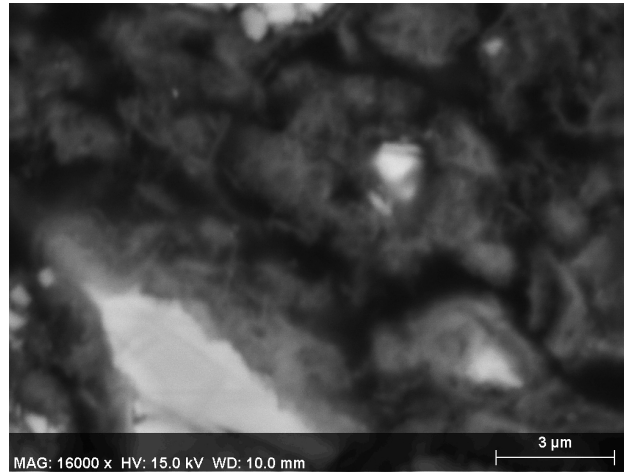
the formation of nuclei. These explanations appear to be the most probable but it remains very difficult to support them experimentally, at least on paste systems.

Observation of alite microstructure mixed at different speeds

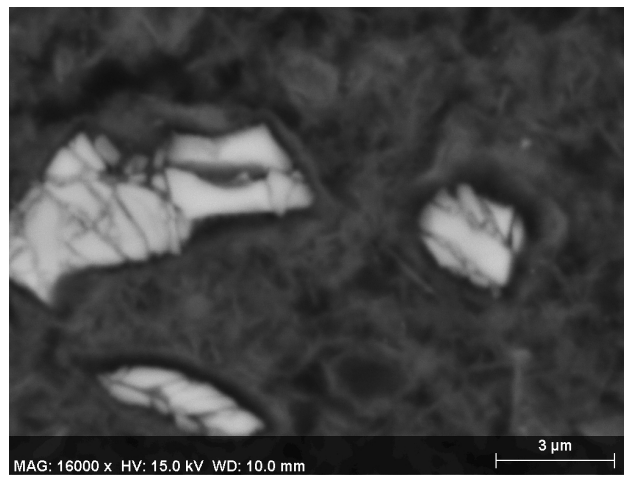
In this section, the influence of mixing speed on the microstructural development of alite systems mixed twice is presented. The first mixing step lasted 2 minutes followed by a delay period of 13 minutes and finally followed by another 1 minute of mixing at the same speed. The motivation for a two mixing steps procedure is explained in a later section. The hydration was stopped at the maximum heat flow of the acceleration period by freeze drying. It can be observed that as the shear forces increase during the mix, the matrix is much denser at the end of the acceleration period. This is in good agreement with a higher density of nuclei and the promotion of nucleation in the surrounding solution as what Thomas and co-workers [41] shown in their seeding experiments.

There is an important difference between samples mixed mechanically compared to the hand mixed one since this latter still shows some capillary porosity. Small crystals of CH embedded in the C-S-H matrix are present in larger amount for pastes mixed at 915 rpm and 1600 rpm compared to the hand mixed system. The microstructure appears even finer at mixing conditions of 1600 rpm. This observation agrees with the fact that the nucleation rate is enhanced when the shearing conditions are more intense as the rate of heat evolved during the acceleration period measured by isothermal calorimetry becomes steeper and as the matrix becomes denser. Homogenisation of the ions in solution is enhanced for higher shearing conditions as Portlandite crystals becomes much finer as well as well dispersed into the matrix when subjected to a mix at 1600 rpm which tends to indicate that supersaturation with respect to this phase is quite homogeneous across the solution as the shearing conditions increase. This microstructural evidence supports that nucleation rate is enhanced either due to a higher and more homogeneous concentration reached in the surrounding solution which might lead to homogeneous nucleation or that a mechanical effect sweeps the nuclei into solution which in both cases lead to a shorter induction period.

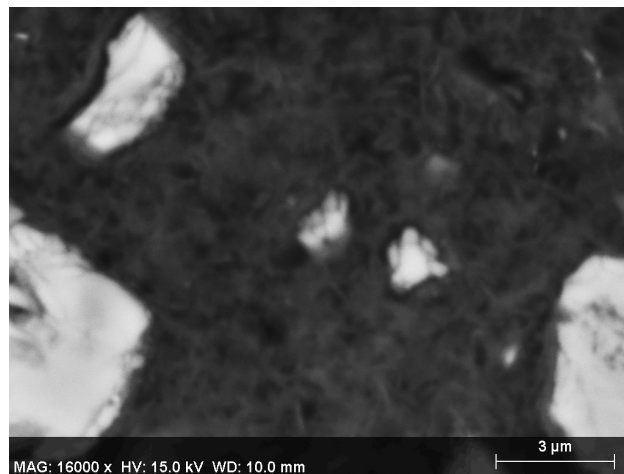
However, these micrographs do not support the view of a diffusion limited reaction through a layer of hydrate at the end of the acceleration period since in two cases, the matrix is completely filled with hydrates. Even in the case of hand mixing, the matrix is quite dense and does not just present a rim around the alite grains. Simulations using the diffusion controlled approach in order to explain the deceleration period of alite systems with different particle size distributions have shown that diffusion coefficients vary over an order of magnitude, indicating that a large variation in the transport properties of C-S-H would need to be assumed [134]. From the micrographs obtained during this study, the idea of densification process as presented by Bishnoi and Scrivener [6], [134] appears a much more likely limiting factor.



(a)



(b)

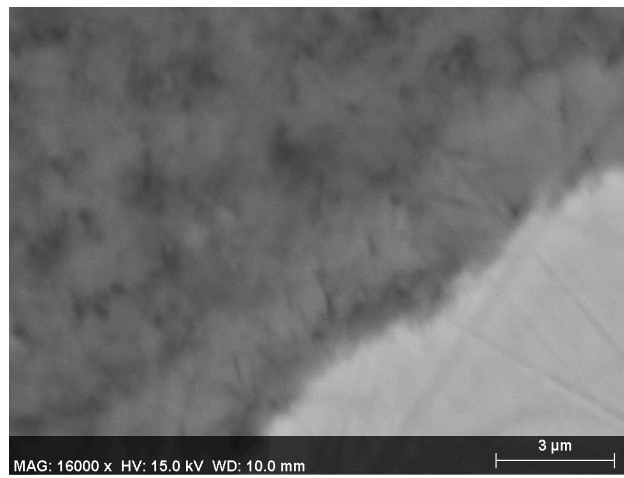


(c)

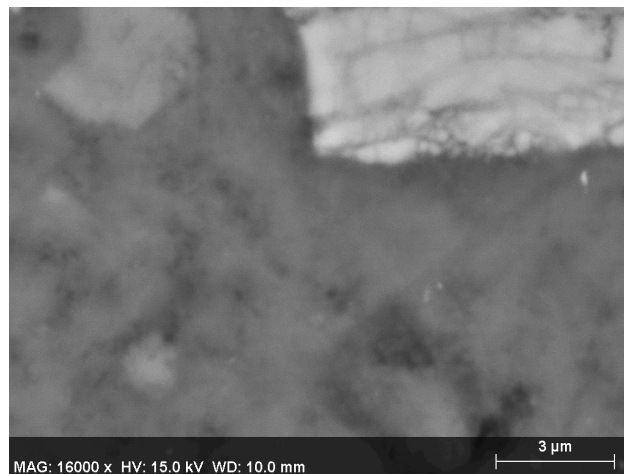
Figure 4.4: Micrographs of polished section of alite samples at the maximum heat flow mixed twice by (a) hand mixing (16h00 of hydration), (b) at 915 rpm (13h30 of hydration) and (c) at 1600 rpm (12h30 of hydration).



(a)



(b)



(c)

Figure 4.5: Micrographs of polished section of alite samples at 7 days of hydration mixed twice by (a) hand mixing, (b) at 915 rpm and (c) at 1600 rpm.

Figure 4.5 shows the microstructures of alite systems at 7 days of hydration. It

can be seen that in the hand mixed specimen some visible capillary pores are still present whereas the two other mixing conditions lead to almost the same dense microstructure at these later ages of hydration. For systems mixed mechanically, even if differences are observable at early age, microstructures seem to become similar over time but the higher mixing conditions still appear to lead to a denser matrix. This points to a densifying process of the cementitious paste. On the other hand, it is obvious that poor mixing does have an influence on the microstructural development since large inhomogeneities are still observed at later ages.

From the results obtained by this series of experiments, it is very likely that the induction is brought to an end by the massive precipitation of hydrates, either C-S-H or CH, but the question of what allows it remains open. The results obtained by C-S-H seeding experiments shows that C-S-H precipitation can efficiently bring the induction period to an end or even eliminate it as shown in Figure 4.6 [41]. The addition of C-S-H seeds are efficient nucleating agents and can eliminate the induction period as growth can take place directly. However we have shown in our annealing experiments that a true induction period can exist without the addition of retarding admixture. Rodgers et al. [36] have also shown that polymerisation of silicate units was not instantaneous. Therefore, we can only conclude that a critical amount of reaction has to proceed before the onset of the acceleration period can take place.

Whether it is the precipitation of CH or C-S-H that brings the induction period to an end, these stable hydrates will consume the released ions and become the rate determining factor of the hydration process during the acceleration period. We therefore cannot conclude to an exact mechanism to explain the onset of the acceleration period.

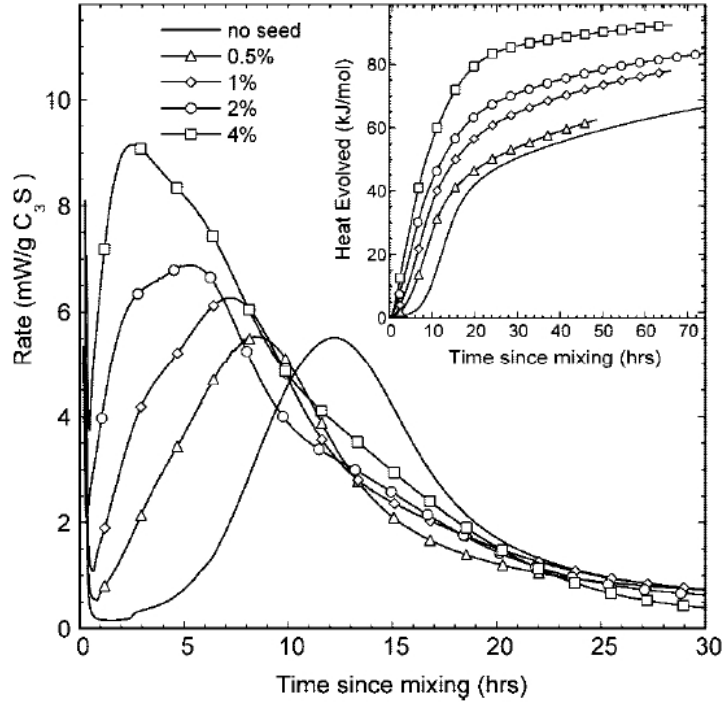


Figure 4.6: Effect of C-S-H seed made with a molar Ca/Si ratio of 1 on the early hydration kinetics of C_3S hydration. The seed amounts refer to the mass of solid C-S-H per mass of C_3S . From [41].

4.2 Influence effect on real cementitious systems

In this section we will discuss the influence of mixing speed and procedures on the early hydration of different cementitious systems. The effect of different types of admixtures (either retarding/superplasticizing or accelerating admixtures) with or without addition of aggregates (silica beads of narrow particle size distribution) will be tested.

4.2.1 Portland Cement systems

The same series of experiments were replicated using Portland cement (Siegentaler, see Annex II for chemical composition). As PC generally has an alite amount ranging between 50 and 70% percent by mass, the kinetics of hydration are dominated by this phase. Therefore similar results found for alite systems are expected to be observed for PC systems.

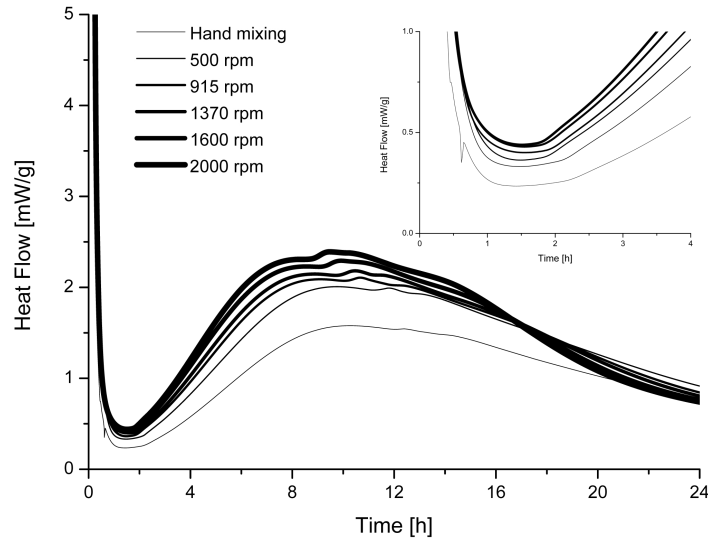


Figure 4.7: Evolution of the kinetics of hydration for an PC paste ($w/c=0.4$) mixed two minutes at various mixing speeds.

Figure 4.7 shows the influence of the mixing speed on the kinetics of hydration of PC paste. The same features as in the pure alite system are encountered. The induction period is shortened and the rate of heat flow increases as the speed of mixing increases. Therefore the same assumptions as the ones for the pure alite system can be made. One can also see that at higher stirring rate, the acceleration of the hydration is not as pronounced as at lower range of mixing rate. This would mean that the thickness of the diffusion boundary layer can no more be significantly reduced at these shearing conditions. However, the system is not yet limited by surface reactions even if there is almost no more enhancement of the hydration kinetics as acceleration of these latter is still possible at higher shearing conditions, for instance when aggregates are added (see Figure 4.8).

In this pure PC system, a series of minors humps are observed. These humps are related to the renewal of the aluminate hydration. It can be seen that aluminate hydration is also accelerated and the maximum heat flow associated with these reactions also increases with the speed of mixing. However, there is still a lack of knowledge as to the reactions taking place at that particular moment. It has been proposed that there is a reprecipitation of ettringite [1].

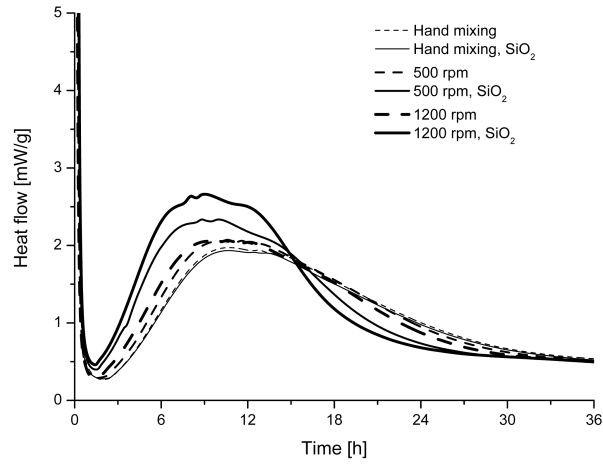
Influence of adding silica beads on PC systems

Mortars were produced in which the typical aggregates were replaced by silica beads (Type S, Sigmund Lindner GmbH) of different narrow particle size distributions with a cement to aggregate weight ratio of 0.66. The w/c was set to 0.4 for all mixes and the mixing time was kept at two minutes. As shown previously, PC systems behave similarly to alite ones, both are presented for comparison.

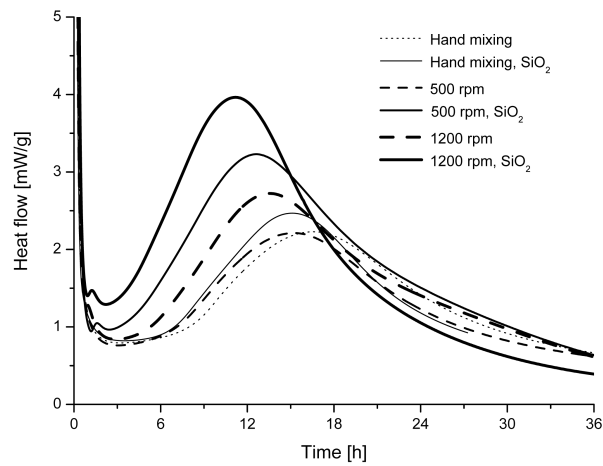
Table 4.2: Characteristics of silica beads.

Diameter (mm)	Bulk density (g.cm^{-3})	Mean specific surface area (g.cm^{-2})
0.1 - 0.2	1.52	$6.3.10^{-3}$
0.2 - 0.3	1.51	$8.8.10^{-3}$
0.3 - 0.4	1.51	$1.25.10^{-2}$
0.4 - 0.6	1.50	$1.5.10^{-2}$
0.5 - 0.75	1.49	$2.2.10^{-2}$

On Figure 4.8, a comparison is made between pastes and mortars containing silica beads of size ranging from 0.3 to 0.4 mm for PC and alite systems.



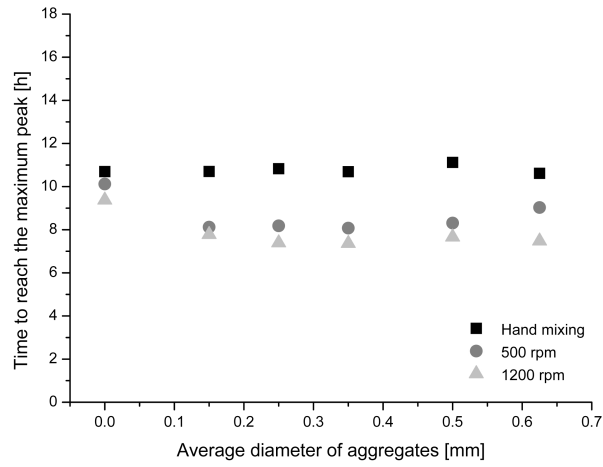
(a)



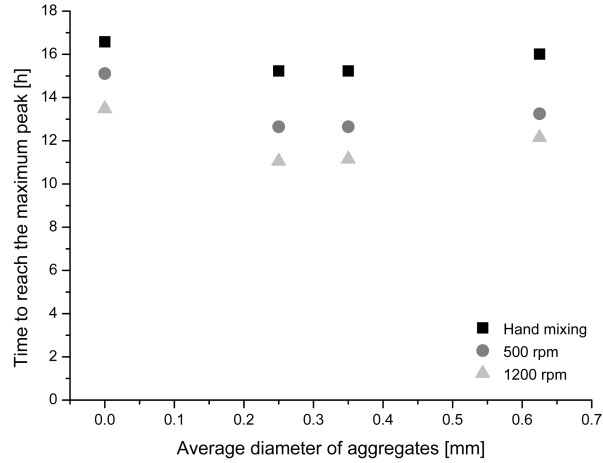
(b)

Figure 4.8: Heat of hydration for pastes (dashed lines) and mortars (solid lines) with a size of beads of 0.3 - 0.4 mm for (a) the PC and (b) the alite systems at different mixing speeds.

It can be seen that as the speed increases, the relative difference between the mortars and pastes becomes greater. The presence of the silica beads seems to accentuate the shearing conditions during mixing and further accelerate the hydration. For very high shear conditions, a small peak is seen before the onset of the induction period. This feature was already observed by Costoya [26] as well as by Makar and Chan [29]. No explanation were proposed in order to correlate this thermal event with a specific reaction. It is possible that it could be due to a subsequent endothermic reaction corresponding to the precipitation of CH as observed by Damidot [32] on dilute suspension experiments. However, this event took place after the induction period in these experiments in diluted conditions. The question remains open and further experimental or modelling work is needed to elucidate this feature. Otherwise the same accelerating features are observed as previously.



(a)



(b)

Figure 4.9: Time to reach the maximum peak of heat flow during the acceleration period in function of the average diameter of aggregates at three different speed of mixing for (a) alite systems and (b) PC systems. Note that hand mixing being negligible compared to mechanical mixing, it is graphically reported as 0.

Figure 4.9 shows the time to reach the maximum heat flow as a function of the

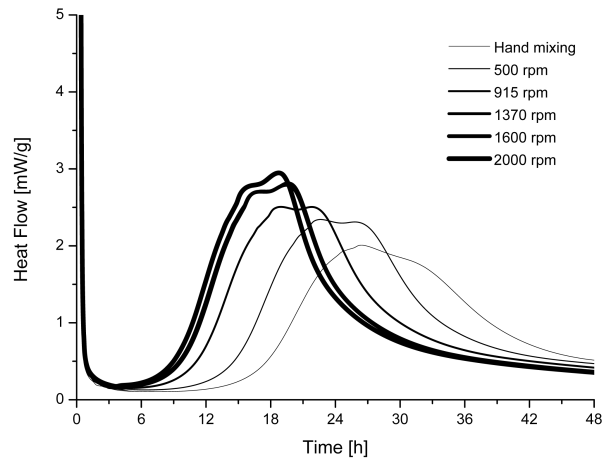
diameter of the silica beads at various speeds of mixing. The values remain almost constant with different bead sizes for each condition of speed. It is quite obvious in PC systems, that in the range of size studied, the size has no effect. However, for alite systems, it seems that finer beads slightly enhance the kinetics of hydration and also increase the maximum heat of hydration.

4.2.2 Retarded/Superplasticised PC systems

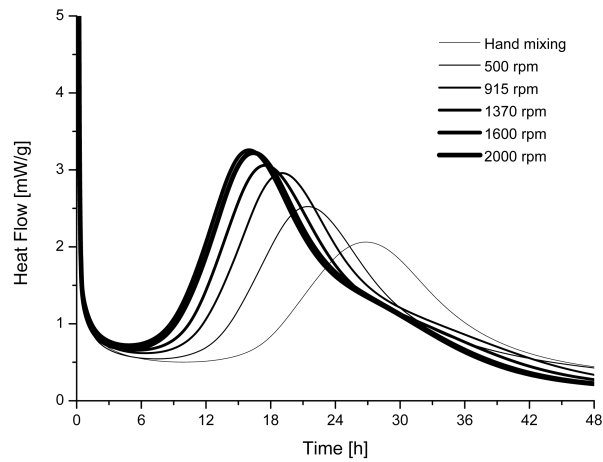
The use of setting retarders (such as gluconates and derivatives of glucose) or viscosity modifiers (superplasticizers) are nowadays commonly used in many civil engineering applications. For instance, in wet-mixed shotcrete applications, setting regulators (retarding admixture) and superplasticizers which regulate the viscosity of the system are used together to ensure a good pumpability of the mortar over a time period of a few hours. The accelerator (discussed in the following section) is then normally added directly at the nozzle. This second mixing stage induces high shearing conditions to the granular fluid. This is why the following systems used a two step mixing procedure in order to mimic real conditions occurring in shotcrete. The two steps mixing procedure was the following: 2 minutes at a given speed followed by a delay of 13 minutes before a second mix of 1 minute at the same speed as initially imposed.

The mechanism of retardation is not well elucidated for cementitious systems. For instance, in the presence of sucrose which is a powerful retarding agent, it is often stated in the literature that sucrose prevents the nucleation of C-S-H on the particle surfaces [41]. It is however possible that it also limits the dissolution due to a strong adsorption on the anhydrous surface of alite which would then limit the step retreat process. Therefore, more studies are needed even though Thomas and co-workers have shown that the retarding effects of sucrose can be negated by adding C-S-H seeds at the time of mixing and can be reversed by adding C-S-H later, after the retarding effect has already been observed [41].

In these experiments an organic admixture RS (for retarder/superplasticizer) was added (1% by weight of binder) during the first step of mixing in order to check the influence of a change in viscosity of these granular fluids, but viscosity was not studied independently. On Figure 4.10, it is observed that the hydration is delayed as expected due to the retarding agent and the presence of the superplasticizer reduces significantly the viscosity of these pastes which leads to lower shearing conditions compared to a paste without superplasticizer for the same mixing speed. The effect of mixing speed exhibits the same trends as for non-admixed systems as can be observed on Figure 4.10: the induction period is shortened and the peak height increases as the mixing speed increase.



(a)



(b)

Figure 4.10: Effect of speed mixing on (a) a retarded/superplasticized cement paste and (b) a retarded/superplasticized alite paste using the two steps mixing procedure.

It can also be seen that for high mixing rates, the acceleration effect becomes limited. This would mean that for these mixing conditions the shearing effect is not sufficient anymore to reduce significantly the thickness of the diffusion boundary layer. Thus the kinetics of hydration are only slightly enhanced when there is an increase of speed compared to systems also mixed at relatively high shearing conditions. Aluminate hydration is also accelerated at higher speed of mixing.

One can also observe that at very high rates of mixing, the alite system presents a sharp change in slope in the decelerating period. This could be due to a differential hydration process where coarser particles react at a lower rate than the smaller ones. This type of feature was observed also in seeding experiments [41]. This feature was not observed for unretarded systems probably due to the higher shearing conditions developed during the mix. The coarser particles may be less affected by the shearing conditions when the viscosity of the paste is lowered leading to this differential hydration. However, this explanation remains purely speculative.

The next two graphs (see Figures 4.11(a) and (b)) represent for paste systems

the time of the end of the induction period and the rate of heat evolution during the acceleration period as a function of the mixing speed. The end of the induction period was arbitrarily defined by taking the intersection between the tangents at the minimum value during the induction period and to the acceleration period. Mixing has a larger impact on the reduction of the induction period of alite compared to PC when no admixture is added. However this difference vanishes when the admixture is added.

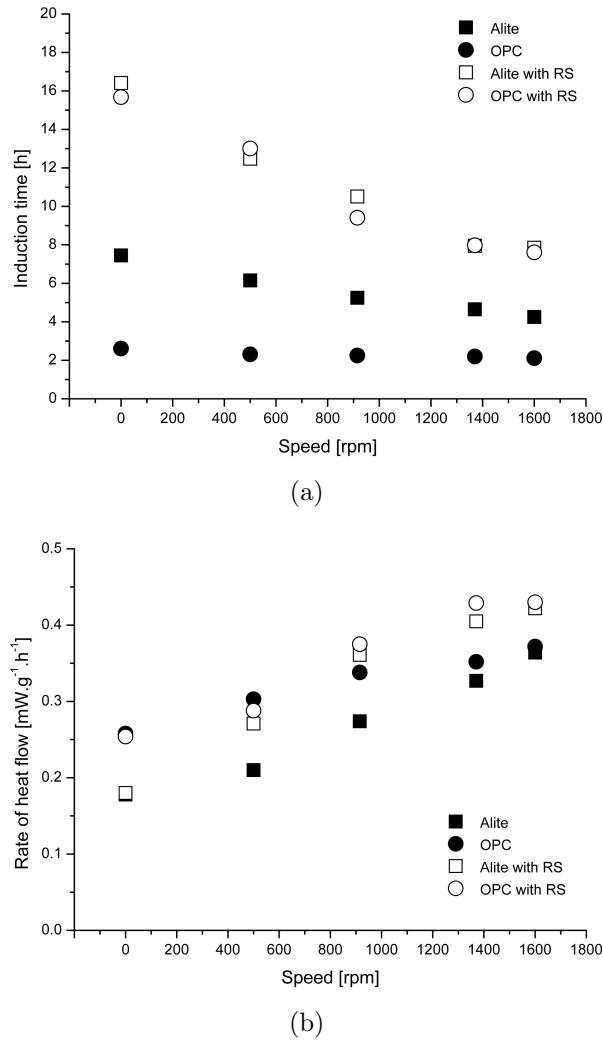


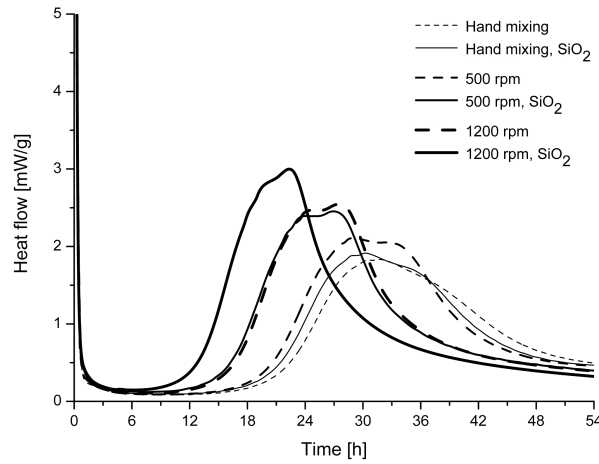
Figure 4.11: Plot of (a) the time at the end of induction period and (b) the rate of heat evolution in function of the speed of mixing.

The presence of the admixture leads to a chemical interaction with the anhydrous phases since the ends of induction period for alite and PC are superimposed and also has a physical effect as an increase of the shearing during the mix induces a more important reduction of the induction period. However, we do not clearly understand what might be the effect of the addition of the RS admixture on the pore solution composition of both systems. Concerning the evolution of the rates of heat flow during the acceleration period, the increase is almost uniform with respect to the speed of mixing, meaning that the same accelerating mechanism appears to occur in

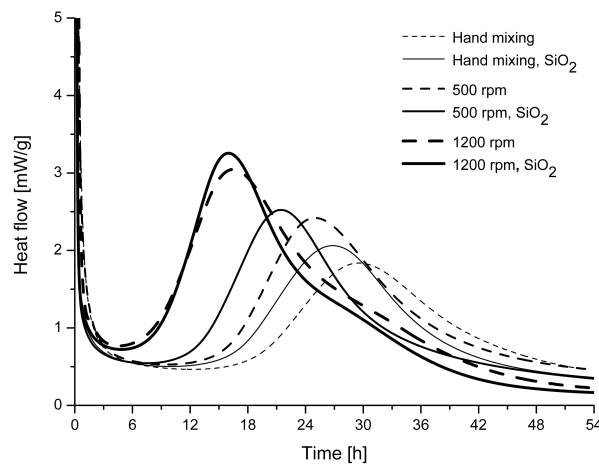
all systems.

Influence of adding silica beads on admixed PC systems

The same procedure is this time replicated for admixed systems in presence of silica beads (Table 4.2). Here again, the trend is the same: a shortening of the induction period, an increase of the rate of heat flow during the acceleration period as well as a pronounced effect on the aluminate reaction due to the presence of the admixture. The relative difference of these features between pastes and mortars is lower in this case compared to non-admixed system. The reason comes from lower viscosity in presence of the superplasticizer which reduces the shearing conditions in pastes as it has been shown in section 4.2.2 but enhances their displacement and therefore increases the velocity profile close to grain surface. Therefore the relative differences between the calorimetry curves are expected to be lower compared to systems without superplasticizer.



(a)



(b)

Figure 4.12: Heat flow for pastes and mortars in presence of RS admixture with beads of 0.3 - 0.4 mm for (a) the cement and (b) the alite system at different level of speed.

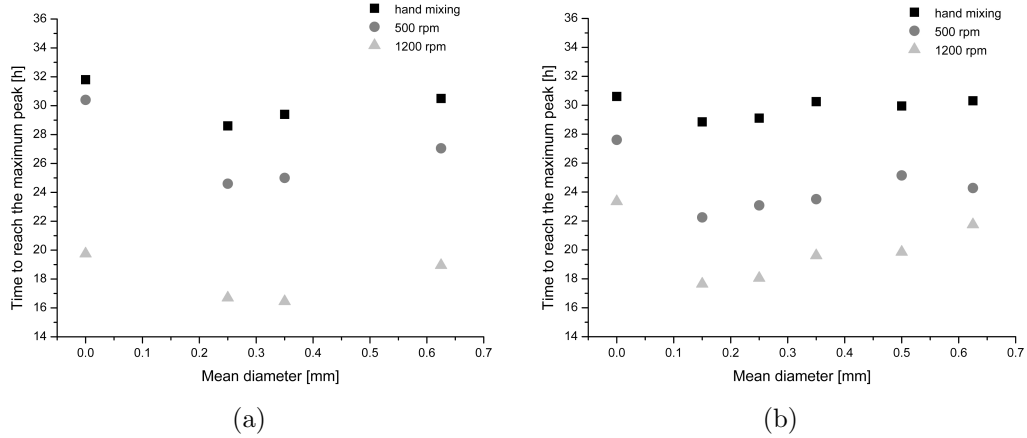


Figure 4.13: Time to reach the maximum peak of heat flow during the acceleration period in function of the average diameter of aggregates at three different speed of mixing for (a) alite systems and (b) PC systems in presence of a RS admixture.

Figure 4.13 represents the time to reach the maximum heat flow peak during the acceleration period as a function of the mean diameter of the silica beads for different speeds of mixing. Compared to the non-admixed systems, the size of the beads does influence the kinetics of hydration but remains pretty marginal. This could be due to a faster displacement of the smaller beads in these systems of reduced viscosity.

4.2.3 Accelerated systems

For these last systems, the same two mixing steps procedure is applied. During the first mixing step, PC is mixed with water at a $w/c=0.4$ and admixed with 1% by weight of RS. The alkali-free accelerator (accelerator A) is only added during the second mix at an amount of 6% by weight of cement. The composition of this accelerator as well as its interactions with cementitious phases will be described in detail in the next chapter. However, it is important to say that the accelerator used in this study is alumino-sulfate based and stabilised by formic acid. Therefore, it will react very rapidly to form ettringite which will provide an early strength development which is required for shotcrete applications. Figure 4.14 shows the influence of mixing on the hydration kinetics of this accelerated PC systems. Here again the same trend is found as previously. As the speed of mixing increases, the induction period is shortened and the rate of heat flow during the acceleration period is enhanced.

The major difference in terms of hydration kinetics concerns the aluminate reactions which are significantly enhanced for accelerated systems and the deceleration period that is also much more pronounced in these cases. These differences increase in intensity as the speed of mixing increases and most probably arise from an excess of aluminium ions brought by the alkali-free accelerator. However the exact mechanism by which the aluminate reaction are reactivated remains to be elucidated.

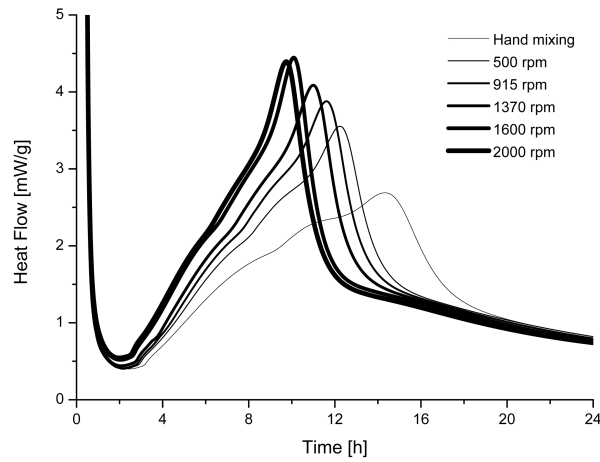


Figure 4.14: Effect of speed mixing on an accelerated cement paste using the two steps mixing procedure.

As for the two previous systems, it can be seen that at high mixing rates, the further acceleration of the kinetics becomes limited. Here also the shearing conditions are not able anymore to reduce the thickness of the diffusion boundary layer leading therefore to a poor enhancement of the hydration kinetics. Figure 4.15 shows a comparison between a pure PC system and an accelerated one both mixed using the same procedure.

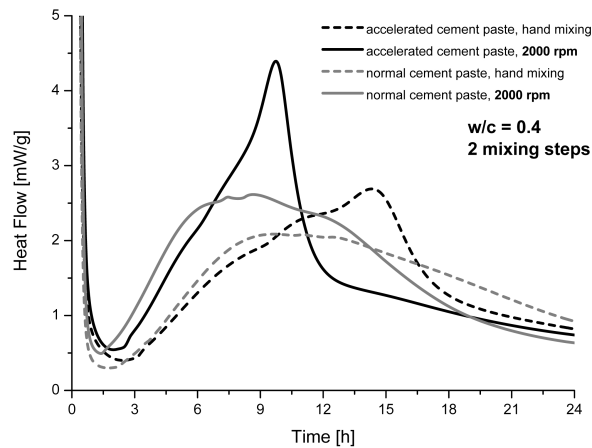


Figure 4.15: Comparison between a pure PC system and an accelerated PC system at two different speeds of mixing.

The kinetics of hydration of the silicate phases are very similar concerning the length of the induction period and the rate of heat flow during the acceleration period. There is a slight delay for the accelerated systems compared to the pure PC one. Nevertheless the addition of the accelerator has completely eliminated the retarding effect of the RS admixture added during the first mixing step. This leads to silicate hydration kinetics very similar to a pure PC system. In terms of rheology, no comparison can be made as the addition of the accelerator will

promote instantaneously the formation of ettringite (see next chapter) and therefore dramatically increases the viscosity of the accelerated system.

Influence of adding silica beads on accelerated PC systems

The same procedure is again replicated for accelerated systems in presence of silica beads (Table 4.2). The trend is again the same as previously reported: a shortening of the induction period, an increase of the rate of heat flow during the acceleration period as well as a pronounced effect on the aluminate reaction due to the presence of the accelerators.

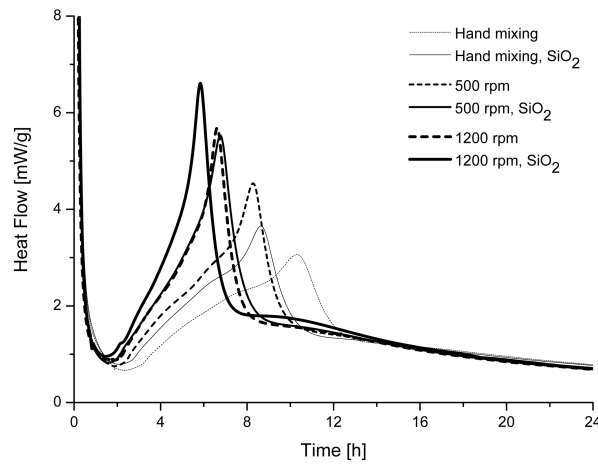


Figure 4.16: Heat flow for pastes and mortars in presence of RS admixture with beads of 0.3 - 0.4 mm for an accelerated PC system at different level of speed.

It can be seen on Figure 4.16 that it becomes very difficult to see the contribution of the silicate hydration as the intensity of the aluminate reactions becomes predominant. Figure 4.17 shows the time to reach the maximum peak during the acceleration period as a function of the mean diameter of the silica beads for different speeds of mixing. As for the retarded/superplasticized system, the size of the beads does influence the hydration kinetics. However, this effect is almost eliminated at the speed of 1200 rpm probably due to the inability to reduce further the diffusion boundary layer.

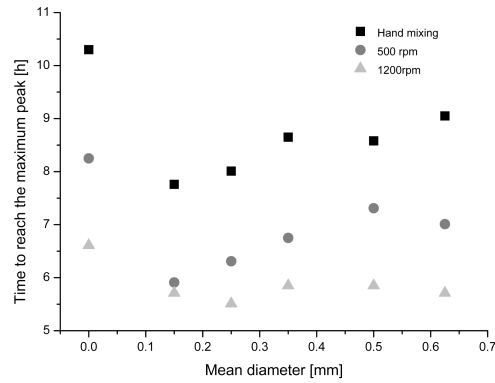


Figure 4.17: Time to reach the maximum peak of heat flow during the acceleration period in function of the average diameter of aggregates at three different speed of mixing for accelerated PC systems.

4.3 Discussion: Effect of mixing conditions on the early hydration of cementitious systems

In this section we will summarise the different effects due to variations in shearing conditions by increased mixing speeds or due to the presence of aggregates as well as due to the addition of admixtures on the hydration kinetics.

It has been shown in previous sections that different processes can increase the shearing conditions in the paste and markedly affect the kinetics of hydration at early age. Speed of mixing and addition of aggregates have shown a remarkable acceleration of the hydration kinetics. Viscosity reduction did also markedly change the shearing effect.

Energy input during mixing

Figure 4.18 reports the temperature measurement of alite and cement pastes before and after each mixing step. For both systems and mixing procedures, the main features observed are a shortening of the induction period, a higher maximum heat flow during the hydration process as well as an increase of the rate of heat flow during the acceleration period with respect to the level of speed. It is also observed that reactivity during the induction period (minimum of heat flow) is enhanced when the mixing speed is increased (see Figure 4.7). Since there is no major change in the shape of the curves it is assumed that kinetics of hydration are accelerated without any modification of the basic mechanisms. It is interesting to note that alite pastes show a longer and more obvious induction period than does the Portland cement. This may be attributed to the fact that alite is prepared in the laboratory, rather than in a rotary kiln, which is known to produce higher defect densities due to a more rapid cooling and also to a different particle size distribution since the grinding process is not as perfectly controlled as in cement plants.

It can be seen that the temperature of the paste increases almost linearly with the

level of speed used during this study. This temperature increase may also enhance the kinetics of hydration at early age as it is known that temperature can enhance markedly the kinetics of hydration [48]. However after 13 minutes, all systems have returned to the same temperature and it can be deduced that the temperature would be even more rapidly stabilised in the isothermal calorimeter. Temperature rise should therefore only affect the first minutes of hydration.

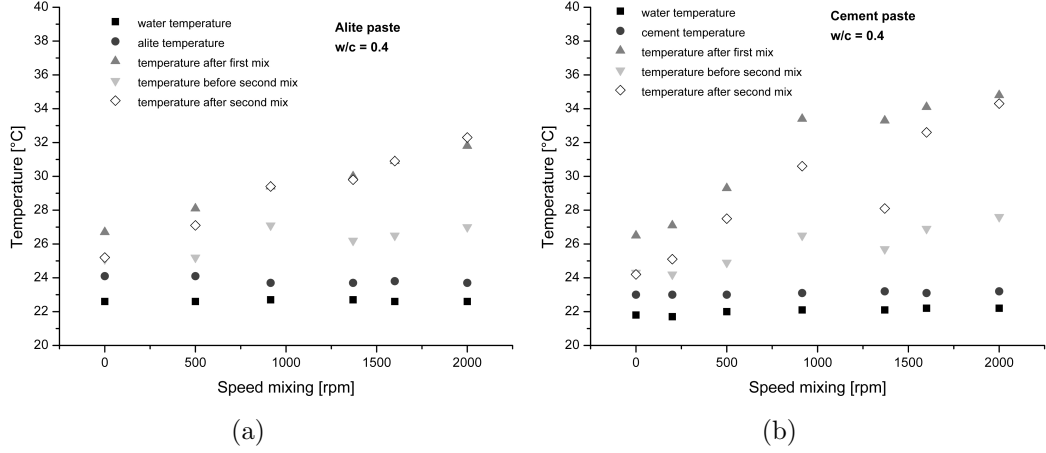


Figure 4.18: Temperature evolution before and after mixing for paste of (a) alite and (b) PC.

To assess the influence of temperature during the mixing itself and the first minutes of hydration, two samples were mixed at the same speed but with different initial temperatures. In order to reach these conditions, two stainless steel mixing paddles were kept at two different temperatures: one at room temperature and the other one in a furnace at 110°C. After one step of mixing at 500 rpm during 2 minutes, the temperature of the pastes was respectively 24°C and 29.5°C. This difference of temperature is almost equal to the largest temperature difference recorded for the least and most intense mixes. The results in Figure 4.19 show that this temperature difference has no effect on the length of the induction period and that the rate of heat released during the acceleration period remains almost the same for both samples. However there is a small difference in the height of the heat evolution peaks as well as the level of heat during the induction period. Nevertheless, it is clear that the temperature during the first few minutes has very little impact on the hydration process compared to the results obtained with different speeds of mixing presented in the previous sections. Therefore we assume that the major features observed are mainly due to the shearing conditions even if an increase of temperature related to the increase of speed could also have affected the hydration process.

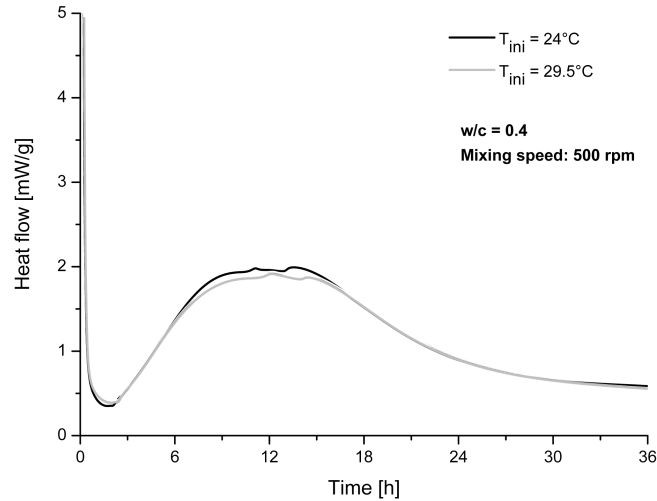


Figure 4.19: Effect of different initial temperatures for the same mixing procedure.

Effect of shearing conditions on the mechanism of early hydration

Regarding theories of crystal dissolution presented in the previous chapters, it has been shown that crystallographic defects as well as solution saturation state are the main parameters affecting the rate of dissolution of a large variety of minerals [17], [15], [108]. The density of internal defects such as dislocations, grain boundaries or vacancies are the reactive sites mainly involved during the first initial dissolution and solution saturation state determines the governing mechanism of dissolution:

1. At large undersaturation (far from equilibrium conditions) mechanism of dissolution by etching pits occurs and leads to a fast rate of dissolution [17].
2. For lower undersaturation (close to equilibrium conditions) dissolution occurs by step retreat and is related to a slow rate of dissolution [15], [108].

These mechanisms have been shown to be valid for cementitious systems. In this chapter, we have seen that hydration of pure alite and PC system are sensitive to stirring rate when the starting solution is deionised water. We could therefore conclude that these systems were limited by the diffusion of calcium ions through an electrical double electrical layer and become progressively limited by surface reactions as the undersaturation of the solution decreases with time. When the starting solution is saturated with lime, the kinetics of hydration were unaffected up to the end of the induction period indicating this time that the overall dissolution rate was only limited by surface reactions but still there is an effect of knocking nuclei off the surface into the solution.

In the case of an intense mixing procedure, the velocity profile close to the surface is high and will prevent to some extent the formation of a large diffusion boundary layer limiting the process of dissolution if the system is transport controlled. This would lead to a thinner diffusion boundary layer which permit a faster rate of dissolution compared to poor or less intensive mixing conditions that are more likely

to have larger electrical double layer. The amount of anhydrous phase dissolved would be higher for high shearing conditions and the conditions of supersaturation related to the precipitating phases should be achieved more rapidly decreasing therefore the duration of the induction period. Therefore, theory of dissolution is well adapted to explain the different features observed up to the end of the induction period. Concerning the acceleration period, an increase of the rate of heat flow was observed when the speed of mixing increased. It was interpreted as an increase of the nucleation density either due to a better homogenisation of the solution which could permit a homogeneous nucleation or by the dispersion in the solution of mechanically detached primary hydrates forming at very early age on the anhydrous surfaces. Higher speeds of mixing resulted also in denser microstructures which tends to confirm both hypothesis. Numerical simulation using for instance μic should be then undertaken to see how the different nucleation and growth parameters should vary in order to simulate the obtained results.

Effect of mixing on the aluminate phase hydration

The secondary humps found in the calorimetry curves of PC systems and related to a renewed hydration of the aluminate phase [48] probably occur when sulfate phases are exhausted in the cement paste as proposed by Sandberg and Roberts [135]. The effect of mixing on the sulphate-aluminate balance could lead to a more rapid exhaustion of the sulphate due to a higher adsorption of sulfates on the C-S-H phase which is present in larger quantity as the speed increases during the acceleration period. This hypothesis could explain the increase of the rate of reaction of aluminate as well as its acceleration with the level of speed. However, further studies regarding the hydration of the aluminate phase are still required to complete the picture of cementitious systems hydration at early age.

The impact of the aluminate hydration is even more pronounced in the case of admixed systems. Since the aluminate phase is more reactive than the silicate phases, specific interactions with the admixture could result. Some authors have studied the effect of certain admixtures on sulfate-aluminate balance and noted that cement can be under-sulfated when hydrated in the presence of admixtures [135]. As the sulphate phases are dissolving more rapidly with higher mixing speeds, these coupled effects could explain why the renewed hydration of the aluminate phase is enhanced in retarded systems.

Application of the dissolution theory could probably be extended to the aluminate phases since the surface features on Figure 4.20 are very similar to etch pits [42]. In this case, the sulfate ions would act as dissolution inhibitors by adsorption onto the anhydrous phases of aluminate as already proposed by Minard et al. [2]. Then, when the gypsum is exhausted, the adsorbed sulfates are released in solution and react further to form ettringite. In the same time, the desorption of the sulfate enables the C_3A to react but again, knowledge on aluminate hydration in real systems is incomplete.

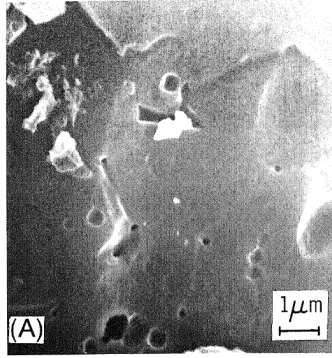


Figure 4.20: C_3A particles after hydration in the presence of $1.5 \cdot 10^{-3}$ M of $CaSO_4$. No hydration time as well as no w/c are specified. From [42]

Effect of aggregates

The surface of the added silica beads did not provide any direct contribution to nucleation as little dependence associated to their size was found in the case of non-admixed systems. The work of Stein and Stevels [61] shows the influence of two different types of silica, one being very fine and the other in the range of the silica beads used in this study (note that the two specific surface areas of the mentioned silica differ by three orders of magnitude), on the hydration of tricalcium silicate. Their calorimetry results show that only the fine silica accelerates clearly the hydration process of alite. The chemical surface characteristics which depend essentially on the compound chemistry and the surface properties of the compound (whether it is amorphous or presents specific crystallographic planes) may have different interaction properties with the ions and the pore solution and could explain why certain fillers act as nucleation sites whereas some do not. The total specific surface area provided by the filler may also play a key role since high water adsorption may occur and therefore lowers the water to cement ratio in the cement paste. This effect would obviously change the kinetics of hydration as well as the rheological properties. Thomas and co-workers [41] also proposed that reactive silica-containing materials first react with calcium ions released by the dissolving cement or C_3S to form C-S-H, which then in turn seeds the hydration process.

We can conclude that the aspect of free surface for nucleation provided by the silica beads used in our experiments can be neglected. Therefore the principal effect of aggregates is to reinforce the shearing conditions during the mixing procedure reducing to a larger extent the thickness of the diffusion boundary layer. However, a relation was found between the size of the beads and kinetics of hydration in the case of admixed systems. This aspect is discussed in the following section.

Role of admixtures

The main parameters affecting the kinetics of hydration in this study are the velocity profiles which depend mainly on the mixing conditions and the viscosity of the paste. A drop in viscosity will lead to the formation of higher velocity profiles

close to the surface of the particles. Therefore the presence of a superplasticizer leads to a higher dependence of the kinetics of hydration with the level of speed during the mix and also a better dispersion of the cement particles due to the electro-steric repulsion induced by the superplasticizer. This effect was observed both in paste and mortar systems (see Figure 4.12). For mortar systems, the presence of the RS admixture leads to a dependence between the size of the beads and the kinetics of hydration. However no specific adsorption of organic compounds on the silica beads was detected by high performance liquid chromatography (HPLC). The only plausible explanation was related to an enhanced displacement of the smaller silica beads in the paste when the viscosity is lowered. This would result in higher velocity profile at the cement grain surfaces when smaller beads are used. This assumption needs confirmation but could be potentially achieved with the help of computational model predicting suspension rheology.

On the following graphics (Figure 4.21), the y-axis represents the ratio between values obtained for the time to reach the maximum peak at a given speed over the one obtained by hand mixing which has been arbitrarily set as the reference. It can be seen that the variation of this ratio with the speed of mixing follows two different trends depending if the system is admixed or not. Admixture containing systems with lower viscosity do show a more pronounced acceleration of their hydration kinetics as the velocity profile at the surface increase during mixing. This observation is valid either for both pastes and mortars systems. These results show therefore the important dependence of the kinetics of hydration with the mixing conditions when the viscosity is reduced.

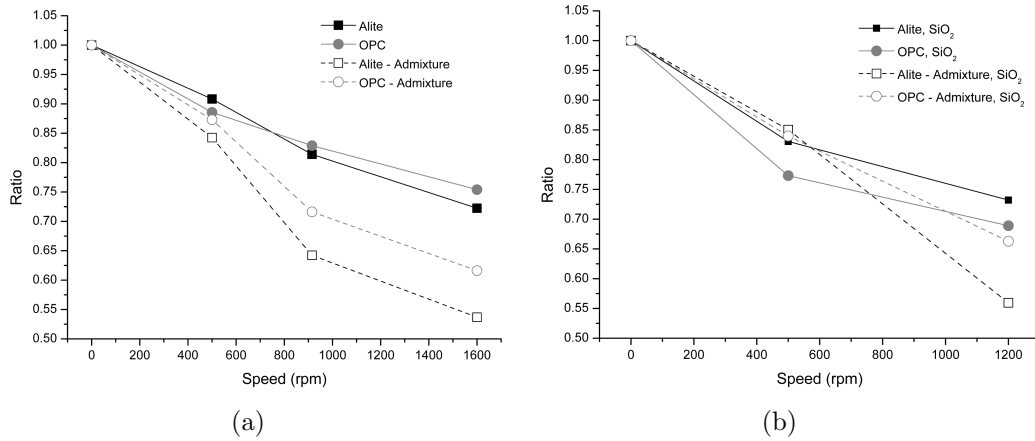


Figure 4.21: Ratio between values obtained for the time to reach the maximum peak at a given speed over the one obtained by hand mixing (a) for paste systems, (b) for mortars systems, in function of mixing speed.

In the case of accelerated systems, the change in viscosity is the opposite as there is an almost instantaneous precipitation of ettringite. However, the formation of ettringite could be seen as an additional aggregate addition helping therefore to homogenise the solution and develop higher shearing stresses during the mix. In addition to that, there is a depletion of calcium ions to form ettringite which should promote the dissolution of calcium-containing phases. This point will be

discussed in more details in the following chapter. The two main effects related to the addition of this accelerator was the elimination of the retardation caused by the presence of the RS admixture as well as an important enhancement of the aluminate hydration. It is possible that the large specific surface area provided by the instantaneous precipitation of ettringite would favour readsorption of the retarding molecules on this hydrate. However, we do not have yet any experimental results to support this hypothesis. Concerning the enhancement of the aluminate reaction, the addition of the alumino-sulfate based accelerator will definitely vary the sulfate-aluminate balance and therefore lead to an uncontrolled aluminate reaction that can take place during the acceleration period of the silicate hydration. This will lead to a competition between the aluminate and silicate reactions to fill the available space. This point is discussed in more details in the following chapter.

Chapter 5

Influence of Alkali-Free Accelerators on the Kinetics of Hydration of Portland Cement

Underground job sites such as tunnels and mines rely on the quality of recently sprayed concrete to secure freshly excavated zones [136]. Rapid setting and high early strength development are required for safety as well as for the rapid progression of the construction site. This is ensured by the addition of accelerating admixtures. These admixtures are of various chemical formulations and have therefore different impacts on the early age hydration kinetics as it will be shown in the following sections. In the past decades, most common types of accelerators used worldwide were alkali products containing aluminate salts. These admixtures have major drawbacks such as safety issues for workers as their high alkalinity can cause severe burns if they come into contact with the skin [136] and also lower ultimate strength at later ages. A new generation of accelerators has been developed to counter these problems. Alkali-free liquid accelerators are based on aluminium hydroxy/sulfate solutions generally stabilised by mineral or organic acids [136]. Their alkaline content is inferior to 0.3% and pH ranges from 3 to 5.5 [137].

As already shown in the last chapter, the addition of an alkali-free accelerator to PC systems has a huge impact on the aluminate hydration. The reason arises from the fact that these admixtures lead to a rapid precipitation of ettringite inducing flocculation and fast setting. It has been reported that alkali-free accelerators result in a delayed setting compared to alkali-rich admixtures resulting in a reduced rebound. Consumption of both clinker phases, C_3A and alite is promoted by both alkaline and alkali-free accelerators [138]. We will therefore concentrate our effort on trying to understand the impact of various alkali-free liquid accelerators on the early hydration kinetics of PC and isolate factors which might enhance the aluminate hydration in accelerated systems since this phase is the most affected by the presence of alkali-free accelerators. The influence of the fast aluminate reaction on the kinetics of hydration at early age will also be discussed.

5.1 Kinetics of hydration on accelerated paste systems

The different results concerning the early age hydration kinetics for PC systems in presence of different alkali-free accelerators are presented in this section. Three different cements were used and their associated kinetics are presented in Figure 5.1. Their chemical composition are given in Annex II. It is seen that the kinetics of hydration are very similar for all cements except for the time of appearance of the second hump related to the renewed aluminate hydration. Wildegger PC (light grey curve in Figure 5.1) was the PC mainly used for this study. Therefore, it is only noted when one of the other cement has been used. All accelerated systems presented in this section are paste systems with the same mixing protocol described in the previous chapter.

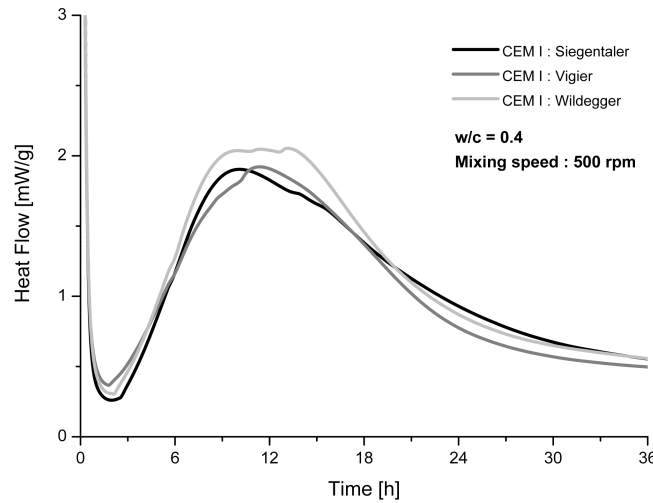


Figure 5.1: Isothermal calorimetry curves of 3 PC systems mixed 2 minutes at 500 rpm with a $w/c=0.4$ at 20°C .

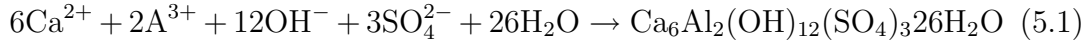
5.1.1 Influence of accelerator type

In Table 5.1, a range of chemical composition is given for the three accelerators used in this study:

Table 5.1: Range of composition for accelerators A, B and C

Compounds	Accelerator A	Accelerator B	Accelerator C
Al ₂ O ₃	10-14%	7-11%	10-14%
SO ₄	18-22%	22-26%	18-22%
A/ \bar{S}	0.55-0.63	0.32-0.42	0.55-0.63%
Formic acid	8-12%	3-5%	-
Phosphoric acid	-	-	1-3%

Ettringite will precipitate massively early on due to initial presence of aluminium and sulfate ions provided by the addition of these alkali-free accelerators with the consequence to deplete the pore solution in calcium ion (see equation 5.1).



Consumption of calcium containing phases is expected to happen and could explain the promotion of C₃A and alite consumption found by Paglia and co-workers [138].

The chemical composition of the accelerator may therefore influence the kinetics of hydration. For instance, Lootens and co-workers [136] have shown that some inorganic acids used for the stabilisation of the accelerator may dramatically retard hydration and the strength development. This feature is clearly seen in Figure 5.2 where accelerators of different chemical compositions were added to paste systems. These show very different and sometimes unusual hydration kinetics. Note that the kinetics of these paste are different from the one presented in the previous chapter due to a change of PC. In the previous chapter, accelerator A was mixed with Siegentaler PC.

The shape of the three calorimetry curves are very similar to under-sulfated systems [4], [3]: the aluminate hydration is enhanced and results in a highly exothermic peak taking place before or during the acceleration period of the silicate phases. The alite hydration is then shifted in time but also reduced in intensity. This behaviour is much more pronounced in the presence of accelerator C where 2 peaks presumably associated to aluminate reactions can be observed before the silicate hydration is taking place. In that case, the silicate hydration is delayed up to 18 hours and the maximum intensity of this peak reaches only 1 mW.g⁻¹ whereas in normal systems it reaches about 2 to 4 mW.g⁻¹.

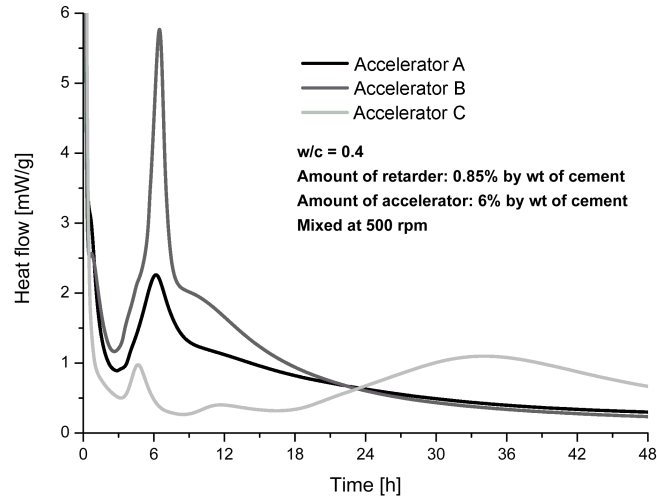


Figure 5.2: Isothermal calorimetry curves for the 3 accelerated systems at 20°C.

In order to better understand the influence of each accelerator during the first 12 hours of hydration, in-situ XRD measurements using kapton foil (X-ray transparent material) that will prevent evaporation and limit carbonation during the measurement, were performed to follow the evolution of the phase assemblage at early age. The time needed to record each diffractogram was set to 13 minutes and the total range of interest of 2θ angles was splitted in two and therefore acquired in two sets of experiments (from 7° to 20° and 20° to 45°). No reference sample of pure PC could be performed using this technique as the amount of free water is too large in that case. This water forms a thin film between the cement paste and the kapton foil leading to a strong adsorption of the X-ray. The temperature in the XRD chamber is 26°C and therefore associated isothermal calorimetry curves were replicated at that temperature (see Figure 5.3). It can be seen that the kinetics of hydration of both silicate and aluminate reactions are enhanced and accelerated for the three cases due to thermal activation. However, it can be seen that the most enhanced system is C with a 12 hours reduction for the onset of the acceleration period.

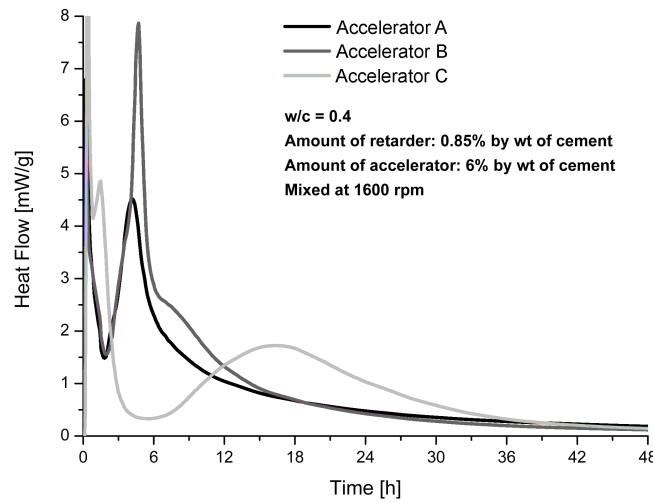


Figure 5.3: Isothermal calorimetry curves of 3 accelerated systems at 26°C.

The following results are all presented in the same manner. Phase development measured by XRD cross-linked with its associated isothermal calorimetry curve at 26°C. To avoid confusion and facilitate the readability of the following graphics, alite and Portlandite were plotted together whereas tricalcium aluminate (C_3A), ettringite and gypsum were plotted on a separated graph. Other phases such as C_2S and C_4AF were not plotted because they do not react very rapidly compare to the other phases. AFm phases are also not reported as it is difficult to isolate these phases properly because of limited intensity relative to the contribution of the background. However, the only AFm phases that have been detected by XRD was hemicarboaluminate which is not surprising as the PC contained 5% of limestone. This phase was also detected in alkali-free accelerated system by Arnold [137] using EDS microanalysis on paste hydrated for 24 hours. The following results are not quantitative as they represent the integral of the area below a specific peak of each phase studied. Problem of X-ray flux fluctuation may have taken place between the start and the end of each experiment as well as between each set of experiments. Therefore, the results remain purely qualitative.

Accelerator A

In Figure 5.4, three distinct stages can be observed for the evolution of CH. Time 0 corresponds to the time after which the first diffractogram has been recorded (13 minutes).

In stage I, which corresponds to the first dissolution and induction periods of alite, CH is not forming (or not in sufficient amounts to be detected). After approximately 90 minutes, CH is being detected by XRD and forms at almost a constant rate up to 5 hours. This period corresponds to stage II on Figure 5.4. After 5 hours of hydration, the rate of formation of CH decreases slightly.

Regarding the alite evolution, it is difficult to see a correlation with the evolution of CH as alite seems to decrease continuously over the time range studied. Nevertheless,

the rate of alite consumption increases slightly when CH starts to precipitate.

A careful analysis also indicates that the formation of CH starts before the minimum heat flow is attained. At the moment CH starts to precipitate massively, the heat flow signal drops sharply. This sharp drop may be associated to the endothermic reaction of CH precipitation. This feature is also visible on Figure 5.6 for the system B.

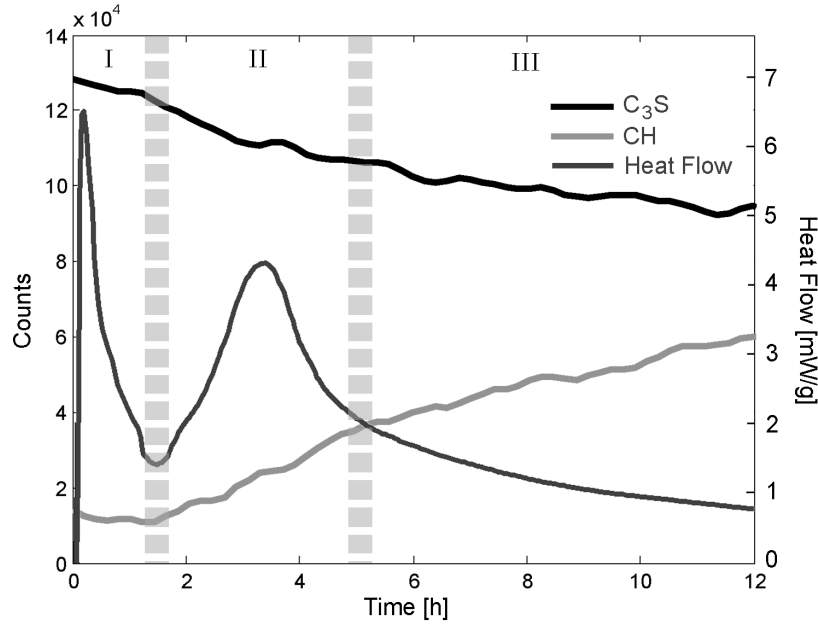


Figure 5.4: Evolution of C_3S and CH amount for the accelerated system A.

Concerning the aluminate and sulfate reactions, 3 stages can be identified according to the rate of formation of ettringite. This phase is forming at a very high rate up to 90 minutes of hydration. In parallel, gypsum dissolves very rapidly whereas C_3A dissolves at a relatively low rate which might be due to the presence of the accelerator which leads to an initial high aluminium concentration.

During the acceleration period, ettringite continues to precipitate at a lower rate until it reaches a maximum. At the same time, C_3A dissolves at a higher rate as aluminium ions provided by the accelerators have probably been all consumed to form ettringite. When gypsum is totally exhausted, ettringite starts to dissolve due to the depletion of sulfate in solution. This behaviour is curious as generally the reaction related to the renew aluminate hydration is believed to take place due to gypsum depletion in the absence of accelerator [4], [135].

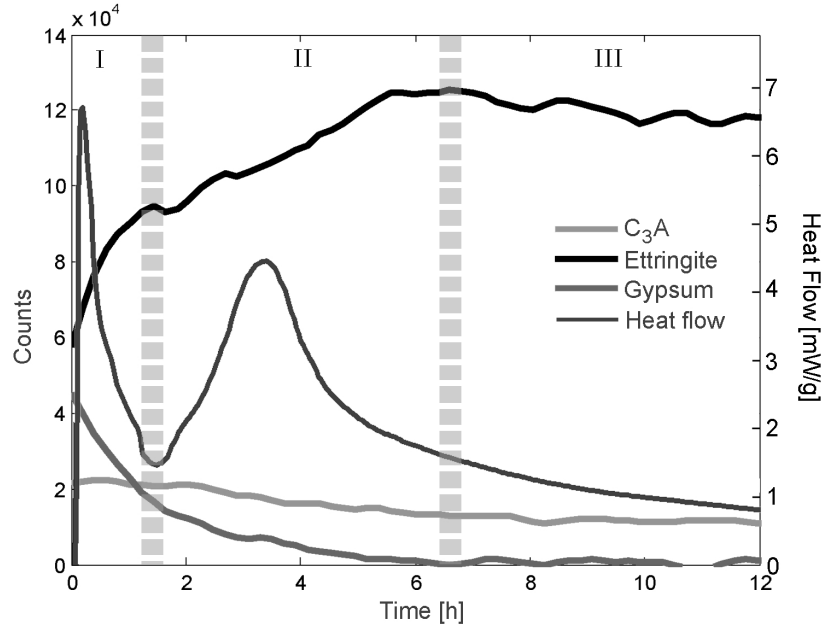


Figure 5.5: Evolution of ettringite and gypsum amount for the accelerated system A.

Accelerator B

The hydration behaviour of the system B is very similar to the system A which is expected as the chemical composition of both accelerators is also quite similar. CH is not detected up to 2 hours of hydration. At this time, the same drop in heat flow signal can be observed on the calorimetry curve which also corresponds to the onset of CH precipitation. CH precipitates at almost a constant rate up to 8 hours of hydration. Compared to system A, CH does not precipitates in large amount and its rate of precipitation levels off after 8 hours of hydration. In this case again, it is very difficult to find a direct correlation between the rate of formation of CH and the rate of dissolution of alite. Alite dissolves at a constant high rate up to 4 hours and the rate of consumption decreases afterwards while the formation of CH continues.

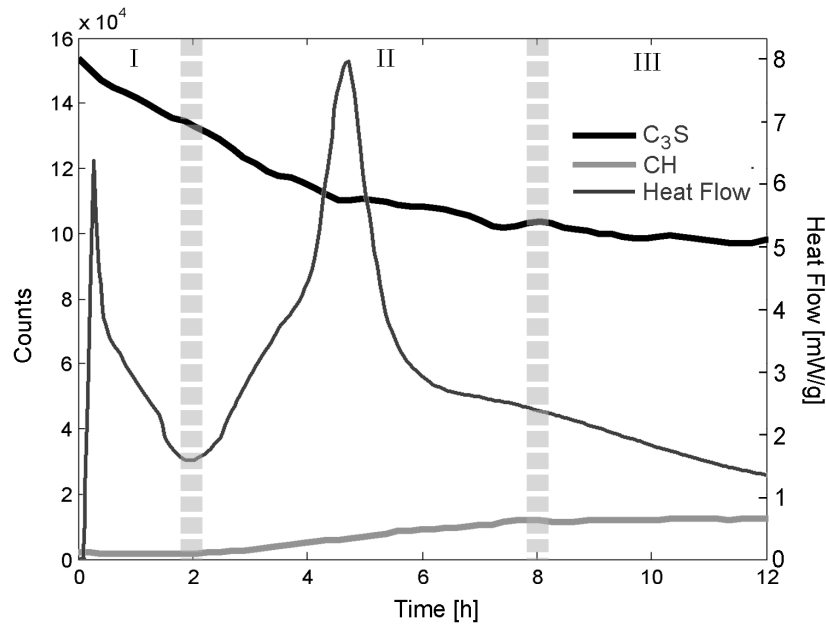


Figure 5.6: Evolution of C₃S and CH amount for the accelerated system B.

Concerning the aluminate and sulfate phases, the same three stages associated with the ettringite evolution can be identified as for system A. Ettringite forms early on at a very high rate due to the addition of the accelerator. At the same time, gypsum dissolves rapidly. After 90 minutes of hydration, ettringite still forms rapidly but at a lower rate than in stage I. At almost the same time (2 hours) C₃A starts to dissolve more rapidly. During this second stage, ettringite grows at a constant rate. It then reaches a maximum and finally starts to dissolve leading to the onset of stage III. During this stage, C₃A dissolves at a lower rate than in stage II. The general trends are here also very close to those found for the system A. It is difficult to assess exactly when the gypsum is totally consumed but it seems in this case that gypsum exhaustion happens before the ettringite consumption.

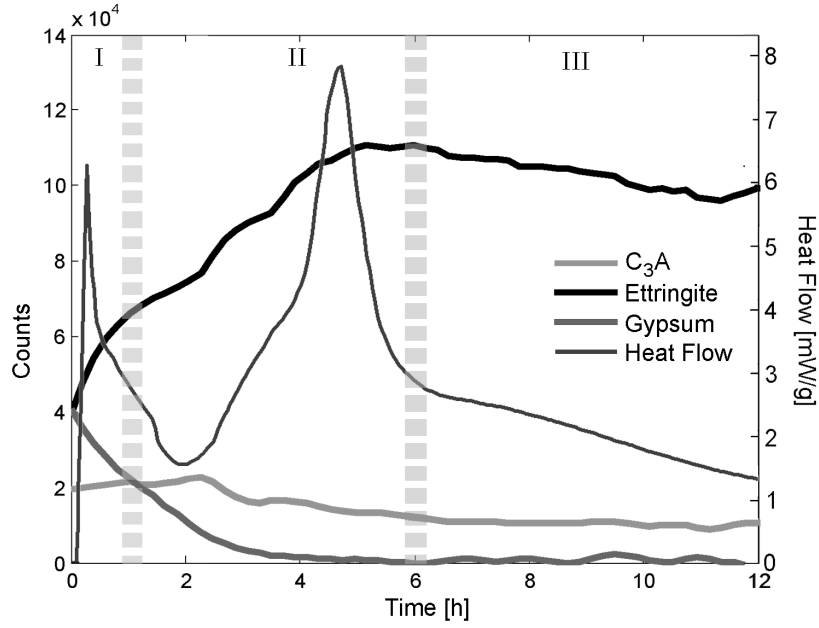


Figure 5.7: Evolution of ettringite and gypsum amount for the accelerated system B.

Accelerator C

The system C does not follow the same hydration behaviour as the the two other systems. In the presence of this accelerator, the aluminate hydration is taking place much faster as it can be observed on the calorimetry curve (see Figure 5.8). The silicate hydration is shifted to later time as most of calcium ions in solution may be consumed to produce aluminate hydrates which will then fill up the available space. Precipitation of CH is negligible for this system, however a strong consumption of alite detected by XRD matches with the onset of the acceleration period observed by isothermal calorimetry.

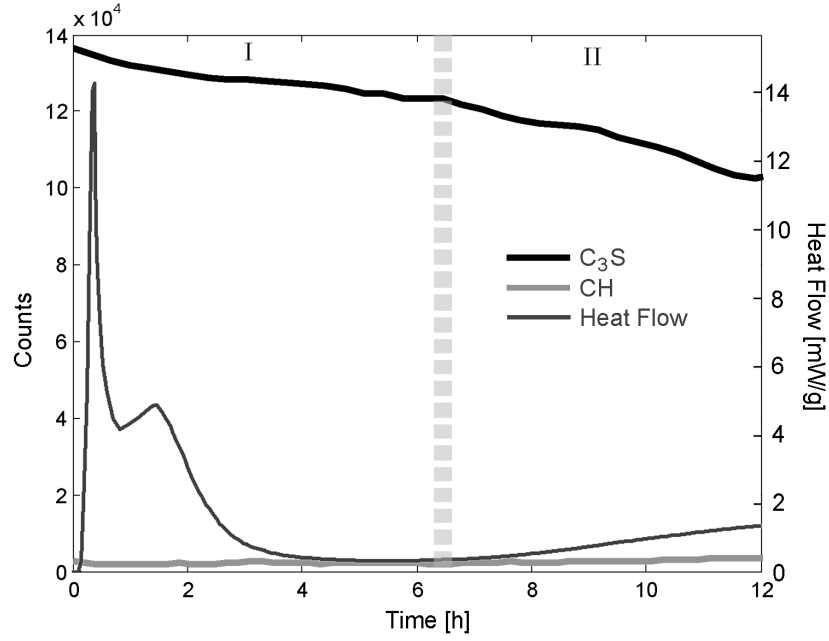


Figure 5.8: Evolution of C_3S and CH amount for the accelerated system C.

The aluminate hydration takes place very rapidly and consumes all the gypsum within less than half an hour. Not enough sulfate ions remain present to control the aluminate reactions leading to similar kinetics of hydration as an undersulfated system. Ettringite is formed very quickly, becomes unstable and starts to dissolve as for the two other systems but in shorter period of time. In this case, the presence of the phosphoric acid could lead to an adsorption of the phosphate ions on alite. Phosphate is known to limit the dissolution of many minerals such as calcite [23], [118], [119], and alite [139] which could explain the long delay before the onset of the silicate acceleration period. Phosphoric acid appears therefore to promote essentially the aluminate hydration and the fast precipitation of ettringite.

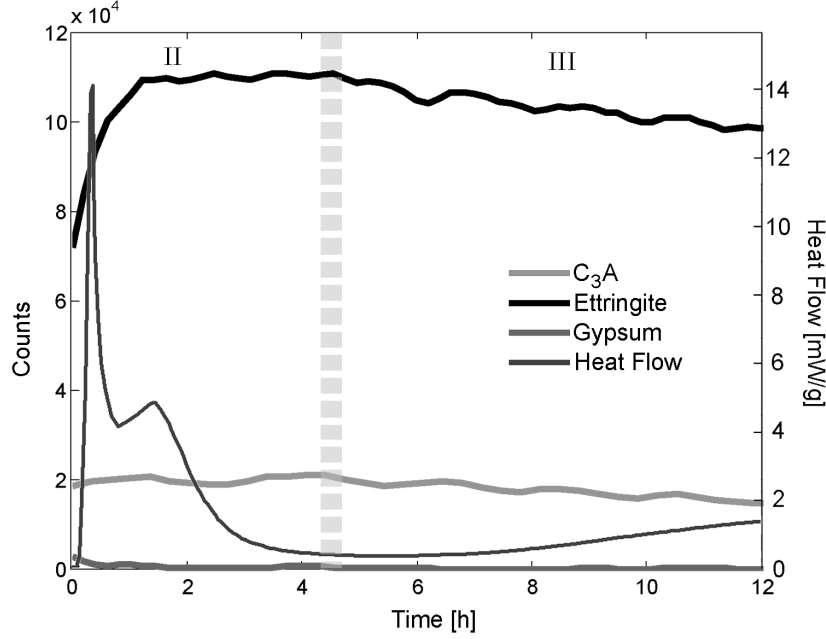


Figure 5.9: Evolution of ettringite and gypsum amount for the accelerated system C.

A general interesting feature is the constant consumption of the alite phase taking place before the onset of its acceleration period. As discussed previously, the massive precipitation of ettringite due to the addition of alkali-free accelerators will consume most of the calcium ions available in the pore solution. Calcium containing phases are therefore expected to dissolve to provide calcium ions needed for the early precipitation of ettringite.

However, the consumption of C_3A is not obvious for all three systems and appears similar in each systems. In addition, the rate of consumption of C_3A measured by XRD does not coincide with the strong exothermic peak monitored by isothermal calorimetry, but the low initial amount of this phase may lead to a strong impact with the process of background subtraction. We will therefore assume that these peaks observed by calorimetry are related to the aluminate hydration.

It can be seen that the A/\bar{S} of ettringite is 0.33 whereas this ratio oscillates between 0.32-0.42 for accelerator B and between 0.55 and 0.63 for accelerators A and C. In the case of accelerator B, the A/\bar{S} ratio almost matches the one of ettringite whereas for accelerators A and C, there is an “excess” of aluminate. For these two systems, aluminate hydration is then expected to be faster since C_3A hydration is limited by the adsorption of sulfate on its surface as proposed by Minard and co-workers [2]. The rapid consumption of the sulfates will lead to the desorption of the sulfate ions from the C_3A surface as well as from the C-S-H gel if this one has already precipitated and C_3A can then react with the solution producing this sharp exothermic peak.

This explanation matches with the lower initial amount of ettringite formed in system B compared to systems A and C as well as the higher rate of ettringite formation after the first rapid precipitation observed in Figure 5.10. This higher rate

of ettringite formation for system B could also explain the low amount of CH detected since the calcium ions released by alite dissolution would be mainly consumed to produce ettringite instead of CH.

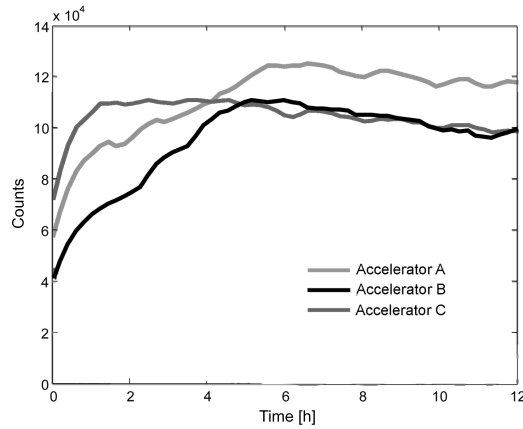


Figure 5.10: Comparison of the evolution of ettringite amount for the three accelerated systems.

All these systems seem to indicate that the precipitation of ettringite due to the addition of the accelerators impairs the capacity of gypsum to control the C_3A hydration. However, the accelerator having the lowest A/\bar{S} ratio appears to better control the C_3A hydration without affecting much the silicate hydration, at least from a kinetic point view as it is observed both by in situ XRD and isothermal calorimetry.

As it can be seen on all previous graphics and especially on Figure 5.8 and 5.9, in situ XRD method has some limitations. The small amounts of phases are greatly influenced by the background as it is the case for the C_3A phase and the CH phase at least at early ages. This makes difficult to determine precisely at which time a phase is being totally consumed or starts to precipitate. However good evolution of ettringite formation could be determined with this technique.

5.1.2 Influence of accelerator dosage

The normal range of dosage for alkali-free accelerators lies between 6 and 8% by mass of cement [136]. Lower dosage ranging from 2% to 6% by weight of cement were tested to check the acceleration effect, if any, on the early hydration kinetics. Two different speeds of mixing (500 and 1600 rpm) were also tested to see the coupled effect of solution composition and shearing conditions (low and high). These experiments were monitored by isothermal calorimetry at 20°C. The results are presented in Figures 5.11, 5.12 and 5.13.

For system A, it can be seen that for a dosage of 6% of accelerators, the intensity of the heat flow is significantly reduced compared to 2% and 4% dosages. It even results in a slight delay of the hydration reactions at early ages compared to the 4% dosage. It is very likely that reactions involving aluminate phases are taking place

during the mix and the first hours strongly affect the later reactions. This is the case for both speeds of mixing. It can also be noticed that the aluminate reactions taking place after the induction period for the 2% and 4% dosage systems are enhanced by the higher shearing conditions as already shown in the previous chapter.

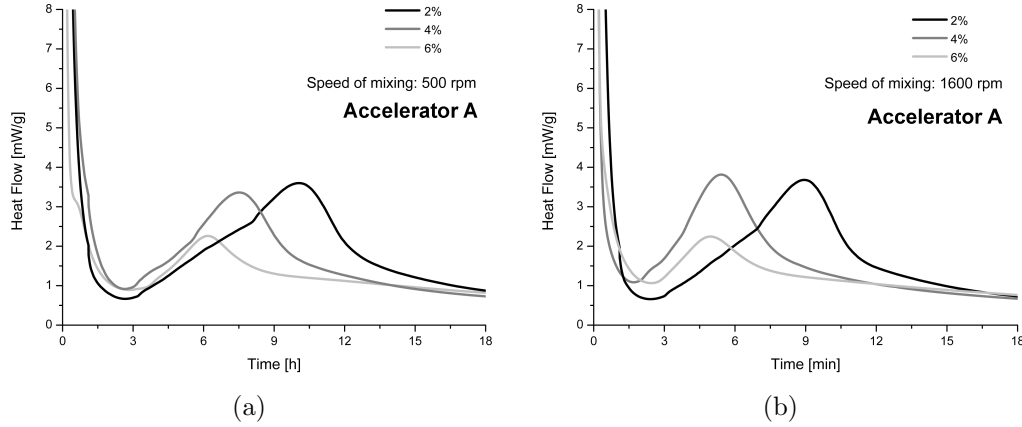


Figure 5.11: Isothermal calorimetry curves of systems A at 20°C with 2%, 4% and 6% of accelerator at (a) 500 rpm and (b) 1600 rpm.

Concerning system B, the increase of accelerator dosage as well as the increase in speed of mixing accelerates the hydration reactions without changing the intensity of the main heat flow peaks. The occurrence of each peak takes place earlier and their associated width becomes thinner showing an enhancement of the reactions. These features appear to also be valid for the peaks at very early ages (less than 3 hours of hydration). It is however impossible in these experimental conditions to better resolved these latter. Compare to the previous system, there is no reduction effect of the rate of reaction at higher dosage since this accelerator has the lowest A/S ratio of all studied accelerators.

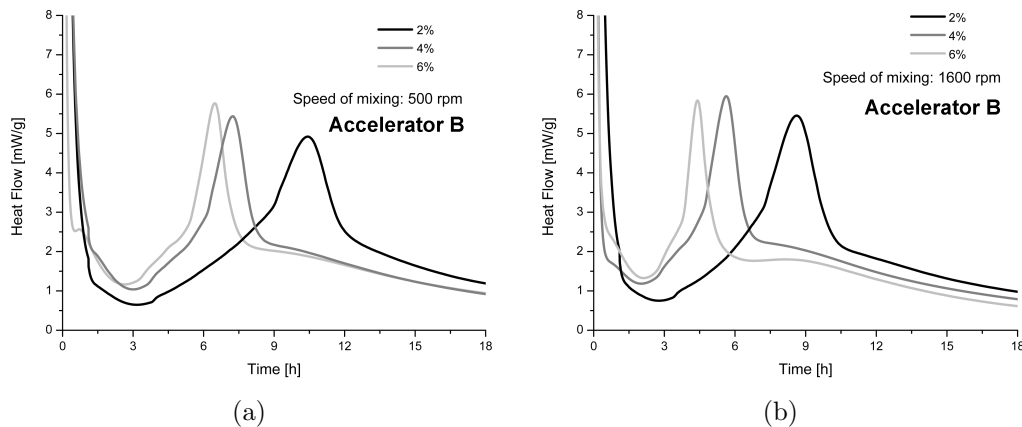


Figure 5.12: Isothermal calorimetry curves of systems B at 20°C with 2%, 4% and 6% of accelerator at (a) 500 rpm and (b) 1600 rpm.

Finally, system C shows here again an unusual hydration behaviour at dosage of

6% at low and high mixing rate, but also at 4% dosage when the paste is submitted to high shearing conditions. In these three cases, the aluminate reactions are enhanced and affect dramatically the hydration of the silicate phases. It was already shown in the previous section that in the presence of this accelerator, the aluminate hydration is very fast and the gypsum is consumed much more rapidly compare to the other two systems probably due to specific interactions between the phosphoric acid and the C_3S phase. In this last system it is now possible to see the destabilisation of the aluminate reactions due to the accelerator dosage and also to the mixing conditions. This destabilisation results in a delayed and reduced hydration of the silicate phases.

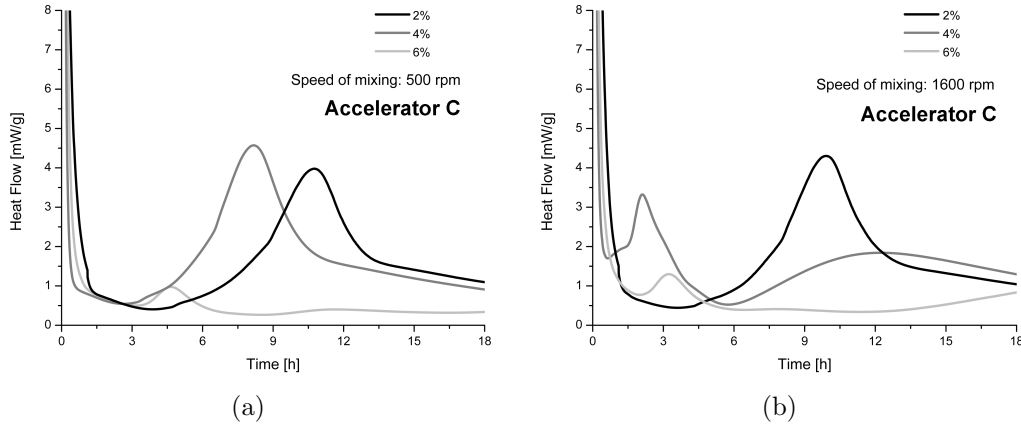


Figure 5.13: Isothermal calorimetry curves of systems C at 20°C with 2%, 4% and 6% of accelerator at (a) 500 rpm and (b) 1600 rpm.

Lower dosage will induce a lower amount of ettringite precipitation which should limit the consumption of the gypsum. If enough sulfates remain present at early age, the renewed aluminate reaction would take place after the onset of the silicate acceleration period. This silicate reaction is therefore not retarded. It depends however on the mixing intensity which can enhance the aluminate hydration under high shear mixing conditions. Though the kinetics of hydration are accelerated with low dosages of accelerator addition, dosage of 2% and 4% by weight of cement are not sufficient to fulfill the requirement for early strength.

5.1.3 Influence of cement type

In the previous sections, we have shown that the rate of mixing, the composition as well as the dosage of the accelerator can greatly influence the hydration of the aluminate phase which may in return affect the silicate hydration. These three parameters are not the only ones susceptible to affect the aluminate hydration. For instance, although it seems from the kinetic point of view that the hydration in deionised water is more or less the same for the three different PC (see Figure 5.1), the addition of an alkali-free accelerator (accelerator A in the present case) leads to large differences in terms of kinetics, especially concerning the aluminate hydration (see Figure 5.15). The aluminium sulfate-balance of the cements can be evaluated

by comparing the ratio of A/\bar{S} ($\text{Al}_2\text{O}_3/\text{SO}_3$) measured by XRF (see Table 5.2 and Figure 5.14; for complete chemical compositions, see Annexe II).

Table 5.2: A/\bar{S} for the three different systems

PC Systems	Siegentaler	Wildegger	Vigier
A/\bar{S}	1.49	1.74	2.21

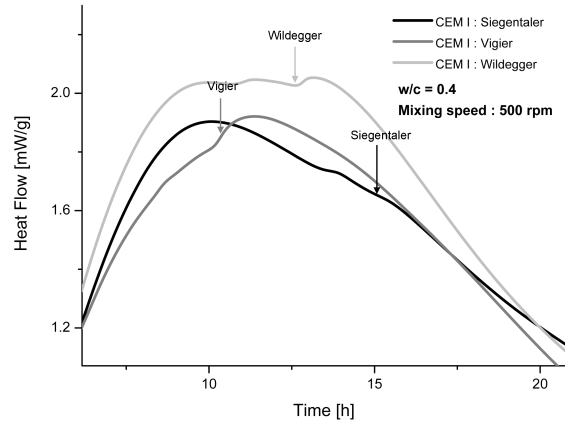


Figure 5.14: Zoom on the maximum heat flow of the three different cements without admixture showing the second hump related to the C_3A reaction. Arrows represent the onset of the main aluminate reaction since a smaller hump is present before each of these.

The arrows on Figure 5.14 represents the renewed aluminate reaction due to sulfate depletion. As the A/\bar{S} ratio increases, the aluminate reaction is taking place earlier meaning that a lower amount of sulfate results in faster aluminate reaction. This effect is even more pronounced in the presence of accelerator A. This confirms that the kinetics of hydration for these accelerated systems are also very sensitive to the aluminium-sulfate balance of the cement. The order of appearance of this aluminate reaction for accelerated systems remains the same as for the non-accelerated systems (see Figure 5.15).

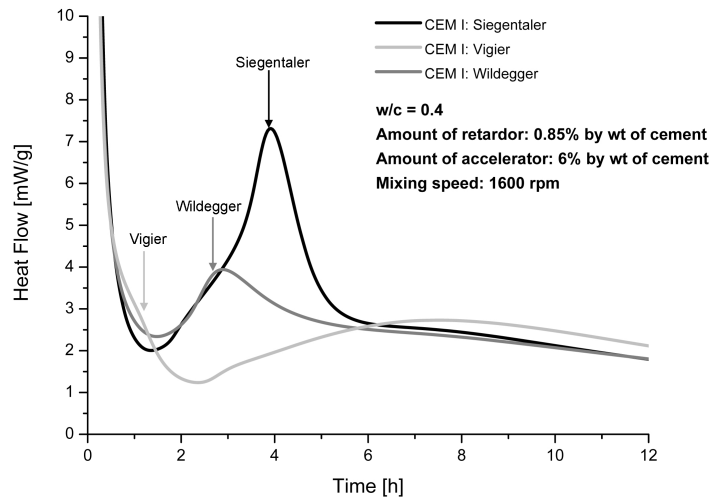


Figure 5.15: Kinetics of hydration for three different PC (Siegentaler, Wildegger and Vigier) accelerated by 6% of accelerator A monitored by isothermal calorimetry at 25°C

Poorly sulfated PC characterised by a high A/\bar{S} ratio are more susceptible to have an uncontrolled C_3A reaction at early age which will retard and decrease the intensity of the silicate hydration as for the Vigier system.

5.1.4 Influence of acid formic content using accelerator A

In order to check the effect of the formic acid content, accelerator A with different amount of formic acid were synthesised (0%, 3%, 6.5%, 9.5%, 12.5% and 15% by weight of acid formic). The influence of formic acid content on the hydration kinetics are presented on Figure 5.16. As the acid content increases, the rate of both reactions is enhanced. The same endothermic peak as observed earlier taking place before the acceleration period is observed. It is most marked for the 9.5% formic acid content. Above 9.5% of acid content, it becomes possible to distinguish two thermal events. Figure 5.16 shows a marked acceleration of the alite hydration without any acceleration of the aluminat hydration despite an increase in rate of reaction. A higher formic acid content seems therefore to specifically favour the silicate hydration.

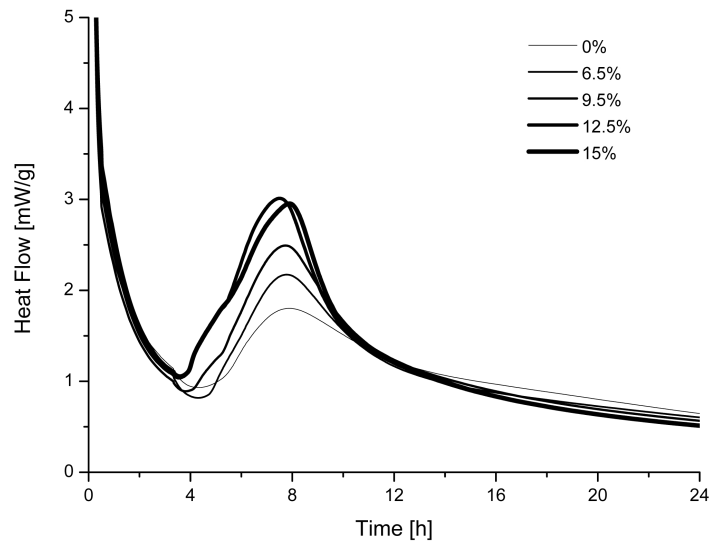


Figure 5.16: Isothermal calorimetry curves for various amount of acid formic content present in the alkali-free accelerator A (percentage by weight of accelerator).

There is certainly more to study regarding the influence of pH changes of the pore solution as well as possible specific interactions depending on the type of acid on the mechanism and kinetics of hydration but these aspects were not studied here.

Beside the effect on the hydration kinetics, it has already been shown in the master thesis of Arnold [137] that ettringite morphology was affected by the formic acid content. We have noticed that for the system A, the ettringite peak was slightly shifted to higher 2θ values compare to the system C (see Figure 5.17). One possible reason in order to explain this decrease in interlayer spacing is that the formiate ions incorporates the ettringite structure as suggested by Pöllmann [140].

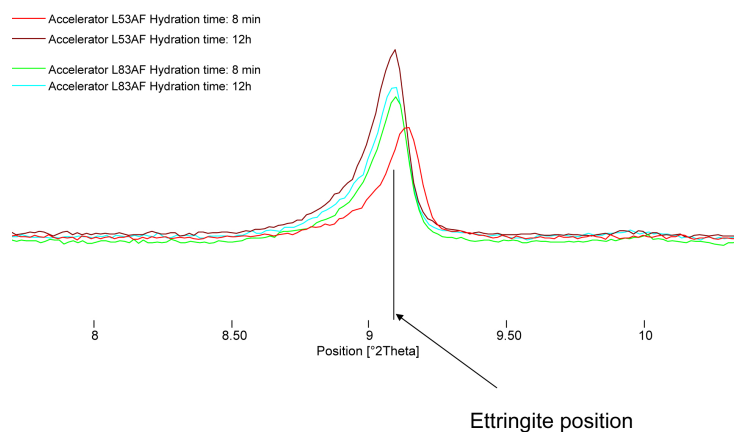


Figure 5.17: Comparison of ettringite peak evolution between accelerated systems A and C.

The mixing procedure remains the same with a speed of 1600rpm. The samples were then analysed by XRD in continuous conditions using a kapton foil. The results

are presented on Figure 5.18. On each graph, the vertical black line represents the reference position of ettringite.

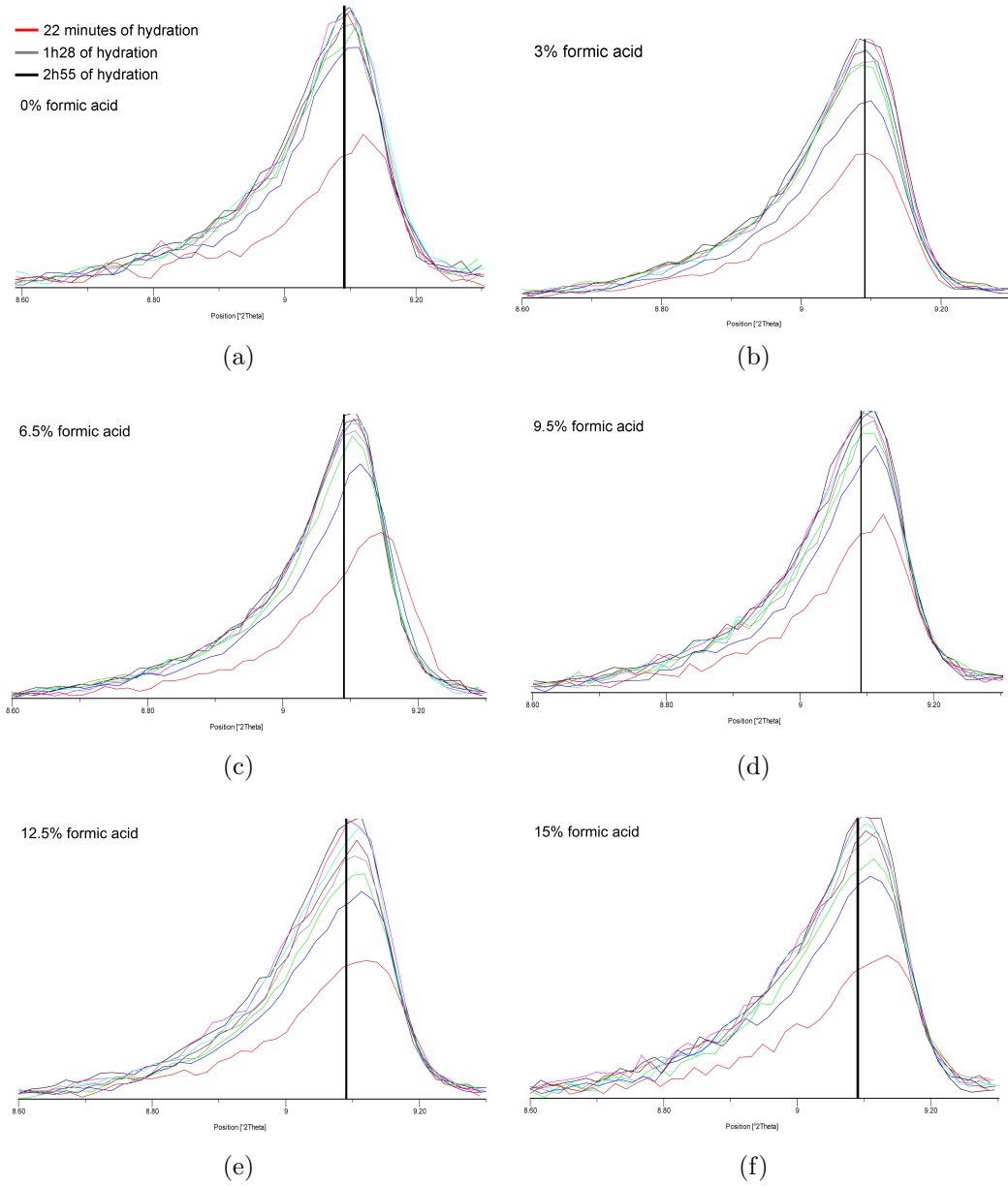


Figure 5.18: X-ray diffraction patterns showing the evolution of the ettringite peak over 3 hours of hydration for accelerated system A containing (a) 0%, (b) 3%, (c) 6.5%, (d) 9.5%, (e) 12.5% and (f) 15% of formic acid content. Diffractograms are recorded every 22 minutes.

From the results obtained for the different systems it is difficult to observe a very clear trend with the increase in formic acid content. At 0%, the first peak recorded after 22 minutes of hydration presents a small shoulder after the reference position of the ettringite peak. This might however be an artifact of measure as at early age the matrix is still full of water and sample's height might change. Otherwise, after 1 hour of hydration, the ettringite peaks are aligned with the reference. We will therefore mainly focus on the diffractogram taken at later time. At 3% of formic

acid content, all the peaks are aligned with the reference. In this case, the acid formic does not affect the interlayer spacing. At 6.5% the ettringite peaks do not align with the reference position which is also the case for the higher contents of formic acid. From these results, it seems possible that the formate ions enters the structure of ettringite if sufficient acid formic is present as proposed by Pllmann [140]. At a content of 6.5%, the interlayer spacing decreases from 9.718 Å to 9.695 Å after 3 hours of hydration. However, more precise acquisitions using for example synchrotron radiation as well as atomistic simulation would ensure and validate these results.

5.2 Shotcrete

In this last section, results related to real shotcrete systems are presented. The kinetics of hydration were monitored by isothermal calorimetry as well as semi-adiabatic calorimetry. This later technique measures the temperature evolution of a large sample compared to isothermal calorimetry. The recorded signal is then corrected to compensate the loss of heat as the system is not perfectly insulated. The mixing protocol is a two step mixing procedure as presented in the previous chapter. A combination of the three cements is mixed with water ($w/c = 0.47 - 0.48$), aggregates (0-4 mm, $c/agg = 0.3$ by weight of cement) and 0.85% (by weight of cement) of RS admixture (retarder-superplasticizer) at a low speed of mixing and then pumped through a nozzle where the accelerator is added (6% by weight of cement). Figure 5.19 shows the evolution of the kinetics of hydration for this system before the addition of the accelerator (bac mixer system) and with the addition of the accelerator after being sprayed. It can be observed that in the presence of the accelerator the aluminate reactions are taking place very early on and dramatically affect the hydration of the silicate phases. This result is also confirmed by the semi-adiabatic calorimetry (see Figure 5.20) which tends to show that this not only a sampling issue (as only 10 grams is required for the isothermal calorimetry sample) for this particular batch even though this hydration behaviour not representative of all shotcretes. This example shows nevertheless the same trend as what was found in paste but in a much more pronounced way. The effect of mixing is probably a key parameter in this case as high shearing conditions develop when the mortar passes through the nozzle. The pattern of the kinetics of hydration are very similar to an under-sulfated system.

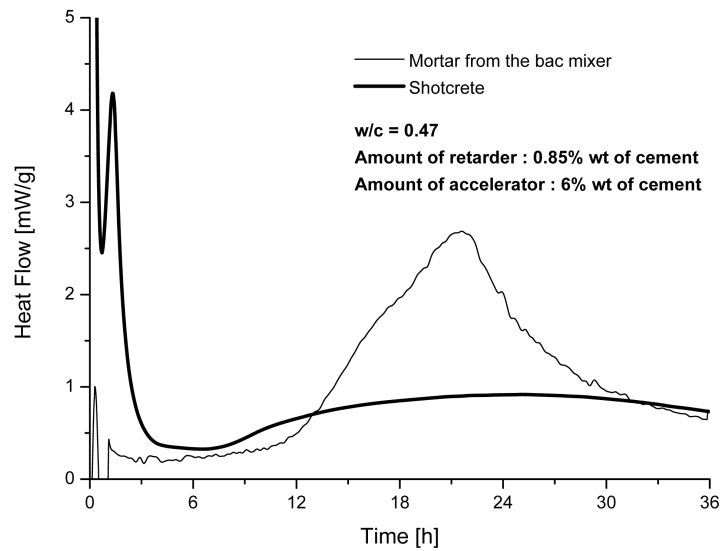


Figure 5.19: Heat flow evolution for a mortar sample before projection monitored by semi-adiabatic calorimetry (sharp line) and a shotcrete sample (system A) after projection monitored by isothermal calorimetry (bold line).

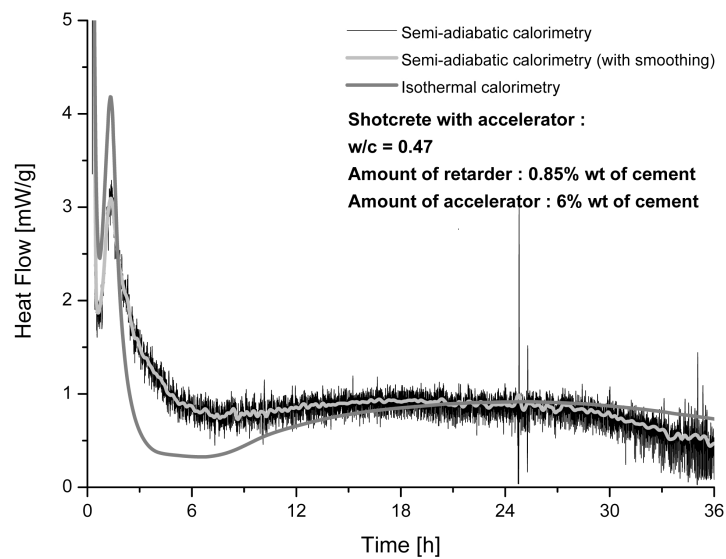


Figure 5.20: Comparison between the heat flow monitored by semi-adiabatic and isothermal calorimetry.

In order to better understand this behaviour, SEM analysis on polished section were performed at three different times: after 6h30, 12h and 24h of hydration (see Figure 5.21). After 6h30 of hydration, according to the isothermal calorimetry, the acceleration period of the silicate hydration has not taken place yet, but some areas of anhydrous alite appear already severely etched. This is in good agreement with the idea that the initial solution is depleted in calcium ions due to the massive formation of ettringite promoting therefore the dissolution of calcium containing phases. The

matrix is already filled with aluminate hydration products such as ettringite and probably some AFm phases. At 12 hours of hydration which corresponds approximately to the middle of the acceleration period of the alite hydration, the matrix densifies, CH crystals are visible but C-S-H is difficult to distinguish as the matrix is already filled with a gel like hydrate. It is possible that this gel like hydrate is an amorphous aluminate hydrate such as AH_3 . Finally at 24 hours, the maximum heat flow of the silicate reaction is attained and the interesting feature is the deep etch pits visible on almost each alite particles. The formation of a rim of C-S-H are sometimes visible around some grains. The matrix appears denser and larger plates of CH are also visible. From this microstructural analysis, part of the kinetic behaviour of the silicate hydration can be explained. As the aluminate hydration reacts very rapidly due to the addition of the accelerator as well as the addition of high shearing conditions induced by the spraying process, the aluminate hydration reacts very rapidly and its hydration products fill up most of the available space of the matrix. The massive precipitation of AFt and AFm phases causes depletion in calcium ions. This depletion induce the consumption of the alite phase before the onset of its acceleration period producing locally some etched areas (see Figure 5.21(a)). As the matrix is already full with aluminate hydration products, less free water and more importantly, less space remains for the silicate hydration to take place normally. This can therefore explain why the heat evolution rate of the reaction is reduced and why the peak is wider. Here again, the uncontrolled aluminate hydration probably due to the rapid gypsum consumption retards dramatically the silicate hydration. The amount of sulfate available appears therefore as the main parameter controlling these accelerated systems.

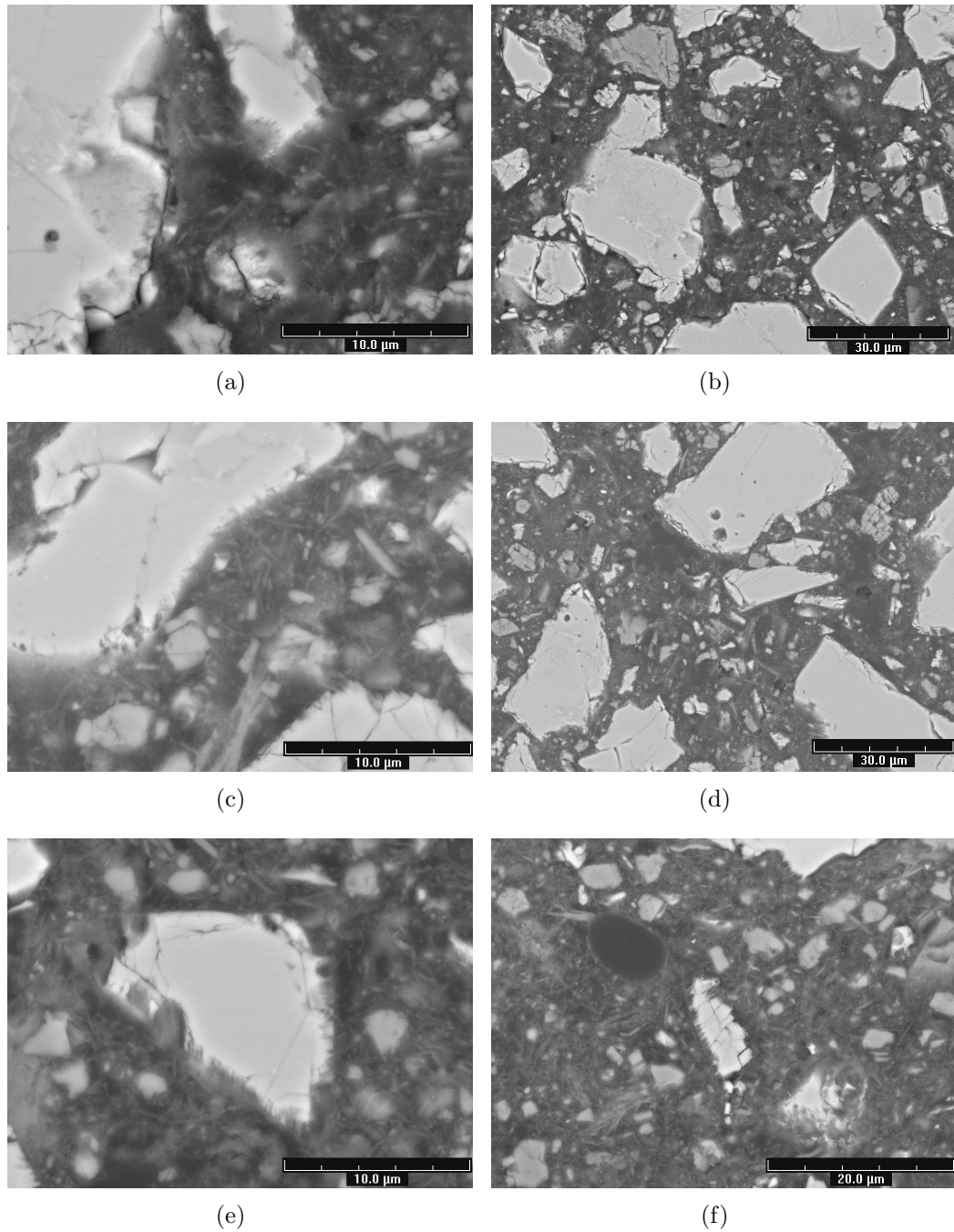


Figure 5.21: SEM micrographs of polished section of shotcrete samples after (a-b) 6h30, (c-d) 12h and (e-f) 24 hours of hydration.

We have tried to mimic this behaviour in laboratory using the same compounds but using the mixing apparatus described in the previous chapter. The kinetics of hydration were not totally replicated but the aluminate reaction does take place quite early (see Accelerated System curve on Figure 5.22). In order to check the validity of the aforementioned hypothesis, two different amounts of gypsum were added to the system, 5% and 10% by weight of cement. The results are presented on Figure 5.22. The addition of gypsum has as an effect to postponed the aluminate peak which is now taking place after the silicate acceleration period but also to

eliminate the retarding effect on the kinetics of the silicate hydration caused by the early aluminate reactions. This result confirms the importance of the sulfate amount in these accelerated systems in order to regulate the aluminate reaction. However, this uncontrolled aluminate reaction may benefit the early strength development as the matrix will be much denser with early hydration products. As noticed by Lootens and co-workers [136], most of the accelerators used in their study show a clear inflection in strength gain after 2 hours followed by a period of much slower gain strength. This slow development of strength may be explained by the reduced and delayed silicate hydration.

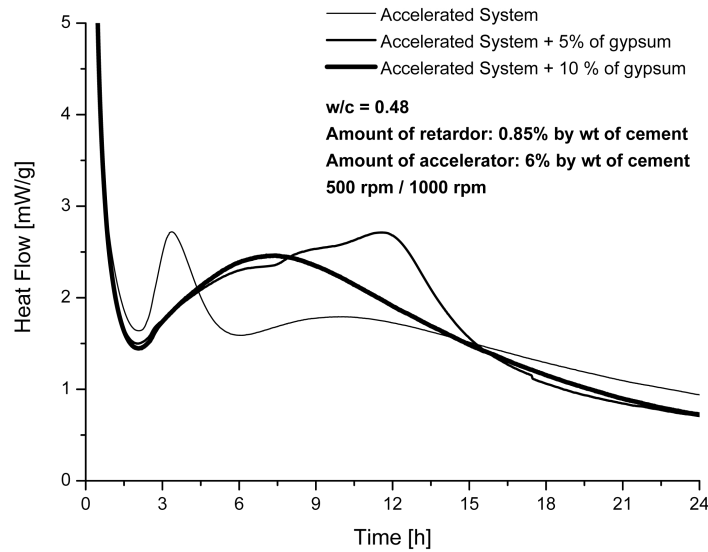


Figure 5.22: Effect of gypsum addition on the kinetics of hydration of an accelerated mortar sample.

5.3 Discussion and Summary

We have shown in this chapter that addition of alkali-free accelerators causes some important changes in terms of hydration kinetics compared to plain cement systems. Particularly, it is the aluminate hydration that is mostly influenced by this type of admixture. Several factors such as the rate of mixing, the chemical composition of the accelerator and the initial sulfate-balance of the plain cement may contribute to these differences in hydration kinetics and might lead to an “uncontrolled” aluminate reaction. The discussion will mainly focus on two aspects. Primarily on the role of the sulfate-balance and finally on the competition between the silicate and aluminate reactions.

5.3.1 Role of sulfate on hydration of accelerated systems

The aluminium-sulfate balance of a plain cement may be a good indication to predict the evolution of the aluminate reaction in presence of an alkali-free accelerator.

High A/\bar{S} ratio will result in a fast and highly exothermic reaction of the aluminate which may take place before or during the acceleration period of the silicate hydration. Lower A/\bar{S} ratio may not have such a dramatic impact on the silicate hydration as it could be seen for the Siegentaler PC.

Addition of gypsum would be needed in large amount to postpone the aluminate reaction sufficiently in time for the alite hydration to take place normally. However, an addition of 5% of gypsum is not applicable in real field condition for durability purposes and another solution remains to be found if we want to better control the aluminate reactions or to accelerate the silicate hydration.

The A/\bar{S} ratio of the accelerator itself is also important as higher ratio may also accelerate the aluminate hydration. Accelerator B which has the lowest A/\bar{S} ratio among all accelerators studied presented the least acceleration of the aluminate reactions. Therefore an optimum sulfate content has to be found regarding the A/\bar{S} ratio of the cement and the accelerator in order to avoid kinetics of reactions similar to under-sulfated systems.

However, the impact of the shearing conditions developed during the mix have to be taken into account as it can accelerate both the aluminate and silicate reactions. Therefore, even if a system would be properly sulfated at low mixing speed regarding the hydration kinetics, these latter might produced a behaviour similar to under-sulfated systems if the mixing conditions are very intense.

5.3.2 Competition between aluminate and silicate reactions

In some extreme cases (high A/\bar{S} ratio of accelerator and cement as well as high shear mixing conditions), sulfate is quickly consummed and a very exothermic event related to C_3A reaction is taking place before or during the silicate acceleration period.

In both cases, a competition between the silicate and aluminate hydration occurs to fill up the available space. If the aluminate reaction is not controlled, this latter can take place before the silicate one and fill up most of the empty space. The consequence is a delayed silicate hydration probably due to a consumption of the calcium ions to produce aluminate hydrates and a limited hydration of the alite as almost all the space is occupied by the aluminate hydrates. If the aluminate reaction happens during the silicate acceleration period, the fastest growing phases will probably fill up most of the available space and limit the parallel reactions. The aluminate hydration is likely to be the fastest process as the solubility product of ettringite is very low, $K_{SP, \text{ettringite}} = 10^{-55.19}$ [damidot:1993].

A compromise should be found in order to limit the aluminate hydration enhanced by the presence of the alkali-free accelerator but resulting in sufficient early strength development and an acceleration of the silicate hydration to ensure a higher rate of strength gain at later ages. Seeding with C-S-H nuclei may be one option to see if these seeds can accelerate the silicate hydration sufficiently to overcome or balance the aluminate hydration. Otherwise, admixtures which would mainly accelerate the silicate hydration could be another possible alternative.

Chapter 6

Conclusion and Perspectives

The main aim of this thesis was to get a better insight into the kinetics of early hydration and the related mechanisms. It has been shown that theory of crystal dissolution developed in the field of geochemistry seems to apply to the hydration of alite up to the onset of the acceleration period. The saturation state of the solution as well as the density of crystallographic defects were shown to be the main rate controlling factors. At high undersaturation, alite dissolution is dominated by the formation of etch pits but the study of mixing indicates that the rate controlling factor of the overall process is limited by transport through an electrical double layer forming at the solid-liquid interface. At lower undersaturation, the step retreat mechanism prevails and the overall rate of dissolution is therefore limited by surface reactions.

These findings enable us to propose a new mechanism for the early hydration of alite where dissolution is the main controlling factor up to the onset of the acceleration period. Explanations of different features such as the retarding effect of calcium hydroxide addition in C_3S seeding experiments, the influence of mixing on the kinetics of hydration and part of the acceleration effect of calcium chloride addition on alite were possible using these concepts of crystal dissolution.

Alkali-free accelerators enhance mainly the aluminate hydration leading to a massive precipitation of ettringite. This latter feature may enhance the dissolution of the silicate phases since calcium ions in the pore solution are rapidly consumed. This enhanced dissolution does not seem to provide an earlier formation of C-S-H and obviously not CH.

The acceleration effect of the aluminate may be at the expense of the silicate hydration producing kinetics similar to under-sulfated systems. The type of acid used to stabilise the accelerator, the shearing conditions of the mix as well as the initial sulfate-balance of the PC and the accelerator are some of the parameters which may be responsible for an “uncontrolled” aluminate reaction having a dramatic effect on the hydration of alite. This may lead to a competition between the silicate and the aluminate reaction to fill up the available space where the aluminate reaction is more likely to dominate. However, these accelerated systems do not always exhibit hydration kinetics similar to under-sulfated systems but the aluminate reaction is in any case enhanced.

Perspectives

Concerning the alite hydration, future works should characterise the nature and the density of crystallographic defects of this phase even though it has been shown in the field of geochemistry that no linear correlation was found between the density of dislocations and the rate of dissolution for many different minerals. Techniques such as VSI (vertical scanning interferometry) using a flow through reactor may enable measurements of the rate of dissolution of alite under different undersaturation conditions.

We were also not able to measure the interfacial energy of the alite-water interface. Direct measurement of this value is experimentally difficult but a range of value may be found using molecular dynamics.

Another field of interest would also be the nucleation and growth process of C-S-H and CH. We were not able to assess which phase is responsible for the onset of the acceleration period. The precipitation of primary hydrates composed of monomeric hydrated silicate units is certainly taking place before the end of the induction period but no clues were found regarding any possible transformation of these primary hydrates to a thermodynamically more stable phase or if nucleation of more stable hydrates is taking place independently.

The mechanisms of C-S-H growth as well as the matrix densification are also of fundamental interest since they regulate the kinetics of hydration after the induction period. Models have already been proposed but new techniques such as FIB and TEM tomography could potentially bring useful information at the micro and nanoscale level.

The kinetics of hydration of the aluminate phases need also to be further investigated. The role of sulfate as regulator of the C_3A reaction is well established but its effect on the renewed aluminate reaction taking place normally after the acceleration period resulting in the further formation of ettringite is still poorly understood. It is known that this reaction is not taking place directly at the exhaustion of gypsum but enough sulfate should be present to precipitate ettringite. One hypothesis would be that the adsorbed sulfate on C-S-H could be desorbed to further react in solution to form ettringite. It would therefore be interesting to follow the evolution of the sulfate content adsorbed on the C-S-H to check the validity of this hypothesis.

Finally, regarding the impact of alkali-free accelerator on the kinetics of hydration, the influence of pH changes of the pore solution as well as possible specific interactions with the anhydrous phases depending on the type of acid used to stabilise these admixture needs to be further studied.

Bibliography

- [1] K.L. Scrivener. The development of microstructure during the hydration of portland cement, 1984.
- [2] H. Minard, S. Garrault, L. Regnaud, and A. Nonat. Mechanisms and parameters controlling the tricalcium aluminate reactivity in the presence of gypsum. *Cement and Concrete Research*, 37:1418–1426, 2007.
- [3] N. Tenoutasse. The hydration mechanism of c_3a and c_3s in the presence of calcium chloride and calcium sulphate. *in 5th ISCC*, 2:372–378, 1968.
- [4] A. Quennoz, E. Gallucci, C.F. Dunant, and K.L. Scrivener. Influence of the gypsum amount on the hydration of tricalcium aluminate in c_3a -gypsum and in alite- c_3a -gypsum systems. *in 17th ibausil, Weimar*, 1:1–0207 – 1–0212, 2009.
- [5] E.M. Gartner, J.F. Young, D.A. Damidot, and I. Jawed. *Structure and Performance of cements*, 2nd edition. Spon Press, 2002.
- [6] S. Bishnoi and K.L. Scrivener. μic : A new platform for modelling the hydration of cements. *Cement and Concrete Research*, 39:266–274, 2009.
- [7] E.M. Gartner and H.M. Jennings. Thermodynamics of calcium silicate hydrates and their solutions. *J. Am. Ceram. Soc.*, 70(10):743–749, 1987.
- [8] D. Ménétrier, I. Jawed, T.S. Sun, and J. Skalny. ESCA and SEM studies on early C_3S hydration. *Cement and Concrete Research*, 9:473–482, 1979.
- [9] P.W. Brown, E. Franz, G. Frohnsdorff, and H.F.W. Taylor. Analyses of the aqueous phase during early C_3S hydration. *Cement and Concrete Research*, 14:257–262, 1984.
- [10] S. Garrault, E. Finot, E. Lesniewska, and A. Nonat. Study of c-s-h growth on c_3s surface during its early hydration. *Materials and Structures*, 38:435–442, 2005.
- [11] G.A. Parks. Surface and interfacial energy of quartz. *Journal of Geophysical research*, 89:3997–4008, 1984.
- [12] A.C. Lasaga. *Kinetic Theory in the Earth Sciences*. Princeton University Press, 1998.
- [13] J. Castaing. Dislocations in ceramics. *Encyclopedia of Materials: Science and Technology*, pages 2271–2278, 2001.

- [14] K. Mori, T. Fukunaga, Y. Shiraishi, K. Iwase, Q. Xu, K. Oishi, K. Yatsuyanagi, M. Yonemura, K. Itoh, M. Sugiyama, T. Ishigaki, T. Kamiyama, and M. Kawai. Structural and hydration properties of amorphous tricalcium silicate. *Cement and Concrete Research*, 36:2033–2038, 2006.
- [15] H.H. Teng. Controls by saturation state on etch pit formation during calcite dissolution. *Geochimica and Cosmochimica Acta*, 68:253–262, 2004.
- [16] P.M. Dove and N. Han. Kinetics of mineral dissolution and growth as reciprocal microscopic surface processes across chemical driving force. in *AIP Conference Proceedings*, 916:215–234, 2005.
- [17] A.C. Lasaga and A. Lüttge. Variation of crystal dissolution rate based on a dissolution stepwave model. *Science*, 291:2400–2404, 2001.
- [18] J. Schott, S. Brantley, D. Cerar, C. Guy, M. Borcsik, and C. Willaime. Dissolution kinetics of strained calcite. *Geochimica et Cosmochimica Acta*, 53:373–382, 1989.
- [19] R.T. Cygan, W.H. Casey, M.B. Boslough, H.R. Westrich, M.J. Carr, and G.R. Holdren. Dissolution kinetics of experimentally shocked silicate minerals. *Chemical Geology*, 78:229–244, 1989.
- [20] W.H. Casey, M.J. Carr, and R.A. Graham. Crystal defects and the dissolution kinetics of rutile. *Geochimica et Cosmochimica Acta*, 52:1545–1556, 1988.
- [21] C.M. Eggleston, M.F. Hochella, and G.A. Parks. Sample preparation and ageing effects on the dissolution rate and surface composition of diopside. *Geochimica et Cosmochimica Acta*, 53:797–804, 1989.
- [22] W. Stumm. *Chemistry of the solid-water interface*. John Wiley & Sons, Inc., 1992.
- [23] P.M. Dove and M.F. Hochella. Calcite precipitation mechanisms and inhibition by orthophosphate: In situ observations by scanning force microscopy. *Geochimica et Cosmochimica Acta*, 57:705–714, 1993.
- [24] P.M. Dove and D.A. Crerar. Kinetics of quartz dissolution in electrolyte solutions using a hydrothermal mixed flow reactor. *Geochimica et Cosmochimica Acta*, 54:955–969, 1990.
- [25] D. Spagnoli, D.J. Cooke, S. Kerisit, and S.C. Parker. Molecular dynamics simulations of the interaction between the surfaces of polar solids and aqueous solutions. *Journal of Materials Chemistry*, 16:1997–2006, 2006.
- [26] M.M. Costoya. Effect of particle size distribution on the hydration kinetics and microstructural development of tricalcium silicate, 2008.
- [27] P. Fierens, J. Tirlocq, and J.P. Verhaegen. Défauts de structure et hydratation du silicate tricalcique. *Ind. Chim. Belg.*, 39:363–367, 1974.
- [28] T. Sakurai, T. Sato, and A. Yoshinaga. The effect of minor components on the early hydraulic activity of the major phases of portland cement clinker. in *5th ISCC*, 1:300–321, 1969.

- [29] J.M. Makar and G.W. Chan. End of induction period in ordinary portland cement as examined by high-resolution scanning electron microscopy. *J. Am. Ceram. Soc.*, 91(4):1292–1299, 2008.
- [30] H. di Murro. Mécanismes d’élaboration de la microstructure des bétons, 2007.
- [31] L. Nicoleau. Interactions physico-chimiques entre latex et les phases minérales constituant le ciment au cours de l’hydratation, 2004.
- [32] D. Damidot and A. Nonat. C₃S hydration in diluted and stirred suspensions: (I) study of the two kinetic steps. *Advances in Cement Research*, 6(21):27–35, 1994.
- [33] D. Damidot, D. Sorrentino, and D. Guinot. Factors influencing the nucleation and growth of the hydrates in cementitious systems: An experimental approach. in *Proceedings of the 2nd International RILEM Symposium*, 13:161–197, 1997.
- [34] D.L. Kantro. Tricalcium silicate hydration in the presence of various salts. *Journal of Testing and Evaluation*, 3(4):312–321, 1975.
- [35] P.W. Brown, C.L. Harner, and H.J. Prosen. The effect of inorganic salts on tricalcium silicate hydration. *Cement and Concrete Research*, 16:17–22, 1985.
- [36] N.J. Clayden S.A. Rodger, G.W. Groves and C.M. Dobson. Hydration of tricalcium silicate followed by ²⁹Si NMR with cross-polarisation. *J. Am. Ceram. Soc.*, 71(2):91–96, feb 1988.
- [37] T.E. Burch, K.L. Nagy, and A.C. Lasaga. Free energy dependence of albite dissolution kinetics at 80°C and pH 8.8. *Chemical Geology*, 105:137–162, 1993.
- [38] D. Damidot, F. Bellman, B. Möser, and T. Sowoidnich. Modelling the effect of electrolytes on the rate of early hydration of tricalcium silicate. in *1st International Conference on Microstructure Related Durability of Cementitious Composites*, W. Sun, K. van Breugel, C. Miao, G. Ye, H. Chen eds., RILEM Proceedings PRO 61, Nanjing (China), pages 1075–1081, 2008.
- [39] A. Zingg, F. Winnefeld, L. Holzer, J. Pakusch, S. Becker, and L. Gauckler. Adsorption of polyelectrolytes and its influence on the rheology, zeta potential and microstructure of various cement and hydrate phases. *Journal of Colloid and Interface Science*, 323:301–312, 2008.
- [40] K. Sangwal. *Etching of crystals*, volume 15. North-Holland, 1987.
- [41] J.J. Thomas, H.M. Jennings, and J.J. Chen. Influence of nucleation seeding on the hydration mechanisms of tricalcium silicate and cement. *J. Phys. Chem. C*, 113:4327–4334, 2009.
- [42] J. Skalny and M.E. Tadros. Retardation of tricalcium aluminate hydration by sulfates. *J. Am. Ceram. Soc.*, 60:174–175, 1977.
- [43] T.K. Kundu, H. Rao, and S.C. Parker. Competitive adsorption on wollastonite: an atomistic simulation approach. *J. Phys. Chem. B*, 109(22):11286–11295, 2005.

- [44] R.A. Berner. Rate control of mineral dissolution under earth surface conditions. *The American journal of science*, 278:1235–1252, 1978.
- [45] M. Jolin, D. Beaupré, and S. Mindess. Tests to characterise properties of fresh dry-mix shotcrete. *Cement and Concrete Research*, 29:753–760, 1999.
- [46] H.M. Jennings and P.L. Pratt. Le béton projeté : nouveaux développements et applications. *Can. J. Civ. Eng.*, 27:383–388, 2000.
- [47] A. Ishida. High strength at an early age. *Tunnels and Tunnelling International*, pages 21–25, 2007.
- [48] H.F.W. Taylor. *Cement Chemistry 2nd Ed.* Thomas Telford Publishing, 1997.
- [49] L. Black, C. Breen, J. Yarwood, C.S. Deng, J. Phipps, and G. Maitland. Hydration of tricalcium aluminate (c_3a) in the presence and absence of gypsum – studied by raman spectroscopy and x-ray diffraction. *Journal of Materials Chemistry*, 16:1263–1272, 2006.
- [50] H.E. Schwiete, U. Ludwig, and P. Jäger. Investigation in the system $3cao.al_2o_3-caso_4-cao-h_2o$. *44th Annual Meeting of the Highway Research Board, Special Report*, 90:353–367, 1966.
- [51] R.F. Feldman and V.S. Ramachandran. Character of hydration of $3cao.al_2o_3$. *J. Amer. Ceram. Soc.*, 49:268–273, 1966.
- [52] H. Manzano, J.S. Dolado, and A. Ayuela. Structural, mechanical and reactivity properties of tricalcium aluminate using first-principles calculations. *J. Am. Ceram. Soc.*, 92:897–902, 2009.
- [53] M. Collepardi, G. Baldini, M. Pauri, and M. Corradi. Tricalcium aluminate hydration in the presence of lime gypsum or sodium sulfate. *Cement and Concrete Research*, 8:571–580, 1978.
- [54] I.G. Richardson. The nature of the hydration products in hardened cement pastes. *Cement and Concrete Research*, 22:97–113, 2000.
- [55] P.Barret, D. Ménétrier, and D. Bertrandie. Mechanism of C_3S dissolution and the problem of congruency in the very initial period and later. *Cement and Concrete Research*, 13:728–738, 1983.
- [56] S. Garrault and A. Nonat. Hydrated layer formation on tricalcium and dicalcium silicate surfaces: Experimental study and numerical simulations. *Langmuir*, 17:8131–8138, 2001.
- [57] I. Odler. *Lea’s Chemistry of Cement and Concrete*. Arnold, 1998.
- [58] J.P. Skalny and J.F. Young. Mechanisms of portland cement hydration. in *7th ISCC*, 1:II–1/3–II–1/45, 1980.
- [59] Le Châtelier. *Recherches expérimentales sur la constitution des mortiers hydrauliques*. Dunod, 1904.

- [60] P. Barret and D. Ménétrier. Filter dissolution of C_3S as a function of lime concentration in a limited amount of lime water. *Cement and Concrete Research*, 10:521–534, 1980.
- [61] H.N. Stein and J.M. Stevels. Influence of silica on the hydration of $3 CaO, SiO_2$. *J. appl. Chem.*, 14:338–346, aug 1964.
- [62] D.L. Kantro, S. Brunauer, and C.H. Weise. Development of surface in the hydration of calcium silicates. II. extension of investigations to earlier and later stages of hydration. *Journal of Chemical Chemistry*, 66(10):1804–1809, 1962.
- [63] J.D. Birchall, A.J. Howard, and J.E. Bailey. On the hydration of portland cement. *Proc. R. Soc. Lond. A.*, 360:445–453, 1978.
- [64] D.D. Double, A. Hellawell, and S.J. Perry. The hydration of portland cement. *Proc. R. Soc. Lond. A.*, 359:435–451, 1979.
- [65] M.E. Tadros, J. Skalny, and R.S. Kalyoncu. Early hydration of tricalcium silicate. *J. Am. Ceram. Soc.*, 59:344–347, 1976.
- [66] O.S. Pokorovsky, S.V. Golubev, and J.A. Mielczarski. Kinetic evidences of the existence of positively charged species at the quartz-aqueous solution interface. *Journal of colloid and Interface Science*, 296:189–194, 2006.
- [67] S.C. Parker, J.P. Allen, C. Arrouvel, D. Spagnoli, S. Kerisit, and D.C. Sayle. Molecular simulation of mineral surfaces and the role of impurities on surface stabilities. *AIP Conference Proceedings*, 916:268–287, 2007.
- [68] J.A. Davis and D.B. Kent. Surface complexation modeling in aqueous geochemistry. in *Reviews of Mineralogy*, 23:177–260, 1990.
- [69] G. Sposito. Molecular models of ion adsorption on mineral surfaces. in *Reviews of Mineralogy*, 23:261–279, 1990.
- [70] P. Fierens and J.P. Verhaegen. Hydration of tricalcium silicate in paste – kinetics of calcium ions dissolution in the aqueous phase. *Cement and Concrete Research*, 6:337–342, 1976.
- [71] I. Odler and H. Dörr. Early hydration of tricalcium silicate II. the induction period. *Cement and Concrete Research*, 9:277–284, 1979.
- [72] S. Garrault-Gauffinet and A. Nonat. Experimental investigation of calcium silicate hydrate (C-S-H) nucleation. *Journal of Crystal Growth*, 200:565–574, 1999.
- [73] J.F. Young, H.S. Tong, and R.L. Berger. Compositions of solutions in contact with hydrating tricalcium silicate pastes. *J. Am. Ceram. Soc.*, 60(5-6):193–198, 1977.
- [74] I. Odler and J. Schüppstuhl. Early hydration of tricalcium silicate III. control of the induction period. *Cement and Concrete Research*, 11:765–774, 1981.
- [75] J.N. Maycock, J. Skalny, and R. Kalyoncu. Crystal defects and hydration I. influence of lattice defects. *Cement and Concrete Research*, 4:835–847, 1974.

- [76] J.G.M. de Jong, H.N. Stein, and J.M. Stevels. Hydration of tricalcium silicate. *J. Appl. Chem.*, 17:246–250, sep 1967.
- [77] R. Kondo and M. Daimon. Early hydration of tricalcium silicate: A solid reaction with induction and acceleration period. *J. Am. Ceram. Soc.*, 52(9):503–508, 1969.
- [78] H.M. Jennings and P.L. Pratt. An experimental argument for the existence of a protective membrane surrounding portland cement during the induction period. *Cement and Concrete Research*, 9:501–506, 1979.
- [79] A.C. Lasaga and A.E. Blum. Surface chemistry, etch its and mineral-water reactions. *Geochimica and Cosmochimica Acta*, 50:2363–2379, 1986.
- [80] R. Petrovich. Rate control in feldspar dissolution – II. the protective effect of precipitates. *Geochimica et Cosmochimica Acta*, 40:1509–1521, 1976.
- [81] C. Correns and W. von Engelhardt. Neue untersuchungen über die verwitterung des kalifeldspates. *Die Naturwissenschaften*, 26:137–138, 1938.
- [82] R. Wollast. Kinetics of the alteration of k-feldspar in buffered solutions at low temperature. *Geochimica et Cosmochimica Acta*, 31:635–648, 1968.
- [83] H.C. Helgeson. Kinetics of mass transfer among silicates and aqueous solutions. *Geochimica et Cosmochimica Acta*, 35:421–469, 1971.
- [84] H.C. Helgeson. Kinetics of mass transfer among silicates and aqueous solutions: Correction and clarification. *Geochimica et Cosmochimica Acta*, 36:1067–1070, 1972.
- [85] M. Lagache, J. Wyart, and G. Sabatier. Dissolution des feldspaths alcalins dans l’eau pure ou chargée de CO_2 à 200 °c. *Mémoires et communications des membres et correspondants de l’académie des sciences*, pages 2019–2022, 1961.
- [86] M. Lagache. Contribution à l’étude de l’altération des feldspaths dans l’eau, entre 100 et 200 °c, sous diverses pressions de CO_2 , et application à la syntèse des minéraux argileux. *Bull. Soc. fr. Minér. Crist.*, pages 223–253, 1965.
- [87] M. Lagache. New data on the kinetics of the dissolution of alkali feldspars at 200°C in CO_2 charged water. *Geochimica and Cosmochimica Acta*, 40:157–161, 1976.
- [88] W.E. Dibble and W.A. Tiller. Non-equilibrium water/rock interactions – I model for interface-controlled reactions. *Geochimica et Cosmochimica Acta*, 45:79–92, 1981.
- [89] R.W. Luce, R.W. Bartlett, and G.A. Parks. Dissolution kinetics of magnesium silicates. *Geochimica et Cosmochimica Acta*, 36:35–50, 1972.
- [90] T. Paces. Steady-state kinetics and equilibrium between ground water and granitic rock. *Geochimica et Cosmochimica Acta*, 37:2641–2663, 1973.

- [91] L. Chou and R. Wollast. Study of the weathering of albite at room temperature and pressure with a fluidized bed reactor. *Geochimica et Cosmochimica Acta*, 48:2205–2217, 1984.
- [92] R. Petrovich, R.A. Berner, and M.B. Goldhaber. Rate control in dissolution of alkali feldspars-I. study of residual feldspar grains by x-ray photoelectron spectroscopy. *Geochimica et Cosmochimica Acta*, 40:537–548, 1976.
- [93] G.R. Holdren and R.A. Berner. Mechanism of feldspar weathering-I. experimental studies. *Geochimica et Cosmochimica Acta*, 43:1161–1171, 1979.
- [94] R.A. Berner and G.R. Holdren. Mechanism of feldspar weathering-II. observations of feldspars from soils. *Geochimica et Cosmochimica Acta*, 43:1173–1186, 1979.
- [95] R.A. Berner, E.L. Sjöberg, M.A. Velbel, and M.D. Krom. Dissolution of pyroxenes and amphiboles during weathering. *Science*, 207:1205–1206, 1980.
- [96] J. Schott, R.A. Berner, and E.L. Sjöberg. Mechanism of pyroxene and amphibole weathering-I. experimental studies of iron-free minerals. *Geochimica et Cosmochimica Acta*, 45:2123 – 2135, 1969.
- [97] R.A. Berner and J. Schott. Mechanism of pyroxene and amphibole weathering-II. observations of soil grains. *American Journal of Science*, pages 1214–1231, 1982.
- [98] B. van der Hoek, W.J.P. van Enkevort, and W.H. van der Linden. Dissolution kinetics and etch pit studies of potassium aluminium sulphate. *Journal of Crystal Growth*, 61:181–193, 1983.
- [99] H.C. Helgeson, W.M. Murphy, and P. Aagaard. Thermodynamic and kinetic constraints on reaction rates among minerals and aqueous solutions. II. rate constants, effective surface area and the hydrolysis of feldspar. *Geochimica et Cosmochimica Acta*, 48:2405–2432, 1984.
- [100] G.A. Parks. Surface energy and adsorption at mineral water interfaces: an introduction. in *Reviews in Mineralogy*, 23:133–175, 1990.
- [101] A.W. Adamson. *Physical chemistry of surfaces*, 4th ed. Jhon Wiley & Sons, New York, 1992.
- [102] N.H. de Leeuw and S.C. Parker. Atomistic simulation of the effect of molecular adsorption of water on the surface structure and energies of calcite surfaces. *J. Chem. Soc., Faraday Trans.*, 93(3):467–475, 1997.
- [103] S. Kerisit, S.C. Parker, and J.H. Harding. Atomistic simulation of the dissociative adsorption of water on calcite surfaces. *J. Phys. Chem. B*, 107:7676–7682, 2003.
- [104] M.F. Hochella. Atomic structure, microtopography, composition and reactivity of mineral surfaces. in *Reviews of Mineralogy*, 23:87–132, 1990.

- [105] A.C. Lasaga. Atomic treatment of mineral-water surface reactions. *in Reviews of Mineralogy*, 23:17–85, 1990.
- [106] A. Mortensen. *Cours-Déformation et Rupture I et III*. 2000.
- [107] R. Petrovich. Kinetics of dissolution of mechanically comminuted rock-forming oxides and silicates – I. deformation and dissolution of quartz under laboratory conditions. *Geochimica et Cosmochimica Acta*, 45:1665–1674, 1981.
- [108] P.M. Dove, N. Han, and J.J. De Yoreo. Mechanisms of classical crystal growth theory explain quartz and silicate dissolution behavior. *PNAS*, 102(43):15357–15362, 2005.
- [109] A.J. Malkin, Y.G. Kuznetsov, and A. McPherson. In situ atomic force microscopy studies of surface morphology growth kinetics, defect structure and dissolution in macromolecular crystallization. *journal of Crystal Growth*, 196:471–488, 1999.
- [110] N. Cabrera and M.M. Levine. On the dislocation theory of evaporation of crystals. *Philos. Mag.*, 1:450–458, 1956.
- [111] A. Lüttge. Crystal dissolution kinetics and Gibbs free energy. *Journal of Electron Spectroscopy and Related Phenomena*, 150:248–259, 2006.
- [112] H.H. Teng, P. Fenter, L. Cheng, and N.C. Sturchio. Resolving orthoclase dissolution processes with atomic force microscopy and X-ray reflectivity. *Geochimica and Cosmochimica Acta*, 65:3459–3474, 2001.
- [113] I.N. Macinnis and S.L. Brantley. The role of dislocations and surface morphology in calcite dissolution. *Geochimica and Cosmochimica Acta*, 56:1113–1126, 1992.
- [114] Fabrizio Moro. *Nanocem calorimetry workshop in Praha*, 2008.
- [115] E.H. Oelkers, J. Schott, and J.-L. Devidal. The effect of aluminum, ph and chemical affinity on the rates of aluminosilicate dissolution reactions. *Geochimica et Cosmochimica Acta*, 58:2011–2024, 1994.
- [116] R.K. Iler. *The chemistry of silica*. Wiley-Science, 1979.
- [117] P.M. Dove and C.J. Nix. The influence of the alkaline earth cations, magnesium, calcium, and barium on the dissolution kinetics of quartz. *Geochimica et Cosmochimica Acta*, 61:3329–3340, 1997.
- [118] L.M. Walter and J.S. Hanor. Effect of orthophosphate on the dissolution kinetics of biogenic magnesian calcites. *Geochimica et Cosmochimica Acta*, 43:1377–1385, 1979.
- [119] E.A. Burton and L.M. Walter. The role of ph in phosphate inhibition of calcite and aragonite precipitation rates in seawater. *Geochimica et Cosmochimica Acta*, 54:797–808, 1990.
- [120] P.M. Dove and S.F. Elston. Dissolution kinetics of quartz in sodium chloride solutions: Analysis of existing data and a rate model for 25 °c. *Geochimica et Cosmochimica Acta*, 56:4147–4156, 1992.

- [121] P.M. Dove. The dissolution kinetics of quartz in aqueous mixed cation solutions. *Geochimica et Cosmochimica Acta*, 63:3715–3727, 1999.
- [122] R.B. Williamson. Constitutional supersaturation in portland cement solidified by hydration. *Journal of Crystal Growth*, 3:787–794, 1968.
- [123] M.C.G. Juenger, P.J.M. Monteiro, E.M. Gartner, and G.P. Denbaur. A soft x-ray microscope investigation into the effects of calcium chloride on tricalcium silicate hydration. *Cement and Concrete Research*, 35:19–25, 2005.
- [124] P. Fierens, J. Tirlocq, and J.P. Verhaegen. Luminescence et hydratation du silicate tricalcique. *Cement and Concrete Research*, 3:549–560, 1973.
- [125] P. Fierens, J. Tirlocq, and J.P. Verhaegen. Influence du mode d’excitation sur la thermoluminescence du silicate tricalcique. *Cement and Concrete Research*, 3:227–232, 1973.
- [126] K.E. Hudson and G.W. Groves. The structure of alite in portland cement clinker – TEM evidence. *Cement and Concrete Research*, 12:61–68, 1982.
- [127] U. Becker, S. Biswas, T. Kendall, P. Risthaus, C.V. Putnis, and C.M. Pina. Interactions between mineral surfaces and dissolved species: From monovalent ions to complex organic molecules. *The American journal of science*, 305:791–825, 2005.
- [128] H.N. Stein. Thermodynamic considerations on the hydration mechanisms of Ca_3SiO_5 and $\text{Ca}_3\text{Al}_2\text{O}_6$. *Cement and Concrete Research*, 2:167–177, 1972.
- [129] K. Mishra and H. Heinz. Atomistic simulation of cleavage energy of c_3s and organic-silicate interactions. *Presentation in Challenges and promises of multi-scale modelling schemes for cementitious materials workshop, Derio (Spain), 2-4 mars*, 2009.
- [130] J.W. Bullard. A determination of hydration mechanisms for tricalcium silicate using a kinetic cellular automaton model. *J. Am. Ceram. Soc.*, 91(7):2088–2097, 2008.
- [131] J.W. Bullard. Three-dimensional structural modelling of cement hydration: Opportunities for bridging length scales. *Presentation in Challenges and promises of multi-scale modelling schemes for cementitious materials workshop, Derio (Spain), 2-4 mars*, 2009.
- [132] D.A. Williams, A.W. Saak, and H.M. Jennings. The influence of mixing on the rheology of fresh cement paste. *Cement and Concrete Research*, 29:1491–1496, 1999.
- [133] D. Dollimore and R.J. Mangabhai. Effect of mixing time on heat evolution pattern of cement pastes. *Thermochimica Acta*, 85:223–226, 1985.
- [134] S. Bishnoi and K.L. Scrivener. Studying nucleation and growth kinetics of alite hydration using μic . *Cement and Concrete Research*, 39:849–860, 2009.

- [135] P. Sandberg and L.R. Roberts. Studies of cement-admixture interactions related to aluminate hydration control by isothermal calorimetry. *in 7th CAN-MET/ACI International conference on superplasticizers and other chemical admixtures in concrete*, 1:SP-217–235, 2003.
- [136] D. Lootens, B. Lindlar, and R.J. Flatt. Some peculiar chemistry aspect of shotcrete accelerators. *in Proceedings of the 1st International Conference on Microstructure Related Durability of Cementitious Composites, Nanjing (China)*, 2:1255–1261, 2008.
- [137] J. Arnold. Influence of the accelerator formulation on the microstructural setting of shotcrete. *Diploma Work, EPFL*, 2005.
- [138] C. Paglia, F. Wombacher, and H. Böhni. The influence of alkali-free and alkaline shotcrete accelerators within cement systems I. characterization of the setting behavior. *Cement and Concrete Research*, 31:913–918, 2001.
- [139] P. Bénard, S. Garrault, A. Nonat, and C. Cau dit Coumes. Influence of orthophosphate ions on the dissolution of tricalcium silicate. *Cement and Concrete Research*, 38:1137–1141, 2005.
- [140] H. Pöllmann. Carboxylic acid anions: The reaction mechanisms and products with the aluminate phase of cement. *in Proceedings of the 9th ICC*, pages 198–204, 1980.

Acknowledgments

I would like to thank the following people who made this work possible:

- Professor Karen L. Scivener, my thesis director; I am most grateful for the advice and support she gave me throughout the duration of this thesis, for making it possible for me to present my work in several international conferences and workshops. I enjoyed our short-lasting but motivating and stimulating discussions.
- Dr. Emmanuel Gallucci, my thesis co-director, for his daily support and scientific guidance. Despite all the very interesting academic discussion, I mainly enjoyed the beers, mountain hiking or ski that we had the chance to share!
- Dr. Robert J. Flatt, from Sika A.G., for stimulating discussions and guidance during this work. I am also very thankful for letting me the liberty of exploring concepts out of the cement field.
- People at Sika, particularly Heinz, Irene, Christian, Marc, Renato, Denise for their helpful contribution during this work and especially Dr. Didier Lootens and Dr. Benedikt Lindlar for their great help during the shotcrete, US experiments performed at Sika.
- LMC people for the good atmosphere and all the good moment spent together outside the lab, particularly at Satellite. I am also thankful to all my office mates but a special thanks to Vanessa and Cyrille for their particular help, academical as well as more practical, it was a great pleasure to spend time with you!
- The undergraduate students who preformed the semester projects!
- Pierre Burdet, Milan Felberbaum and Marco Cantoni for the FIB measurements and data treatment.
- Sika A.G. for financial support.
- Danielle and my family, for their love and support!

Finally, I would like to thank the members of my thesis Jury for reviewing this work: Professor André Nonat from Université de Bourgogne, Dr. Robert J. Flatt from Sika A.G. (Zürich, Switzerland), Dr. Paul Bowen from LTP at EPFL, Professor Karen L. Scivener and Dr. Emmanuel Gallucci from LMC. I am also thankful to Professor Pierre Stadelmann, from CIME at EPFL, who was the president of this Jury.

Annexe I

Nomenclature

Symbol	Definition
C	Free lime - CaO
S	Silica - SiO ₂
A	Alumina - Al ₂ O ₃
F	Iron oxide III - Fe ₂ O ₃
H	Water - H ₂ O
S̄	Sulfur trioxide - SO ₃
C̄	Calcium carbonate - CaCO ₃
N	Sodium oxide - Na ₂ O
K	Potassium oxide - K ₂ O
M	Magnesium oxide - MgO
C ₃ S	Tricalcium silicate - 3CaO.SiO ₂
C ₂ S	Dicalcium silicate - Belite - 2CaO.SiO ₂
C ₃ A	Tricalcium aluminate - 3CaO.Al ₂ O ₃
C ₄ AF	Solid solution of 2CaO.Fe ₂ O ₃ and 2CaO.Al ₂ O ₃ - 4CaO.Al ₂ O ₃ .Fe ₂ O ₃
C \bar{S}	Anhydrite - CaSO ₄
CH	Calcium Hydroxide - Ca(OH) ₂
C-S-H	Calcium silicate hydrate gel - CaO.SiO ₂ .H ₂ O
C ₃ A.3C \bar{S} .32H	Ettringite - 3CaO.Al ₂ O ₃ .3CaSO ₄ .32H ₂ O
AFt	t stands for tri and refers to the three units of CX in the general AFt formula: C ₃ (A,F).3CX.yH ₂ O, where the most important AFt phase is ettringite
AFm	m stands for mono and refers to the single unit of CaX ₂ in the general AFm formula: C ₃ (A,F).CaX ₂ .yH ₂ O, where X may be OH ⁻ , SO ₄ ⁻² and CO ₃ ⁻²

Annexe II

Compositions

Table 6.1: Phases composition determined by XRD-Rietveld refinement

Phases	Siegentaler	Wildegger	Vigier	Mix of 3 cements
C ₃ S	65.9	59.7	64.6	63.5
C ₂ S	8.6	12.9	8.9	10.3
C ₃ A	6	4.3	9.3	6.4
C ₄ AF	8.4	11	6.6	9.2
C	0.7	0.6	0.6	9.2
M	1.4	1	1	1.1
Gypsum	0	3.2	1.3	1.2
Hemi-hydrate	0	0	0.4	0.9
Anhydrite	1.8	0.5	1.1	1
\bar{C}	4.3	4.8	3.8	4.1
K ₂ SO ₄	1.7	1.4	1.6	1.5

Table 6.2: Elements analysis determined by XRF

Phases	Siegentaler	Wildegger	Vigier	Mix of 3 cements
CaO	64	63	64	63.7
SiO ₂	19.6	19.6	19	19.6
Al ₂ O ₃	4.5	5	5.2	4.9
MgO	2	2.1	1.9	1.9
Na ₂ O	0.15	0.16	0.11	0.17
SO ₃	3.02	2.88	2.35	2.79
P ₂ O ₅ 0.2	0.11	0.34	0.21	
K ₂ O1.3	1.33	1.4	1.37	
TiO ₂ 0.27	0.27	0.29	0.27	
Fe ₂ O ₃ 2.75	3.17	2.47	2.61	
LOI	2.1	2.3	3.0	2.4

Curriculum Vitae

Name	Juilland
Surname	Patrick Piya
Date of Birth	October 10 th 1979
Background	<p>1999 – 2005, Materials Science and Engineering at Ecole Polytechnique Fédérale de Lausanne (EPFL); Switzerland.</p> <p>Undergraduate thesis done at the Asian Institute of Technology; Thailand and at EPFL in the Powder Technology Laboratory – “Nanocomposites à matrice en caoutchouc naturel”.</p> <p>1994 – 1999 Collège des Creusts; Sion – Switzerland.</p>
Professional experience	<p>2005 – 2009, Laboratory of Construction Materials, Departement of Materials Science, EPFL; Switzerland.</p> <p>PhD thesis – “Early Hydration of Cementitious Materials”.</p> <p>2004, Internship in Plant toys in the Engineering departement (Thailand)</p> <p>2001 – 2004, Different employment as Assistant-Student in EPFL</p> <p>1999 – 2004, Private Courses in Mathematics and Physics at Ecole Alpha, Sierre, Switzerland.</p>
Special Interests	<p>Drawing and Oil Painting</p> <p>Since 1985, Judo (Monitor JS 1 since 2001)</p>
Languages	<p>French – Excellent knowledge (mother tongue)</p> <p>English – Good knowledge</p> <p>German – Good knowledge</p> <p>Thai – Good knowledge (only spoken)</p>